Molecular Effects on Evaporation and Condensation

Roar Meland
Submitted for the degree
Doktor ingeniør at the
Norwegian University of Science
and Technology.

URN:NBN:no-3346

Abstract

In this thesis the evaporation from and condensation on a plane liquid surface have been studied by analysis and molecular dynamics simulations. The effect of the condensation coefficient on the inverted temperature gradient for a two-surface evaporation-condensation geometry is investigated by the moment method. The influence of the molecular exchange phenomenon on the gas-kinetic treatment of evaporation and condensation is shown to be neglible under certain assumptions. Methods to simulate half-space steady evaporation or condensation in Direct Simulation Monte Carlo simulation are adapted to Molecular Dynamics (MD). A microscopic definition of evaporation and condensation is introduced and values for the evaporation and condensation coefficients are calculated from MD. The velocity distribution functions for the evaporation and condensation modes have been calculated and compared with the standard assumptions in gas-kinetic calculations.

Contents

Preface

This study has been submitted for the degree Doktor Ingeniør at the Norwegian University of Science and Technology. I wish to thank my supervisors, professor Tor Ytrehus and professor Bjørn Hafskjold, for their support and encouragement. The work has been made possible through a grant from the Norwegian Research Council. I am also grateful to the Italian Foreign Ministry for supporting my one-year stay at Politecnico di Milano, my deepest gratitude to the staff at Dipartimento di Matematica for their generous hospitality. Finally I wish to thank my parents for their continuing help and support.

Chapter 1

Introduction

1.1 Preliminaries

Flows involving evaporation and condensation are widespread both in natural processes and in industrial applications. Examples are condensation heat transfer, vacuum distillation, vacuum vapor deposition of thin films in microelectronics technology, isotope separation, laser induced vaporization of metals, growth of droplets in the earth atmosphere that might have an effect on the green house effect, and space applications such as outgassing from surfaces of satellites.

Evaporation and condensation are surface phenomena, molecules that change phase pass through a thin region dividing the phases called the interphase. In kinetic theory treatment of phase change, the Boltzmann equation describes the gas and the effect of the interphase is modeled by an appropriate boundary condition. The standard boundary condition contains a parameter called the condensation coefficient, which may be interpreted as the fraction of the incident molecules that condenses. Values for the condensation coefficient for various substances are poorly known, for instance, reported values for water[1] vary between 0.01 and 1, and often the condensation coefficient has been set to 1 without much justification. However, the results from gas-kinetic calculations are strongly dependent upon the condensation coefficient. The evaporation or condensation mass-flux is an almost linear function of the condensation coefficient. Gas-kinetic calculations shows the theoretical possibility of an inverted temperature profile from what seems physically reasonable in the region between two dense-phase surfaces, kept at slightly different temperatures, with net evaporation from one surface and net condensation on the other. The criterion for the occurrence of the inverted temperature gradient is critically dependent upon the value of the condensation coefficient. Gas-kinetic calculations also predict the so-called blocking effect for condensation; the maximum subsonic Mach number attainable for steady condensation depends strongly on the value of the condensation coefficient.

1.2 Objective and scope

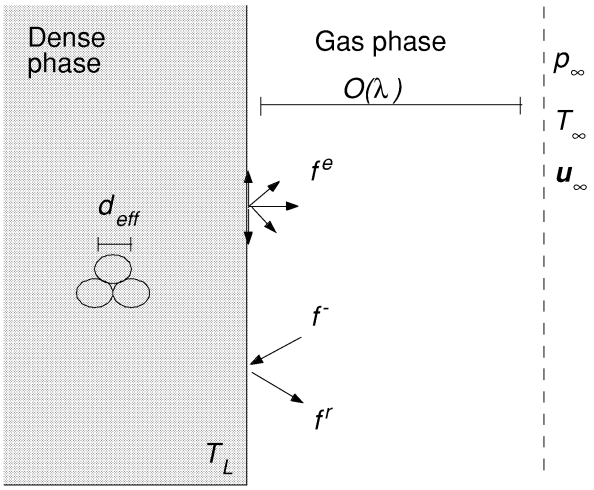

Figure 1.1: Definition sketch for the evaporation/condensation problem

Fig.1.1 shows a sketch of a plane liquid or solid surface and its corresponding vapor to the right. Net evaporation or condensation may occur, depending on conditions in the liquid, such as the temperature T_L, and conditions in the gas phase far from the interphase, for instance the temperature T_∞ and the pressure p_∞. The gas-liquid system contains at least two length scales: in the liquid the effective molecular diameter, d_{eff}, and in the gas the mean free path λ. The mean free path depends on the density of the gas, but is typically several orders of magnitude larger than the molecular diameter. Studies of the interphase must be performed on the molecular scale, for instance with molecular dynamics. Kinetic theory, on the other hand, is valid for dilute gases only, and can resolve the flow in the gas region outside the interphase. The traditional way to model evaporation and condensation has been to specify the distribution functions f^e and f^r outside the interphase for evaporated and reflected molecules, the calculation is then reduced to a well defined gas-kinetic problem. The reflection distribution depends upon the incoming distribution f^-, which is a result of the computation, hence the boundary condition is coupled to the solution.

The initial motivation for this study was to calculate the condensation coefficient and the related evaporation coefficient for a gas-liquid interphase in equilibrium, with molecular dynamics simulation. Later, methods to simulate net evaporation and condensation were developed. It was then decided that the boundary condition itself needed a closer examination, and the distribution function outside the interphase was calculated with data from molecular dynamics.

1.3 Organization of the report

Chapters 2 and 3 introduce the reader to the fields of kinetic theory and molecular dynamics simulation. Chapter 2 presents the Boltzmann equation and the gas kinetic formulation of the evaporation/condensation problem. Then various methods of solution are discussed. In chapter 3, the basic principles of equilibrium molecular dynamics are introduced, some preliminary results for a gas obeying the Soave-Redlich-Kwong (SRK) equation of state are also included and the definition of the interphase is discussed.

The author's contribution starts in chapter 4. The moment solution for slightly weak condensation is trivially extended to the case of evaporation and condensation coefficients differing from each other. Then the criterion for the inverted temperature gradient phenomenon in the two plate geometry is derived for equal evaporation and condensation coefficients. At the end of chapter 4 is an equilibrium molecular dynamics simulation of gas-liquid coexistence, the condensation coefficient is calculated directly from its definition and implications on gas-kinetic predictions for the inverted temperature gradient are examined.

Chapter 5 is a short digression to the molecular exchange phenomenon. An article entitled "Molecular exchange and its influence on the condensation coefficient" with content closely resembling this chapter has been accepted for publication in the Journal of Chemical Physics.

Chapter 6 deals with intense, or strong evaporation. The moment solution is trivially extended to the case of evaporation and condensation coefficients different from each other, and the effect of nonunity coefficients on the Knudsen layer is discussed. A molecular dynamics simulation algorithm for net evaporation is presented, and various ways of calculating the condensation coefficient are discussed. The distribution function outside the interphase is sampled and a comparison with the standard boundary condition in gas-kinetic modelling of evaporation is made.

Chapter 7 deals with intense, or strong condensation. The general transformation is trivially extended to the case of evaporation and condensation coefficients different from each other. A molecular dynamics simulation algorithm for net condensation is presented. The condensation coefficient and the distribution function outside the interphase are calculated from simulation data and a comparison with the standard boundary condition in gas-kinetic modelling of condensation is made.

Chapter 2

Kinetic theory of interphase mass transfer

2.1 Boltzmann equation

A kinetic equation is a closed equation for the time-development of the one-particle distribution $f_1(\mathbf{r}_1, \mathbf{c}_1, t)$, where $f_1(\mathbf{r}_1, \mathbf{c}_1, t)d\mathbf{r}_1 d\mathbf{c}_1$ gives the number of molecules in a volume element $d\mathbf{r}_1$ and velocity element $d\mathbf{c}_1$. $\mathbf{c}$ is the molecular velocity vector with components c_x, c_y and c_z. In general the one-particle distribution $f_1(\mathbf{r}_1, \mathbf{c}_1, t)$ depends on the two-particle distribution $f_2(\mathbf{r}_1, \mathbf{c}_1, \mathbf{r}_2, \mathbf{c}_2, t)$ and so on, thus forming an infinite hierarchy. For dilute gases Boltzmann derived the famous equation named after him which is a closed equation for $f_1(\mathbf{r}_1, \mathbf{c}_1, t)$, henceforth denoted $f(\mathbf{r}, \mathbf{c}, t)$,[2]

$$\frac{\partial f}{\partial t} + \mathbf{c} \cdot \frac{\partial f}{\partial \mathbf{r}} + \frac{\mathbf{K}}{m} \cdot \frac{\partial f}{\partial \mathbf{c}} = C(f) \tag{2.1}$$

The left hand side of the Boltzmann equation is analogous to the substantial derivative in fluid dynamics, but here the molecular velocity is also an independent variable. $\mathbf{K}$ is the net external force acting on a particle. On the right hand side, $C(f)$ is the nonlinear collision integral

$$C(f) = \int\int \left[f(\mathbf{c}') f(\mathbf{c}_1') - f(\mathbf{c}) f(\mathbf{c}_1) \right] |\mathbf{c} - \mathbf{c}_1| \sigma d\Omega d\mathbf{c}_1 \tag{2.2}$$

that gives the rate of change of the distribution function due to binary collisions between the molecules. Primed variables denote post collisional velocities that must be expressed as functions of $\mathbf{c}$ and $\mathbf{c}_1$, and $\sigma d\Omega$ is the differential cross section[2],[3]. The Boltzmann equation can resolve flow structures on the scale of the mean free path.

For the Boltzmann equation, inflow boundary conditions must be specified at boundaries of the computational domain,

$$f(\mathbf{c}) = f_{bc}(\mathbf{c}), \qquad \mathbf{c}\cdot\mathbf{n} > \mathbf{0} \tag{2.3}$$

where $\mathbf{n}$ is normal to the boundary and directed into the domain. It is assumed here that the boundary is not moving. Equivalently, the inflow differential flux $(\mathbf{c}\cdot\mathbf{n})\, f_{bc}$ could be specified instead. The distribution for $\mathbf{c}\cdot\mathbf{n} < \mathbf{0}$ at the boundary is a result of the solution.

The Boltzmann equation is valid only for dilute gases, it is assumed that the range of the intermolecular force is small compared to the intermolecular spacing which in turn is small compared to the average distance a molecule travels between collisions[4]. Hence only two-particle interactions, or 'collisions', need to be taken into account. Between collisions the molecules travel in straight-line trajectories if the external force is neglected. It is also implicit in the derivation that two molecules are uncorrelated before a collision, this is the so-called 'molecular chaos' assumption[5].

2.2 Boundary condition outside the interphase

Since the pioneering work of Hertz[6] and Knudsen[7], it has been known that evaporation and condensation require the use of kinetic theory for an accurate description. In kinetic theory the interphase is modeled as a surface of zero thickness. A molecule that strikes the interphase is either captured, i.e. condensed, or reflected. It is usually assumed that the condensation probability is independent of the incoming velocity. A fraction σ_c of the incoming molecules condenses on the surface, the fraction $1-\sigma_c$ is reflected, see Fig. 2.1. σ_c is often called the condensation coefficient. The distribution function is split into modes for evaporated and reflected molecules. The evaporation mode is usually assumed to be Maxwellian with a liquid temperature T_L and no drift velocity. This is approximately the same distribution as in the liquid, the liquid is close to local equilibrium, and the liquid drift velocity is small compared to the drift velocity in the gas in case of net evaporation or condensation. Hence it is assumed that the evaporation mode passes through the interphase unaltered, which is not particularly plausible as the interphase can be regarded in mean field theory as a potential jump[8]. The reflection mode is usually modeled as diffuse or specular or a combination of both. On the molecular level the interphase is not smooth, the interphase molecules are of course identical to the incoming gas molecules, and there is no reason to assume specular reflection. The diffuse assumption is also convenient since solutions for nonunity condensation coefficient can be obtained from ideal solutions, if the temperature in the reflection mode is assumed to be T_L, i.e. complete accommodation to the liquid temperature[9]. Contrary to the specular model, for diffuse reflection a nonunity condensation coefficient has an important influence on the results[2].

The number density must also be specified, a convenient scale for the evaporation mode is the saturation density $n_s(T_L)$, since it is usually assumed that the evaporation flux is independent of the degree of nonequilibrium and only

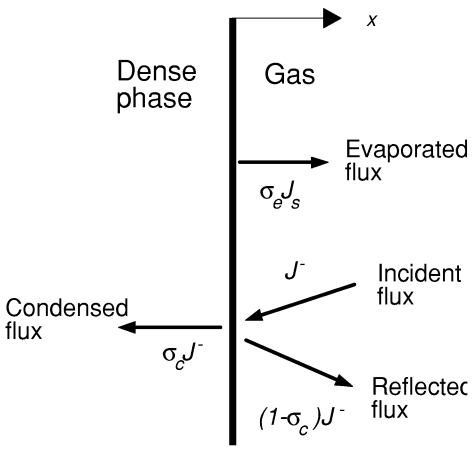

Figure 2.1: Molecular fluxes at the interphase

depends upon T_L. An 'evaporation coefficient' is introduced to account for the deviation of the number density for the evaporating molecules from the saturation density. For the reflection mode it is convenient with a reference density n_i that scales as the flux of reflected molecules. This is the reason for introducing the factor $1-\sigma_c$ in the boundary condition, Eq.(2.4), and as will be seen later, cancellation occurs in the expression for n_i. The boundary condition is written as

$$f^+(\mathbf{c}) = n^+ F^+ = \left[\sigma_e n_s + (1-\sigma_c) n_i\right] F_s \qquad c_x > 0 \tag{2.4}$$

where

$$F_s = \frac{1}{(2\pi R T_L)^{3/2}} \exp\left(-\frac{c_x^2 + c_y^2 + c_z^2}{2RT_L}\right) \tag{2.5}$$

Here $R = k/m$, the gas constant per unit mass. f^+ is the complete distribution function, it includes both the density n^+ and the velocity probability distribution F^+. Lower-case index indicates reference quantities with the distribution normalized to 1 on $-\infty < c_x < \infty$, upper-case indicates physical quantities where the distribution has been normalized to 1 on $c_x > 0$. The reference density n_i for reflected molecules follows from the reflected flux

$$\int_{c_x>0} c_x (1-\sigma_c) n_i F_s \, d\mathbf{c} = \int_{c_x<0} (1-\sigma_c) \left|c_x\right| f^- \, d\mathbf{c} \tag{2.6}$$

Hence

$$n_i = J^- / \sqrt{\frac{RT_L}{2\pi}}. \tag{2.7}$$

where J^- is the incident flux defined by

$$J^- = \int\limits_{c_x<0} |c_x| \, f^- d\mathbf{c} \tag{2.8}$$

In equilibrium n_i is equal to the saturated vapor density n_s. The introduction of the condensation coefficient in the boundary condition hinges on the assumption that the condensation probability is independent of velocity so that the factor $1 - \sigma_c$ can be taken outside of the integrals in Eq.(2.6).

The evaporation coefficient is often defined in terms of fluxes instead of densities. The evaporation flux is

$$J^e = \int\limits_{c_x>0} \sigma_e n_s F_s dc_x \tag{2.9}$$

Hence σ_e may be written as

$$\sigma_e = J^e / J_s \tag{2.10}$$

where $J_s = n_s \sqrt{\frac{RT_L}{2\pi}}$. σ_e and σ_c can not be calculated using kinetic theory, but must be found from measurements, nonequilibrium statistical mechanics or molecular dynamics. In equilibrium, the net flux J through the interphase is zero and the temperature of the system is uniform. J_s and J^- are hence equal since the Mawellians have the same temperature and density, and we must therefore have

$$\sigma_e = \sigma_c = \sigma \tag{2.11}$$

at equilibrium, where σ denotes the common equilibrium value. It has been customary to set σ_e and σ_c equal outside equilibrium too, we suspect that this is more due to ignorance about their true values than theoretical considerations. We have for example never seen a rigorous theoretical derivation of the boundary condition, Eq.(2.4).

In this work the plane, two-phase gas-liquid configuration of a monatomic, one-component substance has been considered. The one-component assumption is crucial. Surface active substances and impurities tend to accumulate in the interphase and reduce the mass transfer by diffusional resistance[10]. The presence of a small amount of noncondensible gas has a dramatic effect on the mass flux in condensation. The noncondensible gas is dragged along by the condensing gas and accumulates near the interphase. Condensing gas molecules then have to diffuse through a layer of the noncondensible gas and the condensation flux is considerably reduced[11],[12].

2.3 Methods of solution

In the last thirty years, a large amount of papers have been devoted to evaporation and condensation within the context of kinetic theory, and most of these have used the moment method, the BKW equation or the DSMC method, which will be briefly described. Assuming steady state, the gas region above the plane interphase is described by the one-dimensional Boltzmann equation, neglecting gravity.

$$c_x \frac{\partial f}{\partial x} = C(f) \tag{2.12}$$

The moment method can give an approximate closed form solution of the one-dimensional Boltzmann equation and has been used extensively in this thesis. If we multiply both sides of the one-dimensional steady Boltzmann equation, Eq.(2.12), by functions $Q_i(\mathbf{c})$ forming a complete set, and integrate over the molecular velocity, we obtain infinitely many relations, called moment equations, to be satisfied by the distribution function f.

$$\frac{d}{dx}\int c_x Q_i f d\mathbf{c} = \int C(f) Q_i d\mathbf{c} = \Delta[Q_i] \tag{2.13}$$

The idea of the so-called moment method[13] is to satisfy only a few moment equations, usually the conserved moments for which $\Delta[Q_i] = 0$ (mass, momentum and energy) and at least one non-conserved moment. This leaves the distribution function largely undetermined and an ansatz is used that complies with the boundary conditions and contains a few adjustable parameters to be determined by the chosen moment equations. The moment method was introduced by Mott-Smith[14] who considered a shockwave in a dilute gas and assumed that the distribution function within the shock may be represented by a linear combination of the Maxwellian distribution functions that apply upstream and downstream of the shock. Liu and Lees[15] applied the moment method to the Couette flow between two infinite flat plates sliding in opposite direction, the distribution function was assumed to be a combination of two half Maxwellians, i.e. with molecular velocities restricted to $c_y < 0$ and $c_y > 0$, respectively. Assuming diffuse reflection at the plates, the ansatz of the distribution function fulfills the boundary conditions. Combining the ideas of Mott-Smith and Liu and Lees, Anisimov[9] and Ytrehus[16],[17] introduced the moment method for the evaporation/condensation problem. The two most significant sources of inaccuracies in the moment method are the a priori assumption for the distribution function and the fact that the result is highly sensitive to the choice of non-conserved moments.

Due to the complexity of the collision term in the Boltzmann equation, collision models have been introduced that give reasonable results if finer details are not required. The most widely used collision model is the Bhatnagar, Gross and Krook(BGK) model[18]

$$C^{BGK}(f) = \nu\,(f_M - f) \tag{2.14}$$

Here ν is a collision frequency proportional to the density and it may also depend on the temperature, but it is assumed to be independent of the molecular velocity. Here f_M is the local Maxwellian distribution, i.e. Maxwellian with the same density, temperature and drift velocity as f. The corresponding kinetic equation is called the Krook equation or BKW equation. The Kyoto group has worked extensively with analytical and numerical solutions of the BKW equation applied to evaporation and condensation[19],[90],[20][21].

Finite difference solution of the Boltzmann equation is awkward since in general a 6-dimensional space $(\mathbf{r}, \mathbf{c})$ must be discretised, it is not clear how to set the bounds in velocity space, and the 5-dimensional integral in the collision term is difficult to approximate numerically. In practice, the Boltzmann equation is often solved by a particle method called Direct Simulation Monte Carlo(DSMC), introduced, and to a large extent, developed by Bird[22],[23]. The particle interactions, or 'collisions' are carried out in an approximate way. The space domain is divided into cells, and particles in the same cell are allowed to collide, with a randomly chosen impact parameter and a collision probability proportional to the relative velocity. Between the collisions, the particles move in straight lines if field forces like gravity are neglected.

The various models and methods have proven to give results that are in good agreement with each other. Recent reviews of kinetic theory applied to evaporation and condensation can be found in Refs.[2],[24],[25].

Chapter 3

Molecular Dynamics Simulation

In molecular dynamics, the classical equations of motion are solved for every molecule in the system. By calculating the motions of individual molecules, one hopes to gain insight into the sometimes puzzling behavior of large collections of molecules. The first successful molecular dynamics simulation, for a system of hard spheres, was published in 1957. Alder and Wainwright[26] showed that a hard sphere gas has a gas-solid phase transition. The first successful simulation of particles interacting via a Lennard-Jones potential was published by Rahman[27] in 1964. In the following years the usefulness of the molecular dynamics method has increased as more powerful computers have become available.

Standard molecular dynamics simulation in a box of volume V and periodic boundary conditions automatically conserves the number of particles N and the total energy E, and averages correspond to the microcanonical ensemble in statistical mechanics. In experiments, the temperature T is often fixed instead of E, then the canonical ensemble is sampled. A crude way of implementing the canonical ensemble in molecular dynamics simulations is simply to rescale the velocities of the molecules at certain time-step intervals[28]. A more refined way to simulate the canonical ensemble of statistical mechanics is to use a so-called Nose-Hoover thermostat[29],[30]. Artificial 'friction' like forces with 'friction coefficients' that can be both positive and negative are introduced that on the average maintain the system at a temperature T and the system samples the canonical ensemble.

In the study of equilibrium behavior, molecular dynamics is used to probe systems that, at least in principle, can be studied by statistical mechanics. However, when one departs from equilibrium, very little theoretical guidance is available, (with the notable exception for dilute gases and the Boltzmann equation) and molecular dynamics is an indispensable tool[31]. In nonequilibrium molecular dynamics(NEMD), a system can be maintained in steady nonequilib-

rium by introducing boundary regions where particles are made to interact with external particle, momentum or energy reservoirs[32]. This is sometimes called boundary driven NEMD.

There is also another approach to NEMD, called synthetic NEMD in Ref.[30], then the equations of motion are perturbed by fictional driving forces. These driving forces homogeneously interact with the molecules in order to mimic precisely the bulk response of a real system to externally imposed temperature or velocity gradients. The system is homogenous and periodic boundary conditions are used[33],[34],[35],[36].

3.1 Principles of equilibrium molecular dynamics

This section gives a brief introduction to the principles of equilibrium molecular dynamics. For a more in-depth description, see the textbook by Haile[37].

For molecules heavier than hydrogen and for temperatures above a few Kelvins, classical dynamics gives sufficient accuracy for the translational and rotational degrees of freedom for molecules in the vibrational ground state[35],[38]. Henceforth only spherically symmetric molecules will be considered. The translational motion of each molecule is calculated according to Newtons second law

$$\mathbf{F}_i = m\mathbf{a}_i \tag{3.1}$$

$\mathbf{F}_i$ is the sum of all forces acting on molecule i, it is often approximated as the sum of pair interactions between the molecules.

The resulting system of nonlinear differential equations is solved numerically. In this study, a variant of the Verlet algorithm[40], called velocity Verlet[39], has been used. For each time-step, the positions and velocities of the molecules are updated according to[33] :

$$\mathbf{r}_i(t+\Delta t) = \mathbf{r}_i(t) + \mathbf{v}_i(t)\Delta t + \frac{1}{2}\mathbf{a}_i(t)\Delta t^2 \tag{3.2}$$

$$\mathbf{v}_i(t+\Delta t) = \mathbf{v}_i(t) + \frac{1}{2}\left[\mathbf{a}_i(t) + \mathbf{a}_i(t+\Delta t)\right]\Delta t \tag{3.3}$$

The time-step must be smaller than the shortest relaxation time of the system. For spherical molecules with no internal structure at typical liquid densities, the time-step is of the order 10^{-14} s, depending on the numerical method used.

The number of molecules in a molecular dynamics simulation is severely limited. Nowadays simulations with 10000 molecules are common, and although a million molecules have been simulated, this is far short of the number encountered under experimental conditions($\sim 10^{23}$). A simulation box with hard physical boundaries would give a large percentage of the molecules sensing the wall, and the effect of the wall would dominate the dynamics. To simulate a

bulk fluid, that is a fluid where wall interactions are not important, periodic boundary conditions must be used [37], see Fig. 3.1 below.

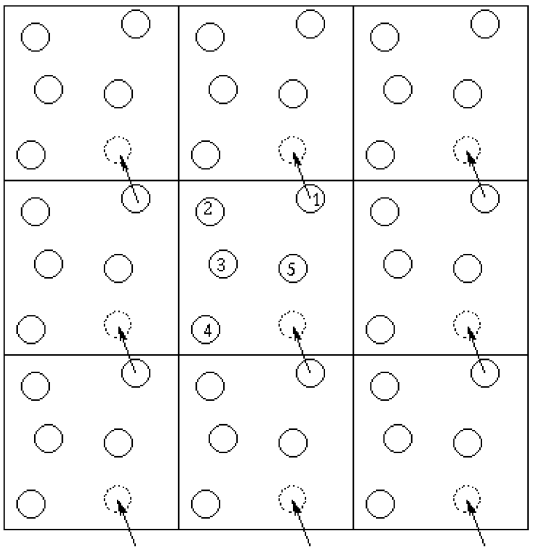

Figure 3.1: Periodic boundary conditions. From Ref. [41]

In this method the rectangular box containing the molecules, is surrounded on all sides by copies of itself. Particles in different boxes interact. Image molecules in image boxes follow trajectories that are exact duplicates of those followed by the molecules in the primary box. Hence molecules that leave the primary box are in effect inserted on the opposite side with the same velocity. The cut-off distance of the interactions is usually much smaller than the dimensions of the box, and hence only molecules near one edge of the primary box interact with molecules on the opposite side of the box. Periodic boundary conditions preserve both energy and momentum, and the exact microcanonical ensemble is not sampled, but denoting the number of molecules by N, the perturbation is of the order $1/N$ and can be neglected[37].

The most time consuming part of a molecular dynamics algorithm is calculation of the forces. In principle, at each time-step, $N(N-1)/2$ distances must be calculated. Computing distances longer than the cut-off distance r_c of the potential wastes computer time. Verlet[40] introduced a neighbor list to reduce this problem. For each molecule i, a list containing all neighbors with distances less than r_L is maintained, only those neighbors are used in force calculations. r_L is slightly larger than r_c so that the same neighbor-list can be used for several time-steps. A new neighbor-list must be constructed when the maximum distance a molecule has moved since the last update exceeds $(r_L - r_c)/2$, it is then possible that it has got new neighbors within the cut-off distance.

Sampling of macroscopic properties is based on the ergodic hypothesis[33] which states that for a macroscopically stationary system, the ensemble average $\langle A \rangle$ equals the time average,

$$\langle A \rangle = \lim_{t \to \infty} \frac{1}{t} \int_{t_0}^{t_0+t} A(t')dt' \approx \frac{1}{\Delta t} \int_{t_0}^{t_0+\Delta t} A(t')dt' \tag{3.4}$$

where Δt is the length of the sampling period.

3.2 Properties of the LJ-spline system

In the simulations a Lennard-Jones-spline (LJ-spline) potential[42] has been used.

$$U_{LJ-spline} = \begin{cases} 4\varepsilon \left[\left(\frac{r_0}{r}\right)^{12} - \left(\frac{r_0}{r}\right)^{6} \right] & r \leqslant r_s \\ k_1(r - r_c)^3 + k_2(r - r_c)^2 & r_s < r \leqslant r_c \\ 0 & r > r_c \end{cases} \tag{3.5}$$

where

$$r_s = \left(\frac{26}{7}\right)^{1/6} r_0 \approx 1.24 r_0, \qquad r_c = \frac{67}{48} r_s \approx 1.73 r_0 \tag{3.6}$$

and

$$k_1 = -\frac{387072}{61009} \frac{\varepsilon}{r_s^3} \qquad k_2 = -\frac{24192}{3211} \frac{\varepsilon}{r_s^2} \tag{3.7}$$

Here r_0 is the inter-molecular separation where the pair-potential is zero, and ε is the potential depth. The LJ-spline potential deviates from the Lennard-Jones potential only in the tail, a cubic spline is fitted from the point r_s of inflection so the potential goes smoothly to zero at r_c. Calculation of the forces with the spline potential is much faster than the conventional Lennard-Jones potential cut at 2.5 r_0, since the neighbor-list is much shorter with the spline. The LJ-spline fluid is a model fluid for spherical molecules, it does not correspond exactly to any substance.

The potential parameters r_0 and ε, in addition to the molecular mass and Boltzmann's constant, are used to make nondimensional quantities, which are denoted by an asterisk. Some frequently used nondimensional quantities are given in Table 3.1.

The Lennard-Jones-spline potential has triple-point temperature $T_3^* \approx 0.55$ and critical temperature $T_c^* \approx 0.9$ [43], the phase diagram is shown in Fig.3.2.

density	$n^* = r_0^3 n$
time	$t^* = \frac{1}{r_0}\sqrt{\frac{\varepsilon}{m}}t$
speed	$c_x^* = \sqrt{m/\varepsilon}c_x$
temperature	$T^* = \frac{kT}{\varepsilon}$
pressure	$p^* = r_0^3/\varepsilon p$
heat capacity	$c_p^* = \frac{k}{m\varepsilon^2}c_p$
viscosity	$\mu^* = \frac{r_0^2}{\sqrt{m\varepsilon}}\mu$
distribution	$F^*(c_x^*) = \sqrt{\varepsilon/m}F$
differential flux	$\phi^*(c_x^*) = r_0^3\phi$
force	$\mathbf{F}^* = \frac{r_0}{\varepsilon}\mathbf{F}$

Table 3.1: Nondimensionalized quantities

In Ref.[43], an approximate Soave-Redlich-Kwong (SRK) equation of state for the LJ-spline fluid in the gas phase was fitted from simulation data. In Lennard-Jones units the SRK-equation is

$$p_{SRK}^* = \frac{T^*}{v^* - b^*} - \frac{a^*}{v^*(v^* + b^*)} \tag{3.8}$$

where

$$v^* = 1/n^* \qquad b^* = 0.0867\frac{T_c^*}{p_c^*} \tag{3.9}$$

$$a^* = e^*\left[1 + d^*\left(1 - \sqrt{\frac{T^*}{T_c^*}}\right)\right]^2 \tag{3.10}$$

$$d^* = 0.487 \qquad e^* = 0.428\frac{T_c^{*2}}{p_c^*} \tag{3.11}$$

$$T_c^* = 0.897 \qquad p_c^* = 0.0776 \tag{3.12}$$

Since the gas is not ideal, the speed of sound is derived from the equation of state[44], but it turns out that the deviation is small.

$$c^* = \sqrt{\left(\frac{\partial p^*}{\partial \rho^*}\right)_{s^*}} = \sqrt{\gamma\left(\frac{\partial p^*}{\partial \rho^*}\right)_{T^*}} = \sqrt{-\gamma\left(\frac{\partial p^*}{\partial v^*}\right)_{T^*} v^{*2}} \tag{3.13}$$

The ratio of the heat capacities, $\gamma = \frac{c_p}{c_v}$, can also be found from the equation of state. Using the cyclical rule[45], [46], the specific heat capacities are related by

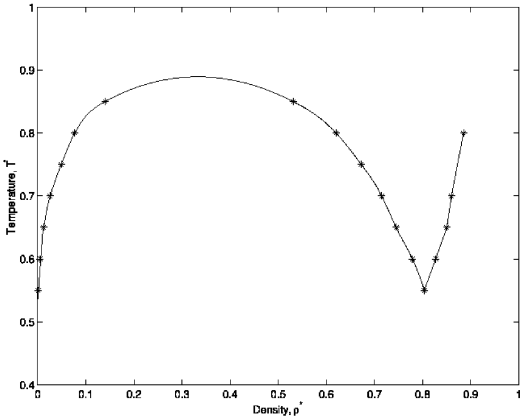

Figure 3.2: Phase diagram for LJ-spline. From Ref.[43]

$$c_v^* = \frac{3}{2} + \int_{\infty}^{v^*} T^* \left(\frac{\partial^2 p^*}{\partial T^{*2}}\right)_v dv^{*\prime} \tag{3.14a}$$

$$c_p^* - c_v^* = T^* \left(\frac{\partial p^*}{\partial T^*}\right)_v \left(\frac{\partial v^*}{\partial T^*}\right)_p = -T^* \frac{\left(\frac{\partial p^*}{\partial T^*}\right)_v^2}{\left(\frac{\partial p^*}{\partial v^*}\right)_T} \tag{3.14b}$$

$$\gamma(T^*, v^*) = \frac{c_p^*}{c_v^*} = 1 - \frac{T^*}{c_v^*} \frac{\left(\frac{\partial p^*}{\partial T^*}\right)_v^2}{\left(\frac{\partial p^*}{\partial v^*}\right)_T} \tag{3.14c}$$

Using the SRK equation of state, the partial derivatives are

$$\left(\frac{\partial p^*}{\partial v^*}\right)_{T^*} = -\frac{T^*}{(v^*-b^*)^2} + \frac{a^*}{v^{*2}(v^*+b^*)} + \frac{a^*}{v^*(v^*+b^*)^2} \tag{3.15}$$

$$\left(\frac{\partial p^*}{\partial T^*}\right)_{v^*} = \frac{1}{v^*-b^*} + \frac{e^*d^*}{\sqrt{T^*T_c^*}} \frac{1+d^*\left(1-\sqrt{\frac{T^*}{T_c^*}}\right)}{v^*\left(v^*+b^*\right)} \tag{3.16}$$

$$\left(\frac{\partial^2 p^*}{\partial T^{*2}}\right)_{v^*} = -\frac{1}{2}\frac{e^*d^*}{T^*\sqrt{T^*T_c^*}} \frac{\left[1+d^*\left(1-\sqrt{\frac{T^*}{T_c^*}}\right)\right]}{v^*(v^*+b^*)} - \frac{1}{2}\frac{e^*d^{*2}}{T^*T_c^*}\frac{1}{v^*(v^*+b^*)} \tag{3.17}$$

and combining with Eq.(3.14a), we finally have

$$c_v^*(T^*,v^*) = \frac{3}{2} + \frac{1}{2}\frac{d^*e^*}{b^*\sqrt{T^*T_c^*}}(d^*+1)\ln\frac{v^*+b^*}{v^*} \tag{3.18}$$

The Mach number far from the interphase is $M_\infty = u_\infty/c$, with $c = \sqrt{\gamma RT_\infty}$ being the speed of sound. In kinetic theory the speed ratio defined as

$$S_\infty = \frac{u_\infty}{\sqrt{2RT_\infty}} \tag{3.19}$$

is often used. When comparing our MD simulations with kinetic theory calculations, equal Mach numbers should be used, and speed ratio is simply derived from the Mach number by $S_\infty = \sqrt{\frac{5}{6}}M_\infty$, and not from the kinetic definition. There is a small difference in the two sets of values.

The usual way to define the mean free path for an arbitrary intermolecular potential is to extend the hard sphere result $\lambda = \frac{\mu}{\rho}\sqrt{\frac{\pi}{2RT}}$. In the Chapman-Enskog expansion the distribution function is written as a power series in the Knudsen number and the viscosity is expanded in Sonine polynomials. In reduced units the first term is[4]:

$$\mu^{*(1)} = \frac{\frac{5}{8}\sqrt{\pi T^*}}{\frac{1}{(4T^*)^4}\int_0^\infty g^{*7}\sigma_\mu^*(g^*)\exp(-\frac{g^{*2}}{4T^*})dg^*} \tag{3.20}$$

$$\sigma_\mu^*(g^*) = 2\pi\int_0^{r_c^*} b^*\sin^2\varkappa db^* \tag{3.21}$$

$$\varkappa = \varkappa(b^*,g^*) \tag{3.22}$$

where $\sigma^*_\mu(g^*)$ is the viscosity cross-section. The deflection angle $\varkappa = \varkappa(g^*, b^*)$ was calculated by solving the equivalent one-body problem with reduced mass $\mu^* = 1/2$ numerically for various g^* and b^*'s. The resulting approximation to the viscosity is shown as a function of reduced temperature in Fig.3.3. The viscosity for the LJ-spline potential is close to the viscosity for the standard Lennard Jones potential cut at $2.5r_0$, the potential tail is apparently not so important for this property.

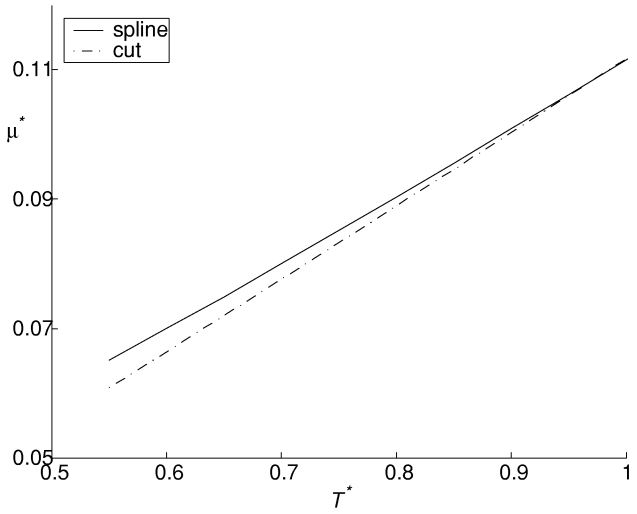

Figure 3.3: Viscosity as a function of reduced temperature for the LJ-spline potential and the LJ potential cut at $2.5r_0$.

In kinetic theory calculations of phase change, it is customary to use a reference mean free path evaluated for an equilibrium gas with a temperature equal to the temperature at the liquid side of the interphase[24].

$$\lambda^*_s = \frac{\mu^*(T^*_L)}{n^*_s(T^*_L)}\sqrt{\frac{\pi}{2T^*_L}} \tag{3.23}$$

This mean free path is independent of the strength of the phase change, i.e. it does not change with M_∞, contrary to a physical reference mean free path defined from conditions at infinity

$$\lambda^*_\infty = \frac{\mu_\infty(T^*_\infty)}{n^*_\infty}\sqrt{\frac{\pi}{2T^*}} \tag{3.24}$$

An effective 'hard sphere diameter' can be defined from the above value for λ^*_∞. Using the hard sphere result $\lambda^*_\infty = \frac{1}{\sqrt{2}n^*_\infty \pi d^{*2}}$, we have

$$d^*_{eff} = \frac{1}{\sqrt{\sqrt{2} n^*_\infty \pi \lambda^*_\infty}} \tag{3.25}$$

d^*_{eff} is always between r_s and r_c. An alternative definition of an equivalent hard sphere diameter can be found in Ref.[47].

The average distance between molecules is given by the density :

$$\delta^* = \sqrt[3]{\frac{1}{n^*}} \tag{3.26}$$

The degree of rarefaction can be expressed by δ^*/d^*_{eff}. Bird[23] uses

$$\delta^*/d^*_{eff} > 7 \tag{3.27}$$

as a limit for the dilute gas approximation. For a LJ-spline gas-liquid system in equilibrium, this limit is actually never attained. For high Mach number evaporation the density of the gas is approximately 1/4 of the saturation density for a condensation coefficient of 0.7[24] and a maximum $\delta^*/d^*_{eff} \approx 4$ was attained in our simulations.

λ^*_∞ is proportional to $1/n^*_\infty$ and hence $\lambda^*_\infty \sim \delta^{*3}_\infty$. The distance from the interphase measured in λ^*_∞'s, for which equilibrium flow is attained, is a function of the Mach number. Hence, with a potential that fulfills the $\delta^*/d^*_{eff} > 7$ criterion, the MD simulation box would have to be very long to contain the given mean free paths, and since the time for reaching steady state is related to the time it takes a sound wave to traverse the box, just relaxing the system to steady state would take a very long time, beyond the capabilities of computers we had access to.

3.3 Microscopic definition of evaporation and condensation

A precise definition of where the interphase ends and the gas phase begins, is necessary for measurement of the velocity distribution function used as the boundary condition in gas-kinetic calculations. The boundary condition should be put as near the liquid as possible, as long as the Boltzmann equation is valid. The Boltzmann equation implies the ideal equation of state, but for the chosen potential the gas in a two-phase gas-liquid equilibrium deviates from ideal for all temperatures down to the triple point, so the ideal gas criterion can not be used.

In a recent simulation of net condensation[43], the Soave-Redlich-Kwong (SRK) equation of state for the LJ-spline fluid in the gas phase was used to find the 'dividing line' between the gas and the interphase, here called the gas boundary. We have defined the gas boundary as the position 'near the liquid'

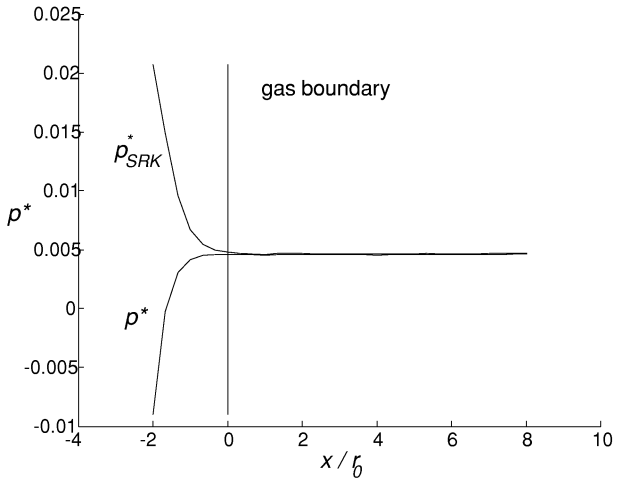

Figure 3.4: Deviation of SRK equation near the interphase

where $|p - p_{SRK}|$ is greater than the maximum of $|p - p_{SRK}|$ in the gas phase, i.e. larger than statistical fluctuations. This is indicated in Fig.3.4.

For net evaporation, there is a Knudsen layer in which $T_{||}$ and $T_{\perp}$ are differing significantly, see Fig.6.10 on page 68. $T_{||}$ and $T_{\perp}$ are defined by

$$T_{||} = \frac{1}{Rn}\int (c_x - u)^2 f d\mathbf{c} \qquad T_{\perp} = \frac{1}{2Rn}\int \left(c_y{}^2 + c_z^2\right) f d\mathbf{c} \tag{3.28}$$

The gas is not in local equilibrium in the Knudsen layer and the validity of the equilibrium equation of state is far from obvious. For evaporation, moment solutions and DSMC simulations for strong evaporation give $T_{\perp}$ increasing towards the interphase as T does, but $T_{||}$ is decreasing. In the liquid there is local equilibrium and $T_{||}$ is equal to T. Hence the derivative of $T_{||}$ has to change sign, and the position where this happens is a possible definition of the gas boundary. It turns out that the two criteria for finding the gas boundary gives almost identical results. In Fig.3.5 the position of the gas boundary from the SRK definition is plotted together with the temperatures for a Mach number at infinity $M_\infty = 0.78$. The minimum in $T_{||}$, indicated by an $\times$ in the figure, is $0.6r_0$ from the SRK definition of the gas boundary. In Fig.3.5 the liquid boundary has also been plotted, its exact definition will be given shortly.

The SRK criterion for the gas boundary gives a reasonable result both for evaporation and condensation, and since it is easier to apply the SRK criterion than the $T_{||}$ criterion for small Mach numbers for evaporation, the SRK definition of the gas boundary was chosen both for evaporation and condensation.

It is desirable to split the distribution function into contributions from evaporated and reflected molecules so comparison with the assumptions made in

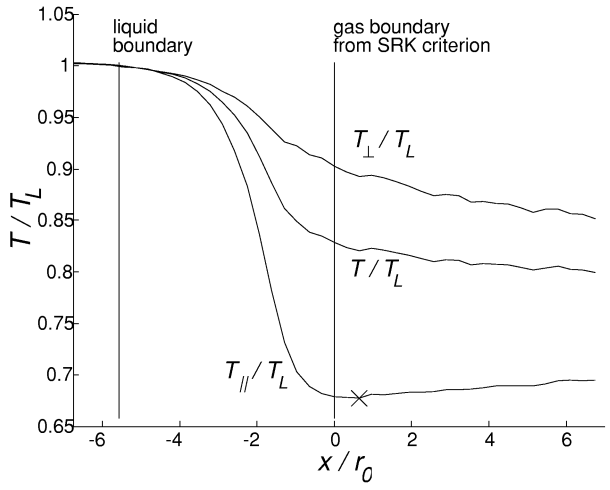

Figure 3.5: Temperatures in the interphase region. $\times$ denotes minimum in $T_{\|}/T_L$

gas-kinetic calculations can be made. Then microscopic definitions of evaporation and condensation are necessary. The most obvious suggestion is perhaps to monitor the potential energy of each molecule and define evaporation or condensation as the potential energy exceeding certain limits. However, in this work it was decided to use sharply divided liquid, interphase and gas regions. A molecule is considered as evaporated if it originated in the liquid region and crosses the interphase into the gas region, condensed if it originated in the gas region, crosses the interphase and enters the liquid region, and reflected if it originated in the gas region, crosses into the interphase and moves back to the gas region without having been in the liquid region, as indicated in Fig. 3.6.

Since evaporation, condensation and reflection are not instantaneous, the molecules have to enter or cross the interphase, it is necessary to have a start-up period after the stationary state has been reached so all molecules that were originally in the interphase are or have been outside of the interphase. Then the history of all the interphase molecules is known, and when a molecule crosses the gas boundary from the interphase, it is immediately clear if this is an evaporation or a reflection.

It is necessary to define a liquid boundary between the liquid and the interphase analogously as was done for the gas boundary. The SRK equation describes a phase transition, but liquid state points were not taken into account when the parameters in SRK equation of state, Eq.(3.8), was adjusted from molecular dynamics simulations of the Lennard-Jones-spline fluid[43]. If the liquid boundary is positioned into the bulk liquid phase, it may happen that some of the molecules that are in the corresponding interphase region at the beginning, do not leave the region during the entire simulation. Hence we used

a rather ad hoc definition of the liquid boundary that shifts the liquid boundary a little away from the liquid. A classical way to define the thickness of a shock wave is the distance required to span the density change by the maximum density gradient within the wave, the so-called density-gradient thickness[44], [4]. The liquid boundary here is defined by a similar construction. In a plot of the density in the interphase region, a tangent line is attached to the point where the density equals $(n_\infty + n_{liq}^{\max})/2$. Here $n_{liq}^{\max}$ is the maximum density in the liquid, for evaporation the density is highest close to the interphase where the temperature is lower than in the bulk. The liquid boundary is defined as the position where the tangent line crosses the line given by $n_{liq}^{\max}$, see Fig. 3.6.

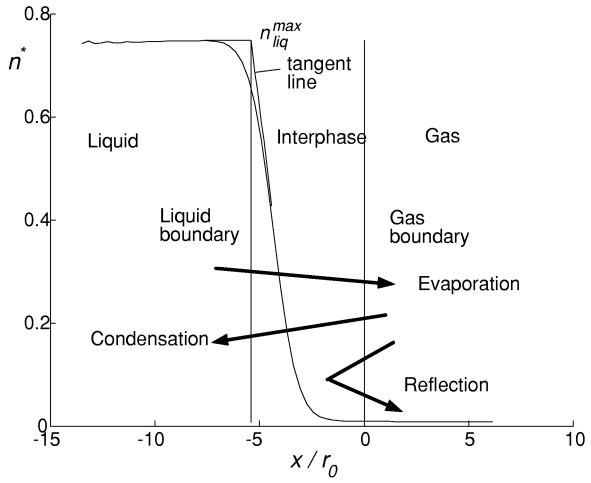

Figure 3.6: Definition of liquid boundary and microscopic definition of evaporation and reflection

The "liquid" temperature T_L used in gas-kinetic calculations of interphase transfer is associated with the temperature at the liquid boundary in molecular dynamics simulations.

Chapter 4

The inverted temperature gradient

4.1 Introduction

The evaporation from and condensation on a liquid or solid surface have been the subject of a variety of studies because of its importance in various fields of physics, chemistry and engineering. The classical Hertz-Knudsen mass flux formula across the interphase is still popular today because of its simplicity, despite an approximative nature and severe limitations on the theoretical side. The formula was significantly improved by Schrage[48] who took into account the bulk velocity of the gas, but without solving the gas-kinetic equations for the problem. The case of weak, linear processes was considered by Patton and Springer[49], Pao[50], [51], Shankar and Marble[11] and by Cipolla *et al.* [52].

Pao[50] noted the theoretical possibility of an inverted temperature profile in the region between two dense-phase surfaces, kept at slightly different temperatures, with net evaporation from one surface and net condensation on the other. If the normalized latent heat per unit mass, L/RT_L, is larger than a critical parameter β_c, the temperature profile in the gas may be inverted of what seems physically reasonable. For a unity evaporation and condensation coefficient, $\sigma = 1$, the value of β_c is approximately 4.8. For water L/RT_L is approximately 13. This remarkable finding has been recomputed and confirmed by several authors, for instance Murakami and Oshima[53], Gajewski *et al.* [54], Sone and Onishi[55], Matshushita[56] and Aoki and Cercignani[57]. Koffman *et al.*[58] suggested that the boundary conditions at the interphase could be responsible for the 'unphysical' temperature profiles, and Cercignani *et al.*[59] subsequently generalized these conditions and looked at their effect on the inverted temperature gradient. Cercignani *et al.* used the moment method with nonunity condensation coefficient and specular reflection, but the value of β_c did not change much when the condensation coefficient was varied from 0 to 1. However, Sone *et al.*[60] had considered the same problem with diffuse reflection for a gas of

hard spheres between two parallel plates, they solved the linearized Boltzmann equation numerically and found a modified critical $\overline{\beta}_c$ strongly dependent upon σ. Ytrehus[61] used the moment method to calculate the half-space problem for slightly strong condensation and the two-surface evaporation-condensation problem with a common condensation and evaporation coefficient $\sigma = 1$, and later[62] considered the condensation half-space problem with nonunity coefficient and diffuse reflection at the interphase. In the latter problem the special condition of a saturated state at infinity was assumed, and an inverted temperature profile for a modified critical $\overline{\beta}_c$ with σ-dependence similar to Sone *et al.* was found, i.e.

$$\overline{\beta}_c = 4.8 + 8\frac{1-\sigma}{\sigma} \tag{4.1}$$

A condensation coefficient less than 0.5 would be sufficient to avoid the inverted temperature gradient for water. In this chapter we have extended Ytrehus' solution to show the effect of the condensation coefficient on the two-surface evaporation-condensation problem, and in particular the inverted temperature gradient. The saturation condition at infinity is then not necessary. The critical parameter for the inverted temperature gradient still turns out to be identical to Eq.(4.1). Then, the condensation coefficient is calculated with molecular dynamics for a spherical symmetric model potential. The inverted temperature gradient phenomenon is predicted for this particular potential for temperatures close to the triple point, but it disappears at higher temperatures.

4.2 Half-space condensation

We consider a monatomic vapor at temperature T_∞ approaching its colder condensed phase at temperature T_L, assuming that a steady state has been reached. We assume a "slightly strong" flow process[63] such that

$$|S_\infty| = \frac{|u_\infty|}{\sqrt{2RT_\infty}} << 1 \tag{4.2}$$

where u_∞ is the bulk speed of the gas far from the interphase and $R = k/m$ is the gas constant per unit mass. The flow is divided into two regimes as shown in Fig. 4.1 : a Knudsen layer on the scale of the molecular mean free path λ next to the boundary, and an external Navier-Stokes region on the scale $\lambda/|S_\infty| >> \lambda$. It is further assumed that the flow is uniform far from the interphase, at given temperature T_∞ and pressure p_∞.

4.2.1 Navier-Stokes solution

In the Navier-Stokes region a perturbation solution to first order in the speed ratio S_∞ has been given[55],[64] :

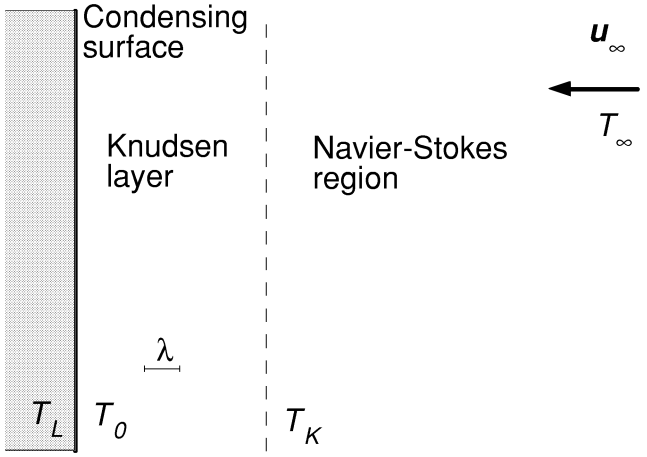

Figure 4.1: Sketch of the half-space problem

$$u = u_\infty \qquad p = p_\infty \tag{4.3}$$

The temperature satisfies the equation

$$\rho_\infty u_\infty c_p \frac{dT}{dx} = K \frac{d^2T}{dx^2} \tag{4.4}$$

where K is the thermal conductivity, which is regarded as a constant since $\frac{T_\infty - T_K}{T_\infty}$ is assumed to be of the order $|S_\infty| << 1$. For a monatomic gas, $c_p = \frac{5}{2}R$. The boundary conditions are

$$T(0) = T_K \qquad T(\infty) = T_\infty \tag{4.5}$$

where T_K is the temperature at the external edge of the Knudsen layer. The solution to Eq.(4.4) is

$$T - T_\infty = (T_K - T_\infty) \exp\left(\frac{\rho_\infty c_p u_\infty}{K} x\right) \tag{4.6}$$

There is a well-behaved solution for $u_\infty < 0$, i.e. only for condensation. For evaporation the matching is to be done directly between the Knudsen layer and the external equilibrium state[65]. The solution Eq.(4.6) was derived already by Plesset[66], although the matching to the Knudsen layer was missing.

4.2.2 Knudsen layer solution

In the Knudsen layer, an approximate solution of the Boltzmann equation (2.1) can be found in this case from the moment method[9],[16],[24],[61]. Assuming partial condensation and diffuse reflection of the molecules at the interphase, the boundary condition at the interphase is given by Eq.(2.4).

Outside the Knudsen layer, there is a Navier-Stokes region. An approximate form of the corresponding Chapman-Enskog distribution function is[4]

$$f_K = f_M(n_K, T_K, u_K) \cdot [1 - \Phi_1] \tag{4.7}$$

where

$$\Phi_1 = \frac{2\sqrt{2}}{5\sqrt{RT_K}} \frac{C_x}{\sqrt{2RT_K}} \left(\frac{C^2}{2RT_K} - \frac{5}{2} \right) \frac{K}{n_K k T_K} \frac{dT}{dx}_{|K} \tag{4.8}$$

and f_M is the local Maxwellian

$$f_M(n, T, u) = nF_M(T, u) = \frac{n}{(2\pi RT)^{3/2}} \exp\left(-\frac{(c_x - u)^2 + c_y^2 + c_z^2}{2RT} \right) \tag{4.9}$$

and $C_x = c_x - u_x$. The Navier-Stokes solution, Eq.(4.6), gives

$$\frac{dT}{dx}_{|K} = \frac{dT}{dx}_{|0} = (T_\infty - T_K) \frac{5}{2} R \frac{\rho_\infty |u_\infty|}{K} \tag{4.10}$$

The pressure from the Navier-Stokes solution is constant, hence the ideal gas equation of state gives $n_K k T_K = n_\infty k T_\infty$.

The order of magnitude of the correction Φ_1 in the distribution function is estimated as follows : $\frac{C_x}{\sqrt{2RT_K}} \sim 1$, we assume $\Delta\widehat{n}_K = \frac{n_K - n_L}{n_L}$ and $\Delta\widehat{T}_K = \frac{(T_K - T_L)}{T_L}$ are of order S_∞, and furthermore $S_\infty = \frac{u_\infty}{\sqrt{2RT_L}}$ is equal to $\frac{u_\infty}{\sqrt{2RT_K}}$ to first order. This gives for the perturbation Φ_1 in Eq.(4.7):

$$\Phi_1 \sim \frac{1}{\sqrt{2RT_K}} \frac{K}{n_\infty k T_\infty} (T_\infty - T_K) R \frac{\rho_\infty |u_\infty|}{K} = \frac{|u_\infty|}{\sqrt{2RT_K}} \frac{T_\infty - T_K}{T_\infty} \tag{4.11}$$

Hence $\Phi_1 \sim S_\infty^2$ and can be neglected. The distribution function at the edge of the Knudsen layer is therefore approximated by a drifting Maxwellian, which is next linearized around the reference Maxwellian at the interphase, $f_s = n_s F_s = f_M(n_s, T_L, 0)$,

$$\begin{aligned} f_K &= f_M(n_k, T_k, u_K) \\ &= f_M(n_s, T_L, 0) + \frac{\partial f_M}{\partial n}(n_K - n_s) + \frac{\partial f_M}{\partial T}(T_K - T_L) + \frac{\partial f_M}{\partial u} u_K \\ &= f_s \cdot \left[1 + \Delta\widehat{n}_K + \left(\frac{c^2}{2RT_L} - \frac{3}{2} \right) \Delta\widehat{T}_K + \frac{c_x u_\infty}{RT_L} \right] \\ &= f_s \cdot \left[1 + \Delta\widehat{p}_K + \left(\frac{c^2}{2RT_L} - \frac{5}{2} \right) \Delta\widehat{T}_K + \frac{c_x u_\infty}{RT_L} \right] \end{aligned} \tag{4.12}$$

where $u_K = u_\infty$ from the Navier-Stokes solution. We have furthermore introduced the nondimensional pressure difference $\Delta\widehat{p}_K$ across the Knudsen layer

$$\begin{aligned} \Delta\widehat{p}_K &= \frac{p_K - p_s}{p_s} = \frac{n_K T_K}{n_s p_s} - 1 \\ &= (1 + \Delta\widehat{n}_K)(1 + \Delta\widehat{T}_K) - 1 = \Delta\widehat{n}_K + \Delta\widehat{T}_K \end{aligned} \tag{4.13}$$

The factor $\Delta\widehat{n}_K \Delta\widehat{T}_K$ has been neglected, which is consistent with the linearization. Since the pressure is constant in the Navier-Stokes region, it also follows that

$$\Delta\widehat{p}_K = \frac{p_k - p_s}{p_s} = \frac{p_\infty - p_s}{p_s} = \Delta\widehat{p}_\infty \tag{4.14}$$

where $p_s = p_{sat}(T_L)$ is the saturation pressure.

A trimodal ansatz for the distribution function[9],[16],[61] is assumed in the Knudsen layer

$$f = a_0(x) f^+ + a_K^+(x) f_K^+ + (1 + \delta(x)) f_K^- \tag{4.15}$$

where f_K^+ and f_K^- are half range restrictions of f_K, Eq.(4.12), and by linearization $\delta(x)$ is assumed to be of order S_∞.

The boundary conditions for $a_0(x)$, $a_K^+(x)$ and $\delta(x)$ follow from Eq.(2.4) and the fact that at infinity $f = f_K$,

$$\begin{array}{lllll} x = 0: & a_0 = 1 & a_K^+ = 0 & \delta = \delta_0 \\ x = \infty: & a_0 = 0 & a_K^+ = 1 & \delta = 0. \end{array} \tag{4.16}$$

Here δ_0 is an unknown that must be obtained from the solution. $x = \infty$ is here at the end of the Knudsen layer. Terms of second order are dropped, and the distribution function for the incident molecules at the interphase is

$$\begin{aligned} f^-(0) &= (1 + \delta_0) f_K^- \\ &= n_s F_s^- \left[1 + \Delta\widehat{p}_\infty + \left(\frac{c^2}{2RT_L} - \frac{5}{2} \right) \Delta\widehat{T}_K + \frac{c_x u_\infty}{RT_L} + \delta_0 \right]. \end{aligned} \tag{4.17}$$

Here $f_s^- = n_s F_s^-$ is the usual half range restriction for $c_x < 0$. With the form of f^- known, the density in the reflected mode n_i can be calculated from Eq.(2.7)

$$n_i = n_s \left(-\sqrt{\pi} S_\infty + 1 + \Delta\widehat{p}_\infty - \frac{1}{2}\Delta\widehat{T}_K + \delta_0 \right) \tag{4.18}$$

The linearized form of the trimodal ansatz is therefore expressed as

$$\begin{aligned} f &= a_0(x) \left[\sigma_e + (1-\sigma_c) \left(-\sqrt{\pi} S_\infty + 1 + \Delta\widehat{p}_\infty - \frac{1}{2}\Delta\widehat{T}_K + \delta_0 \right) \right] f_s^+ \\ &\quad + a_K^+(x) \left[1 + \Delta\widehat{p}_\infty + \left(\frac{c^2}{2RT_L} - \frac{5}{2} \right) \Delta\widehat{T}_K + \frac{c_x u_\infty}{RT_L} \right] f_s^+ \\ &\quad + \left[1 + \Delta\widehat{p}_\infty + \left(\frac{c^2}{2RT_L} - \frac{5}{2} \right) \Delta\widehat{T}_K + \frac{c_x u_\infty}{RT_L} + \delta(x) \right] f_s^- \end{aligned} \tag{4.19}$$

The moment method is based on integrals in velocity space of the one dimensional, steady Boltzmann equation, Eq.(2.12), multiplied with a function $Q(\mathbf{c})$ of the molecular velocity $\mathbf{c}$.

$$\frac{d}{dx} \int c_x Q f d\mathbf{c} = \Delta\left[Q\right] \tag{4.20}$$

The continuity, x-momentum and energy equation follow from the collision invariants $Q = \left\{ m, mc_x, \frac{1}{2}mc^2 \right\}$, with the collision integral $\Delta\left[Q\right]$ then being zero, which leads to

$$\int c_x Q f d\mathbf{c} = const = \int c_x Q f_K d\mathbf{c} \tag{4.21}$$

i.e. the fluxes of the collision invariants are constant. The mass flux normalized with $mn_s\sqrt{\frac{RT_L}{2\pi}}$, reads in detail

$$\begin{aligned} &a_0(x) \left[\sigma_e + (1-\sigma_c) \left(1 + \delta_0 - \sqrt{\pi} S_\infty - \tfrac{1}{2}\Delta\widehat{T}_K + \Delta\widehat{p}_\infty \right) \right] \\ &+ a_K^+(x) \left[1 + \sqrt{\pi} S_\infty - \tfrac{1}{2}\Delta\widehat{T}_K + \Delta\widehat{p}_\infty \right] \\ &- \delta(x) - 1 + \sqrt{\pi} S_\infty + \tfrac{1}{2}\Delta\widehat{T}_K - \Delta\widehat{p}_\infty \\ &= 2\sqrt{\pi} S_\infty \end{aligned} \tag{4.22}$$

The momentum flux normalized with $mn_s RT_L$, reads

$$\begin{aligned} &a_0(x) \left[\sigma_e + (1-\sigma_c) \left(1 + \delta_0 - \sqrt{\pi} S_\infty - \tfrac{1}{2}\Delta\widehat{T}_K + \Delta\widehat{p}_\infty \right) \right] \\ &+ a_K^+(x) \left[1 + \tfrac{4}{\sqrt{\pi}} S_\infty + \Delta\widehat{p}_\infty \right] + \delta(x) - \tfrac{4}{\sqrt{\pi}} S_\infty = 1 + \Delta\widehat{p}_\infty \end{aligned} \tag{4.23}$$

The energy flux normalized with $2mn_s\sqrt{\frac{RT_L}{2\pi}}RT_L$, similarly reads

$$\begin{array}{l} a_0(x)\left[\sigma_e+(1-\sigma_c)\left(1+\delta_0-\sqrt{\pi}S_\infty-\frac{1}{2}\Delta\widehat{T}_K+\Delta\widehat{p}_\infty\right)\right] \\ +a_K^+(x)\left[1+\frac{5}{4}\sqrt{\pi}S_\infty+\frac{1}{2}\Delta\widehat{T}_K+\Delta\widehat{p}_\infty\right] \\ -1-\delta(x)+\frac{5}{4}\sqrt{\pi}S_\infty-\frac{1}{2}\Delta\widehat{T}_K-\Delta\widehat{p}_\infty \\ =\frac{5}{2}\sqrt{\pi}S_\infty \end{array} \tag{4.24}$$

Introducing the boundary conditions at the interphase, $x=0$, the state at the interphase is related to the state outside the Knudsen layer by the system

$$\sigma_e-\sigma_c\left(1+\delta_0-\sqrt{\pi}S_\infty-\frac{1}{2}\Delta\widehat{T}_K+\Delta\widehat{p}_\infty\right) = 2\sqrt{\pi}S_\infty \tag{4.25a}$$

$$\left.\begin{array}{l}\sigma_e-\sigma_c\left(1+\delta_0-\sqrt{\pi}S_\infty-\frac{1}{2}\Delta\widehat{T}_K+\Delta\widehat{p}_\infty\right) \\ +2\delta_0-\frac{1}{2}\Delta\widehat{T}_K-\left(\frac{4}{\sqrt{\pi}}+\sqrt{\pi}\right)S_\infty\end{array}\right\} = 0 \tag{4.25b}$$

$$\sigma_e-\sigma_c\left(1+\delta_0-\sqrt{\pi}S_\infty-\frac{1}{2}\Delta\widehat{T}_K+\Delta\widehat{p}_\infty\right)-\Delta\widehat{T}_K = \frac{9}{4}\sqrt{\pi}S_\infty \tag{4.25c}$$

This is a linear system of three equations and four variables δ_0, S_∞, $\Delta\widehat{T}_K$ and $\Delta\widehat{p}_\infty$. Hence only one parameter of these four can be chosen freely. The pressure difference $\Delta\widehat{p}_\infty$ is usually considered as the driving 'force' of the flow, and hence the remaining unknowns are expressed in terms of $\Delta\widehat{p}_\infty$.

$$\left[\begin{array}{lll}\frac{\sigma_c}{2} & -\sigma_c & \sqrt{\pi}(\sigma_c-2) \\ \frac{\sigma_c}{2}-\frac{1}{2} & -\sigma_c+2 & \sqrt{\pi}\sigma_c-\sqrt{\pi}-\frac{4}{\sqrt{\pi}} \\ \frac{\sigma_c}{2}-1 & -\sigma_c & \sqrt{\pi}(\sigma_c-\frac{9}{4})\end{array}\right]\cdot\left[\begin{array}{l}\Delta\widehat{T}_K \\ \delta_0 \\ S_\infty\end{array}\right]=\left[\begin{array}{l}\sigma_c\Delta\widehat{p}_\infty-\sigma_e+\sigma_c \\ \sigma_c\Delta\widehat{p}_\infty-\sigma_e+\sigma_c \\ \sigma_c\Delta\widehat{p}_\infty-\sigma_e+\sigma_c\end{array}\right] \tag{4.26}$$

The solution to the system reads

$$\left[\begin{array}{l}\Delta\widehat{T}_K \\ \delta_0 \\ S_\infty\end{array}\right]=\left[\begin{array}{l}\frac{1}{\overline{\beta}_c(\sigma_c)}\left[\Delta\widehat{p}_\infty+\Delta\widehat{\sigma}\right] \\ \frac{9\pi-32}{4\pi}\frac{1}{\overline{\beta}_c(\sigma_c)}\left[\Delta\widehat{p}_\infty+\Delta\widehat{\sigma}\right] \\ -\frac{4}{\sqrt{\pi}}\frac{1}{\overline{\beta}_c(\sigma_c)}\left[\Delta\widehat{p}_\infty+\Delta\widehat{\sigma}\right]\end{array}\right] \tag{4.27}$$

Here $\Delta\widehat{\sigma}$ has been introduced, the deviation between the condensation and evaporation coefficients :

$$\Delta\widehat{\sigma}=\frac{\sigma_c-\sigma_e}{\sigma_c} \tag{4.28}$$

and

$$\overline{\beta}_c(\sigma_c) = \beta_c + 8\frac{1-\sigma_c}{\sigma_c} \tag{4.29}$$

where β_c is a numerical factor, $\beta_c = \frac{9\pi+32}{4\pi} \approx 4.8$. In terms of $\Delta\widehat{T}_K$ the solution is easier:

$$\begin{bmatrix} \Delta\widehat{p}_\infty \\ \delta_0 \\ S_\infty \end{bmatrix} = \begin{bmatrix} \overline{\beta}_c(\sigma_c)\Delta\widehat{T}_K - \Delta\widehat{\sigma} \\ \frac{9\pi-32}{4\pi}\Delta\widehat{T}_K \\ -\frac{4}{\sqrt{\pi}}\Delta\widehat{T}_K \end{bmatrix} \tag{4.30}$$

The temperature of the gas at the interphase may be calculated from Eq.(4.30) and the standard definition of temperature. We have

$$T(0) = \frac{1}{3R}\frac{\int\left[(c_x^2-u_0)^2+c_y^2+c_z^2\right]\left[f^+ + (1+\delta_o)f_K^-\right]d\mathbf{c}}{\int\left[f^+ + (1+\delta_o)f_K^-\right]d\mathbf{c}}, \tag{4.31}$$

which yields in nondimensional form :

$$\frac{T(0)-T_L}{T_K-T_L} = \frac{(3\pi+8)}{6\pi}\frac{\sigma_c}{\sigma_e} \tag{4.32}$$

From this result we observe that the evaporation and condensation coefficients have an influence on the resulting temperature $T(0)$ only if the coefficients have different values. In the case of $\sigma_e = \sigma_c = \sigma$, the temperature becomes independent of that common value. As has been remarked before[24],[62], most of the temperature jump is over the interphase for weak transfer processes. We have in the special case of $\sigma_e = \sigma_c$ that $[T(0)-T_L]/[T_K-T_L] \approx 0.92$, and hence only 8 percent of the temperature change takes place in the gas phase.

The condensation mass flux follows from Eq.(4.27) :

$$\begin{aligned} J_m &= mn_s\sqrt{\frac{RT_L}{2\pi}}2\sqrt{\pi}S_\infty = -8mn_s\sqrt{\frac{RT_L}{2\pi}}\Delta\widehat{T}_K \\ &= -8mn_s\sqrt{\frac{RT_L}{2\pi}}\frac{1}{\overline{\beta}_c(\sigma_c)}\left[\Delta\widehat{p}_\infty + \Delta\widehat{\sigma}\right] \end{aligned} \tag{4.33}$$

where it is anticipated that the speed ratio S_∞ is negative since $u_\infty < 0$ for condensation.

For equilibrium, we have $\sigma_e = \sigma_c = \sigma$, and it is often assumed that the coefficients are also equal outside equilibrium and equal to the equilibrium value. Hence we assume from now on that $\Delta\widehat{\sigma}$ is of second order in S_∞, or smaller, so $\Delta\widehat{\sigma}$ can be neglected and $\overline{\beta}_c(\sigma_c)$ is replaced by $\overline{\beta}_c(\sigma)$ in Eqs.(4.27) and (4.30), where σ is assumed to be the equilibrium value.

From numerical simulation of the BKW and Boltzmann equations it has been inferred that two parameters in steady subsonic condensation can be fixed, for instance the temperature ratio between the gas and the liquid, and the pressure ratio or the velocity at infinity[21],[67], [68]. From the linearized moment solution above it seems as if there is only one free parameter, but remember that the Navier-Stokes solution left T_∞ unspecified. In this particular moment solution for slightly strong condensation, T_∞ does not influence the solution. This can be justified by noting that a nonlinear moment solution for condensation[24] for $\sigma = 1$ was only weakly dependent upon T_∞/T_L, and that this dependence disappeared in the limit of weak flow rate[55],[62].

In Ref.[62], half-space condensation was considered, and the state at infinity was assumed to be saturated('worst case'), and hence predictions for an inverted temperature gradient in the Navier-Stokes region could be made. Since the state at infinity is in general not saturated, we will refrain from this step here and rather look at the inverted temperature gradient in connection with the two-surface problem.

4.3 The two-surface problem

The flow in the gas region between two dense-phase surfaces, kept at slightly different temperatures with evaporation from one surface and condensation on the other, Fig. 4.2, can be found by matching two Knudsen layer solutions for evaporation and condensation, provided that $Kn = \frac{\lambda}{l} << 1$, where l is the distance between the surfaces and λ is a characteristic mean free path. In half-space evaporation, there is no external Navier-Stokes region, the Knudsen layer is to be matched directly to the external equilibrium flow[61],[65],[69].

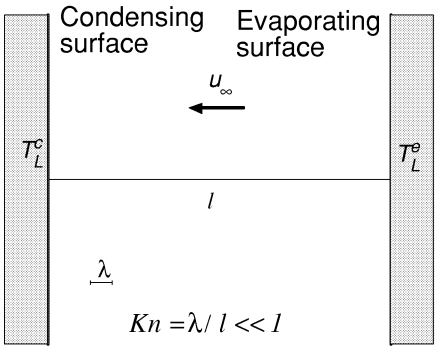

Figure 4.2: Two-surface geometry

The Chapman-Enskog distribution function at the edge of the Knudsen layer for condensation was linearized, resulting in a simple, drifting Maxwellian.

Hence the Knudsen layer equations for slightly strong evaporation and condensation are identical, as are the solution, Eq.(4.27), the temperature jump, Eq.(4.32) and the mass flux, Eq.(4.33).

Defining Δ reverse for evaporation, $\Delta\phi^e = \phi_L^e - \phi_K^e$, and taking into account that the plates are opposite to each other, the positive direction for velocity at the evaporating plate is opposite to that of the condensing plate, the Knudsen layer solutions for condensation and evaporation are as follows:

Condensation:

$$\begin{bmatrix} \Delta\widehat{T}_K^c \\ \delta_0^c \\ S_K^c \end{bmatrix} = \begin{bmatrix} \frac{1}{\beta_c}\Delta\widehat{p}_K^c \\ \frac{9\pi-32}{4\pi}\frac{1}{\beta_c}\Delta\widehat{p}_K^c \\ -\frac{4}{\sqrt{\pi}}\frac{1}{\beta_c}\Delta\widehat{p}_K^c \end{bmatrix} \tag{4.34}$$

Evaporation :

$$\begin{bmatrix} \Delta\widehat{T}_K^e \\ \delta_0^e \\ S_K^e \end{bmatrix} = \begin{bmatrix} \frac{1}{\beta_c}\Delta\widehat{p}_K^e \\ \frac{9\pi-32}{4\pi}\frac{1}{\beta_c}\left[-\Delta\widehat{p}_K^e\right] \\ -\frac{4}{\sqrt{\pi}}\frac{1}{\beta_c}\Delta\widehat{p}_K^e \end{bmatrix} \tag{4.35}$$

where $\Delta\widehat{p}_K^c = \frac{p_K^c - p_s^c}{p_s^c}$ and $\Delta\widehat{p}_K^e = \frac{p_s^e - p_K^e}{p_s^e}$.

Since the velocity is constant in the Navier-Stokes region for condensation, the velocities at the edge of the Knudsen layers for evaporation and condensation are to be matched, $S_K^e = S_K^c$. Hence

$$\Delta\widehat{p}_K^e = \Delta\widehat{p}_K^c \tag{4.36}$$

and furthermore

$$\Delta\widehat{T}_K^e = \Delta\widehat{T}_K^c \tag{4.37}$$

and

$$\delta_0^e = -\delta_0^c \tag{4.38}$$

The reference states at the interphases are per definition saturated, and the Clausius-Clapeyron equation[46] is valid :

$$\frac{dp}{dT} = \frac{Lp}{RT^2} \tag{4.39}$$

Here L is the latent heat per unit mass, which equals the difference in specific enthalpies in the gaseous and liquid states. We have assumed that the specific

volume of the dense phase is negligible compared to that in the vapor. The linearized version follows from approximating $\frac{dp}{dT}$ with $\frac{\Delta p}{\Delta T}$, which yields

$$\Delta\widehat{p} = \frac{L}{RT_L}\Delta\widehat{T} = \beta\Delta\widehat{T}, \tag{4.40}$$

where $\Delta\widehat{T} \equiv \frac{T_L^e - T_L^c}{T_L}$ and $\beta = \frac{L}{RT_L}$. The states are assumed to be so close that L can be considered constant, and any of the states may be used in the denominator of β, $\Delta\widehat{p}$ and $\Delta\widehat{T}$. The pressure is constant in the Navier-Stokes region, hence

$$\Delta\widehat{p} \equiv \frac{p_s^e - p_s^c}{p_s} = \Delta\widehat{p}_K^c + \Delta\widehat{p}_K^e = 2\Delta\widehat{p}_K^c \tag{4.41}$$

Here p_s is either p_s^e or p_s^c, to first order, the result is the same. The temperature jump over the two Knudsen layers together is $2\Delta\widehat{T}_K^c$, which can be related to the total temperature jump by using the Clausius-Clapeyron equation.

$$2\Delta\widehat{T}_K^c = \frac{2\Delta\widehat{p}_K^c}{\overline{\beta}_c(\sigma)} = \frac{\Delta\widehat{p}}{\overline{\beta}_c(\sigma)} = \frac{\beta}{\overline{\beta}_c(\sigma)}\Delta\widehat{T} \tag{4.42}$$

An inverted temperature profile in the Navier Stokes region is therefore predicted if $2\Delta\widehat{T}_K^c > \Delta\widehat{T}$, i.e. if

$$\beta > \overline{\beta}_c(\sigma) \tag{4.43}$$

This is identical to the condition Ytrehus[62] derived for an inverted temperature gradient in half-space weak condensation, with the upstream state at infinity assumed to be on the saturation curve.

As noted in Ref.[62], $\overline{\beta}_c(\sigma)$ is significantly larger than the ideal ($\sigma = 1$) value $\beta_c \approx 4.8$ if σ is considerably less than 1, say 0.5 or below, as is shown in Fig. 4.3. Sone *et al.*[60] considered the same two-plate problem for a gas of hard spheres. They solved the linearized Boltzmann equation numerically for arbitrary σ and obtained a critical parameter $\overline{\beta}_c(\sigma)$ for the inverted temperature gradient almost identical to our expression (4.29). The expression for $\overline{\beta}_c$, Eq.(4.29), with equal evaporation and condensation coefficients, may be written as

$$\overline{\beta}_c = \beta_c + 8\frac{1-\sigma}{\sigma} = \frac{\beta_c}{\sigma} + \frac{1-\sigma}{\sigma}\alpha_c \tag{4.44}$$

where $\beta_c = \frac{9\pi+32}{4\pi} \approx 4.80$ and $\alpha_c = \frac{23\pi-32}{4\pi} \approx 3.20$. The latter equality follows from the fact that $a_c + \beta_c = 8$. Sone *et al.* obtained the values $\beta_c \approx 4.70$ and $\alpha_c = \frac{23\pi-32}{4\pi} \approx 3.06$.

Let the saturation pressure be denoted $p_s = n_s k T_L$. The Clausius-Clapeyron equation can be used to show that the gas outside the evaporation Knudsen

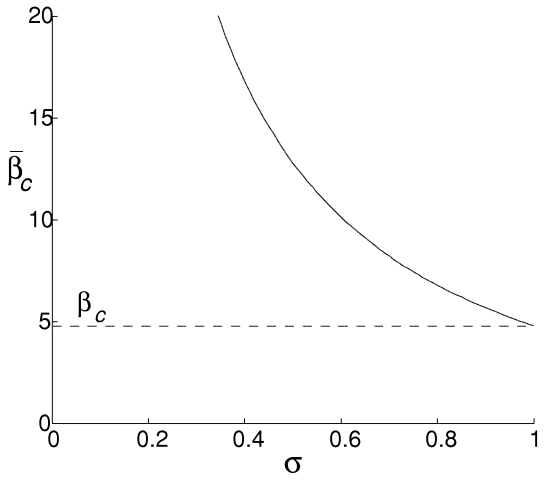

Figure 4.3: The inverted temperature gradient is predicted if $\beta = \frac{L}{RT_L}$ lies above the curve $\overline{\beta}_c(\sigma)$, for a given value of σ.

layer is supersaturated if $\beta > \overline{\beta}_c$. This is schematized in Fig.4.4, from which supersaturation is found to occur if

$$\Delta p_K^e < \beta \frac{p}{T} \Delta T_K^e, \tag{4.45}$$

which is equivalent to

$$\Delta \widehat{p}_K^e < \beta \Delta \widehat{T}_K^e \tag{4.46}$$

since $\beta \frac{p}{T}$ is the derivative of the vaporization curve. From $\Delta \widehat{p}_K^e = \overline{\beta}_c \Delta \widehat{T}_K^e$ follows the criterion for supersaturation :

$$\beta > \overline{\beta}_c \tag{4.47}$$

This could also have been seen directly by comparing Eq.(4.35) with the linearized Clausius-Clapeyron equation, Eq.(4.40). Expression (4.47) is identical to the criterion for the inverted temperature gradient phenomenon in two-plate geometry. This means that the gas has already been through a metastable state prior to a temperature inversion, as observed by Ytrehus[24] in the present case of $\sigma \neq 1$, and by Hermans and Beenakker[70] among others in the ideal case of $\sigma = 1$.

The mass flux across the gap follows from Eqs.(4.34) and (4.41).

$$J_m = m n_s \sqrt{\frac{RT_L}{2\pi}} 2\sqrt{\pi} S_K = 4 m n_s \sqrt{\frac{RT_L}{2\pi}} \frac{\Delta \widehat{p}}{\overline{\beta}_c(\sigma)} \tag{4.48}$$

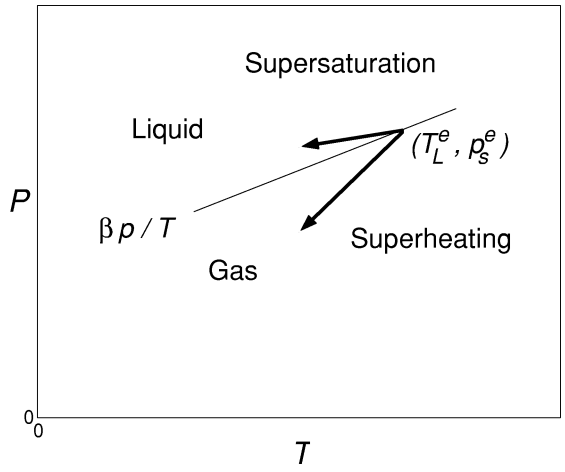

Figure 4.4: Part of the vaporization curve

where n_s can be n_s^c or n_s^e, T_L can be T_L^c or T_L^e, to first order, it does not matter which ones are used. As seen from this formula and from Fig.4.3, the mass flux is strongly dependent upon the value of σ through $\overline{\beta}_c(\sigma)$ in the denominator.

4.4 Equilibrium molecular dynamics simulation

In molecular dynamics, Newtons 2. law

$$\mathbf{F} = m\mathbf{a} \tag{4.49}$$

is solved numerically for every molecule in the system.

Here the Verlet method [40] has been used for a system of 1800 particles. The simulation is conducted in a rectangular box that is elongated in the x-direction, so the gas region can be relatively long with the number of liquid molecules limited. We are not interested in the dynamics in the liquid, and calculation of the trajectories of liquid molecules is computationally expensive since the liquid molecules have more neighbors than the gas molecules. But the interphase must be correctly reproduced, and this requires a liquid slab of say 10 molecular diameters thickness. A usual setup is a liquid slab in the middle of the simulation box surrounded by two gas regions, it is then easier to keep the liquid in place by for instance specifying that the center of mass is fixed. Other authors have constrained the liquid at a wall, using a short range potential which mimics the attractive forces that would be the result from a uniform liquid phase on the other side of the wall[71],[72], but then unphysical ordering near the wall makes it necessary to simulate a thicker liquid phase. In

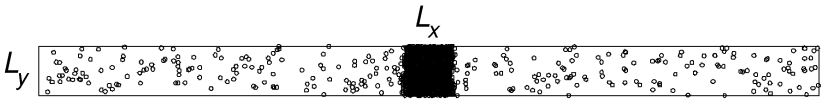

Figure 4.5: Simulation box for molecular dynamics

Fig.4.5, a snapshot of the configuration in an equilibrium simulation of 1800 molecules is shown for the case $L_x/L_y = 16$. L_z is not shown in the figure, but is equal to L_y and the simulation box has a quadratic cross-section.

The standard periodic boundary condition has been used in the simulations. Molecules that cross the box boundary are inserted on the opposite side with the same velocity, as though the simulation box were periodically replicated. A molecule interacts with periodic images of the other molecules if the distances are smaller than the cut-off distance of the potential.

In the middle of the liquid and at the far left and far right in the gas regions the temperature is thermostatted by simple velocity rescaling. Fluctuations of the center of mass of the liquid can be larger than the width of the interphase. Such behavior would 'smear out' density profiles, etc. Therefore the liquid slab is kept in the middle by shifting the x-coordinates, this does not change the relative distance between the molecules. The shifting is determined by the requirement that there shall be an equal number of molecules in both halves of the box. Particles that are moved outside of the x-boundaries in the centering algorithm are inserted on the opposite side with the same velocity.

4.4.1 Calculation of the condensation and evaporation coefficients

The evaporation and condensation coefficients are calculated from their definitions in terms of fluxes, as indicated in Fig.2.1. The definitions in terms of fluxes, as discussed in chapter 2.2, are

$$\sigma_e = \frac{J^e}{J_s} \tag{4.50}$$

$$\sigma_c = \frac{J^c}{J^-} \tag{4.51}$$

Here $J_s = \int\limits_{c_x>0} n_s F_s dc_x = n_s\sqrt{\frac{RT_L}{2\pi}}$, J^e is the evaporated flux, J^c is the condensation flux, and J^- is the incident flux on the gas boundary.

To determine if the criterion for the inverted temperature gradient is violated, the parameter $\beta = \frac{L}{RT_L} = \frac{\Delta h}{RT_L}$ must be calculated. The enthalpy difference is defined as $\Delta h = h_g - h_l$, where h_g and h_l are the specific enthalpies in the gas and liquid respectively. The specific enthalpy is calculated from the molecular dynamics simulation as

$$h = u_p + 3/2RT + p/\rho \tag{4.52}$$

Here u_p is the internal potential energy, and ρ is the mass density. Some results from equilibrium simulations are listed in Table 4.1 and are shown graphically in Fig.4.6 together with results of Røsjorde *et al.*[73], and Tsuruta's results for a Lennard-Jones potential, cut at $3.5r_0$ (private communication).

To calculate $\overline{\beta}_c(\sigma)$, an average of σ_e and σ_c has been used. An inverted temperature profile and supersaturation outside the evaporating boundary is predicted for weak flow conditions if $\frac{L}{RT_L} > \overline{\beta}_c(\sigma)$. The $\overline{\beta}_c(\sigma)$ curve crosses the $\frac{L}{RT_L}$ curve for $\sigma \approx 0.75$. From Table 4.1 it is seen that $L/(RT_L)$ and σ are monotone decreasing functions of T^*, and hence for the Lennard-Jones-spline fluid in our simulations, the $\frac{L}{RT_L} > \overline{\beta}_c(\sigma)$ condition is fulfilled, and hence an inverted temperature gradient is predicted, for $T^* \precsim 0.61$.

From Table 4.1 we see that the evaporation and condensation coefficients are equal, as they should be in equilibrium, and their values decrease with increasing temperature. The degree of rarefaction can be expressed by δ/d_{eff}, where δ is the mean molecular spacing, $\delta = n^{-1/3}$, and d_{eff} is an effective hard sphere molecular diameter, here defined from the mean free path at infinity,

$$\lambda_\infty = \frac{1}{\sqrt{2}n_\infty \pi d_{eff}^2}. \tag{4.53}$$

Bird[23] uses $\delta/d_{eff} > 7$ as a limit for dilute gas as discussed at the end of chapter 3.2. For our Lennard-Jones-spline potential, this limit is actually never attained for the gas in two-phase gas-liquid equilibrium. In our simulations the maximum value of δ/d_{eff} was 3.9, and a comparison with results from gas-kinetic calculations must therefore be interpreted with caution.

4.4.2 Comparison with other MD simulations of the condensation coefficient for spherically symmetric molecules

Values for the condensation coefficient for the ordinary Lennard-Jones potential used by most authors, and from the Lennard-Jones-spline potential we have used in our simulations, are not directly comparable since many physical characteristics, for instance the saturation density, deviate significantly for the same value of T^*. Besides, since there is no unique microscopic definition of evaporation

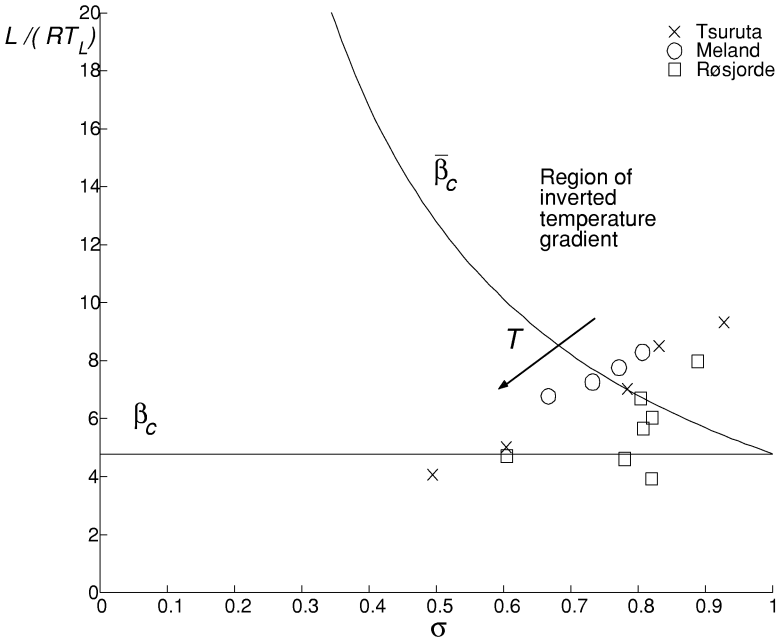

Figure 4.6: Plot of normalized latent heat vs. condensation coefficient from various molecular dynamics simulations; our own, Røsjorde et al.[73] and Tsuruta(private communication). For our own and Tsuruta's simulations, both σ and the normalized latent heat are monotone decreasing functions of the temperature, as shown by the arrow.

and condensation of a single molecule, different approaches used by the various authors contribute to a spread in the simulated values of the condensation coefficient.

Røsjorde *et al.*[73] used the same Lennard-Jones-spline potential as in this study. The resistivity to mass transfer was measured in simulations of weak condensation. An expression for the resistivity to mass transfer involving the condensation coefficient has been derived[52],[74] by comparing expressions for weak heat and mass transfer from kinetic theory and from irreversible thermodynamics. From the measured values of resistivity to mass transfer it was then possible to calculate the condensation coefficient. Røsjorde *et al.*[73] found values of the condensation coefficient scattered around $\sigma = 0.82$. It should be remarked that their 'surface temperature' is not calculated at a specific position as our T_L, but is calculated as an average over molecules in a suitably defined interphase region. Since there is a lot more molecules on the liquid side of the surface region than on the gas side, we conclude that their surface temperature deviates little from our T_L, and in the figure 4.6 they are treated as equal.

Yasuoka and Matsumoto[76] used the Lennard-Jones potential with cut-off

T^*	σ_c	σ_e	$\frac{L}{RT_L}$	$\overline{\beta}_c(\sigma)$	δ/d_{eff}
0.575	0.81	0.80	8.3	6.7	3.9
0.6	0.77	0.77	7.7	7.2	3.5
0.625	0.73	0.73	7.2	7.7	3.1
0.65	0.67	0.67	6.8	8.8	2.9

Table 4.1: Results for equilibrium simulations

at $4.4r_0$ and simulated two-phase coexistence in equilibrium. Their 'coefficient of self-condensation' corresponds to our condensation coefficient. Yasuoka and Matsumoto looked at the depletion of molecules initially in the gas that have not condensed and related the rate of depletion to the condensation coefficient. For $T^* = 0.67$ and $T^* = 0.83$ the values for the condensation coefficient were 0.85 and 0.88, respectively. Their results are not plotted in Fig.4.6 since values for the latent heat are not available.

Tsuruta[77] used the Lennard-Jones potential, cut at $3.5r_0$. For $T^* = 0.70$ and $T^* = 0.85$ the values for the condensation coefficient were reported to be 0.93 and 0.79, respectively. Values for the normalized latent heat were not given in the article but has been obtained through a private communication. Corresponding values for σ and $\frac{L}{RT_L}$ have been plotted together with our results in Fig.4.6. Although the intermolecular potential Tsuruta used is not the same as ours, the σ versus $\frac{L}{RT_L}$ values do not differ significantly. The two sets of data lead essentially to the same general conclusion, namely that an inverted temperature gradient may occur at low temperatures close to the triple point, but not for higher temperatures.

4.5 Conclusion

The inverted temperature gradient phenomenon is critically dependent upon the value of the condensation coefficient for the given substance. If gas-kinetic predictions can be applied to the slightly non-ideal gas in our molecular dynamics simulations, then the inverted temperature gradient phenomenon is predicted to occur for temperatures close to the triple point. To verify this result, direct molecular dynamics simulations of the two-plate geometry for weak flow conditions, and carefully designed experiments, are therefore required to see if the inverted temperature phenomenon really occurs. The very basis of kinetic theory applied to interphase transfer, the assumed form of the distribution function at the interphase, must also be checked from molecular dynamics simulations, before the final word can be said on the inverted temperature gradient.

Chapter 5

Molecular Exchange

5.1 Introduction

When a molecule condenses, potential energy is converted into kinetic energy which is dissipated by collisions. There is then the possibility that a condensing molecule may kick out a molecule in the interphase or in the liquid, Matsumoto[78] calls this effect 'molecular exchange'. Matsumoto reported a strong correlation between condensation and evaporation fluxes and introduced a redefined condensation coefficient taking molecular exchange into account. The redefined condensation coefficient was calculated from molecular dynamics simulations for several substances and a considerable number of papers was published[79],[80],[81], [82]. Since the redefined condensation coefficient always is equal to or smaller than the original definition of the coefficient, it was thought that the molecular exchange mechanism might remove the seemingly unphysical inverted temperature gradient phenomenon predicted by gas-kinetic calculations,[50],[51],[62].

However, the simulation expression Matsumoto *et al.* used, appears to be erroneous, it has inconsistent dimensions. In this paper it is shown that molecular exchange, under suitable assumptions, has no influence on the gas-kinetic treatment of phase change, but anyway, a correlation expression for the fraction of condensing molecules that induces molecular exchange is derived.

5.2 Molecular exchange

In this chapter the notation for the fluxes is a bit different than in the rest of the thesis. In addition to the averaged values of the fluxes, instantaneous values are also required. Hence J is here instantaneous flux and $\langle J \rangle$ is the averaged flux. Eqs.(2.7) and (2.10) can then be written

$$n_i = \langle J^- \rangle / \sqrt{\frac{RT_L}{2\pi}} \tag{5.1}$$

$$\sigma_e = \frac{\langle J^e \rangle}{J_s} \tag{5.2}$$

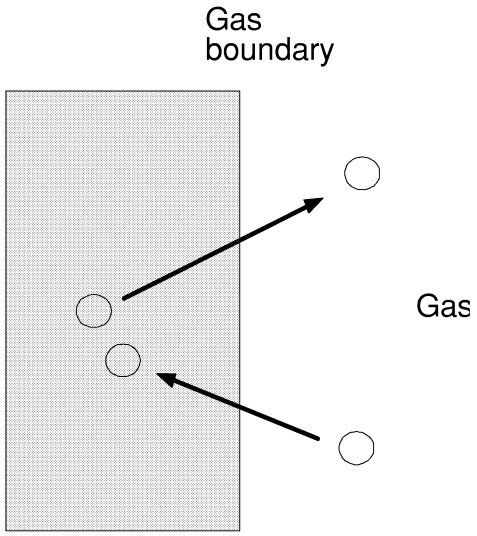

Figure 5.1: Molecular exchange mechanism

Molecular exchange is modeled by assuming that certain molecules that condense, kick out one molecule each from the liquid or the interphase, as indicated in Fig. 5.1. The evaporation and condensation fluxes are hence split into two modes, taking molecular exchange into account.

$$J^e = J^e_{effective} + J^e_{induced} \tag{5.3}$$

$$J^c = J^c_{effective} + J^c_{inducing} \tag{5.4}$$

The subscripts have been written out here to ease the interpretation of the various fluxes. $J^e_{effective}$ is the "true" evaporation flux, independent of the incoming flux. $J^e_{induced}$ is the evaporation flux due to molecular exchange which depends on the incoming flux. $J^c_{effective}$ is the flux of molecules condensing which is not inducing molecular exchange. $J^c_{inducing}$ is the flux of the condensing molecules inducing molecular exchange. The averaged fluxes $\langle J^e_{induced} \rangle$ and $\left\langle J^c_{inducing} \right\rangle$ are equal and opposite since it has been assumed that each condensing molecule

which excites molecular exchange, only excites one molecule to evaporate. The common value is denoted by $\left\langle J^{exchange}\right\rangle$ or short $\langle J^{ex}\rangle$, $J_{effective}$ will be written J_{eff} henceforth.

$$\langle J^e_{induced}\rangle = \left\langle J^c_{inducing}\right\rangle = \langle J^{ex}\rangle \tag{5.5}$$

The 'effective' index in Eq.(5.3) is hence appropriate since $\left\langle J^c_{inducing}\right\rangle$ and $\langle J^e_{induced}\rangle$ cancel each other, they do not contribute to the net flux. Matsumoto[78] defined an effective condensation coefficient taking molecular exchange into account, in our notation it can be written as

$$\sigma_c' = \frac{\left\langle J^c_{eff}\right\rangle}{\langle J^-\rangle} = \sigma_c - \frac{\left\langle J^c_{inducing}\right\rangle}{\langle J^-\rangle} = \sigma_c - \frac{\langle J^{ex}\rangle}{\langle J^-\rangle} \tag{5.6}$$

The effective condensation coefficient is equal to or smaller than the original condensation coefficient. We extend Matsumoto's treatment by also defining a new evaporation coefficient. The new one, not counting the induced evaporated molecules, is

$$\sigma_e' = \frac{\left\langle J^e_{eff}\right\rangle}{J_s} = \sigma_e - \frac{\langle J^e_{induced}\rangle}{J_s} = \sigma_e - \frac{\langle J^{ex}\rangle}{J_s} \tag{5.7}$$

If there is no molecular exchange then $\sigma_c = \sigma_c'$ and $\sigma_e = \sigma_e'$.

The molecular exchange flux may be written in two ways,

$$\langle J^{ex}\rangle = \langle J^c\rangle - \left\langle J^c_{eff}\right\rangle = (\sigma_c - \sigma_c')\left\langle J^-\right\rangle \tag{5.8a}$$

$$\langle J^{ex}\rangle = \langle J^e\rangle - \left\langle J^e_{eff}\right\rangle = (\sigma_e - \sigma_e')J_s \tag{5.8b}$$

We will now show that the gas-kinetic treatment of phase change is unaffected by molecular exchange, if we do the assumption that the molecular exchange molecules are emitted from the interphase with a half-Maxwellian distribution with the liquid temperature T_L. At the interphase one more mode for the evaporated molecular exchange molecules must be added, a half-Maxwellian with unknown number density n'. As will be shown later, it is convenient to extract the factor $(\sigma_e - \sigma_e')$.

$$f^{ex} = (\sigma_e - \sigma_e')n'F_s \tag{5.9}$$

n' is determined from a flux condition

$$(\sigma_e - \sigma_e')\int\limits_{c_x>0} n'F_s d\mathbf{c} = (\sigma_e - \sigma_e')n'\sqrt{\frac{RT_L}{2\pi}} = (\sigma_e - \sigma_e')J_s \tag{5.10}$$

The last equality follows from Eq.(5.8b). Here $J_s = n_s\sqrt{\frac{RT_L}{2\pi}}$, hence $n' = n_s$ and

$$f^{ex} = (\sigma_e - \sigma_e')n_s F_s \tag{5.11}$$

The evaporation distribution is

$$\begin{aligned} f^e &= f^e_{eff} + f^{ex} \\ &= \sigma_e' n_s F_s + (\sigma_e - \sigma_e')n_s F_s = \sigma_e n_s F_s \end{aligned} \tag{5.12}$$

as though molecular exchange was not present. The complete distribution function at the interphase is

$$\begin{aligned} f^+ &= \sigma_e' n_s F_s + (\sigma_e - \sigma_e^{'})n_s F_s + (1-\sigma_c)n_i F_s \\ &= \left[\sigma_e n_s + (1-\sigma_c)n_i\right] F_s \end{aligned} \tag{5.13}$$

Eq.(5.13) is identical to Eq.(2.4). Hence, molecular exchange, if it exists, has no effect upon the kinetic theory results, for instance mass flux formulas are unaltered.

The distribution for the evaporated molecular exchange molecules can also be written as

$$f^{ex} = (\sigma_c - \sigma_c^{'})n'' F_s \tag{5.14}$$

Here n'' is determined from the following flux condition

$$(\sigma_c - \sigma_c^{'}) \int\limits_{c_x>0} n'' F_s d\mathbf{c} = (\sigma_c - \sigma_c^{'})n''\sqrt{\frac{RT_L}{2\pi}} = (\sigma_c - \sigma_c^{'})\left\langle J^- \right\rangle \tag{5.15}$$

The last equality follows from Eq.(5.8a). Hence

$$n''\sqrt{\frac{RT_L}{2\pi}} = \left\langle J^- \right\rangle \tag{5.16}$$

Comparing with Eq.(2.7), it is seen that $n'' = n_i$.

The complete distribution function at the interphase can be written as

$$\begin{aligned} f^+ &= \sigma_e' n_s F_s + (\sigma_c - \sigma_c')n_i F_s + (1-\sigma_c)n_i F_s \\ &= \left[\sigma_e' n_s + (1-\sigma_c')n_i\right] F_s \end{aligned} \tag{5.17}$$

The distribution function is similar to Eq.(2.4) without molecular exchange, the only difference is that σ_c is replaced by σ_c' and σ_e by σ_e'. This description of molecular exchange is equivalent to Eq.(5.13), but as we will see later, it is much harder to calculate σ_e' and σ_c' than σ_e and σ_c, hence the redefined coefficients taking molecular exchange into account should not be used in the boundary condition.

5.3 Molecular dynamics simulation expression

We will now derive an expression for the fraction of condensing molecules that induces molecular exchange. First we look at the induced evaporation flux. There is a time delay before gas molecules crossing the gas boundary can excite 'molecular exchange molecules' in the interphase or the liquid and those molecules cross the gas boundary. The most general linear relationship between the instantaneous flux $J^e_{induced}$ and the incoming numberflux J^- outside the interphase is assumed

$$J^e_{induced}(t) = \int_0^\infty \alpha(t^{'}) J^-(t-t')dt' \tag{5.18}$$

$\alpha(t')$ is the so-called memory function. Hence the average of Eq.(5.3) can be written as

$$\langle J^e \rangle = \langle J^e_{eff} \rangle + \int_0^\infty \alpha(t^{'}) \langle J^-(t-t') \rangle \, dt' \tag{5.19}$$

Equilibrium is not assumed, it is only necessary that macroscopic values are stationary, i.e. may have net condensation or evaporation. We want to find an expression for the memory function so that $\langle J^e_{induced} \rangle$ can be calculated. Substraction of Eq.(5.3) with Eq.(5.19) gives

$$\Delta J^e(t) = \Delta J^e_{eff}(t) + \int_0^\infty \alpha(t^{'}) \Delta J^-(t-t')dt' \tag{5.20}$$

Here Δ means deviation from the average. Then Eq.(5.20) is multiplied by $\Delta J^-(t_1)$ and averaged, here $t_1 < t$.

$$\begin{aligned} \langle \Delta J^-(t_1) \Delta J^e(t) \rangle &= \langle \Delta J^-(t_1) \Delta J^e_{eff}(t) \rangle \\ &\quad + \int_0^\infty \alpha(t^{'}) \langle \Delta J^-(t_1) \Delta J^-(t-t') \rangle \, dt' \end{aligned} \tag{5.21}$$

The fluxes $J^-(t_1)$ and $J^e_{eff}(t)$ should be uncorrelated since the flux-dependent part of the evaporation flux is $J^e_{induced}$. Hence

$$\langle \Delta J^-(t_1) \Delta J^e_{eff}(t) \rangle = 0 \tag{5.22}$$

In Eq.(5.21), $t = t_1 + \delta t$ is introduced

$$\langle \Delta J^-(t_1) \Delta J^e(t_1+\delta t) \rangle = \int_0^\infty \alpha(t^{'}) \langle \Delta J^-(t_1) \Delta J^-(t_1+\delta t-t') \rangle \, dt' \tag{5.23}$$

It is assumed that the fluctuations of the incoming flux J^- have a correlation time τ which is small compared to the time it takes before $\alpha(t')$ is significantly different from 0. Hence $\langle \Delta J^-(t_1)\Delta J^e(t_1+\tau)\rangle \approx 0$ and we can assume that $\delta t >> \tau$ in the subsequent discussion. We model the autocorrelation function inside the integral as a Gaussian curve.

$$\left\langle \Delta J^-(t_1)\Delta J^-(t_1+\delta t-t')\right\rangle = \left\langle \Delta J^-\Delta J^-\right\rangle e^{-\left(\frac{t'-\delta t}{2\tau/\sqrt{\pi}}\right)^2} \tag{5.24}$$

The actual form of the autocorrelation function is not important, any function that is 1 if $\delta t = t'$ and gets narrower as τ gets smaller can be used as long as it is properly normalized. The expression for the autocorrelation function must be consistent with a common definition of the correlation time[83],

$$\tau = \int_0^\infty \frac{\langle \Delta J^-(0)\Delta J^-(t)\rangle}{\langle \Delta J^-\Delta J^-\rangle} dt. \tag{5.25}$$

Then Eq.(5.23) becomes

$$\left\langle \Delta J^-(t_1)\Delta J^e(t_1+\delta t)\right\rangle = \left\langle \Delta J^-\Delta J^-\right\rangle \int_0^\infty \alpha(t')e^{-\left(\frac{t'-\delta t}{2\tau/\sqrt{\pi}}\right)^2} dt' \tag{5.26}$$

Since $e^{-\left(\frac{t'-\delta t}{2/\sqrt{\pi}\tau}\right)^2}$ is a very narrow function centered on δt, there will be no significant contribution to the integral outside a couple of τ's distance from δt. $\alpha(t')$ varies little over τ and may hence be approximated with a Taylor expansion.

$$\alpha(t') \approx \alpha(\delta t) + \alpha'(\delta t)\,(t'-\delta t) \tag{5.27}$$

The first term gives an integral

$$\int_0^\infty e^{-\left(\frac{t'-\delta t}{2\tau/\sqrt{\pi}}\right)^2} dt' = \tau + \mathrm{erf}\left(\frac{\delta t}{2\tau/\sqrt{\pi}}\right)\tau \tag{5.28}$$

τ is assumed to be small, $\delta t >> \tau$, hence $\mathrm{erf}\left(\frac{\delta t}{2\tau/\sqrt{\pi}}\right) \approx 1$ and we have

$$\int_0^\infty e^{-\left(\frac{t'-\delta t}{2\tau/\sqrt{\pi}}\right)^2} dt' \approx 2\tau \tag{5.29}$$

Then Eq.(5.26) simplifies to

$$\left\langle \Delta J^-(t_1)\Delta J^e(t_1+\delta t)\right\rangle = \left\langle \Delta J^-\Delta J^-\right\rangle \left[2\tau\alpha(\delta t) + \frac{2\tau^2}{\pi}e^{-\left(\frac{\delta t}{2\tau/\sqrt{\pi}}\right)^2}\alpha'(\delta t)\right] \tag{5.30}$$

Since $\tau << \delta t$, we have $e^{-\left(\frac{\delta t}{2\tau/\sqrt{\pi}}\right)^2} \approx 0$, hence the last term in Eq.(5.30) may be neglected and

$$\left\langle \Delta J^-(t_1)\Delta J^e(t_1+\delta t)\right\rangle = 2\tau\alpha(\delta t)\left\langle \Delta J^-\Delta J^-\right\rangle \tag{5.31}$$

This result is equivalent to the correlation function $\langle \Delta J^-(t_1)\Delta J^-(t_1+\delta t-t')\rangle$ written as

$$\left\langle \Delta J^-(t_1)\Delta J^-(t_1+\delta t-t')\right\rangle = 2\tau\left\langle \Delta J^-\Delta J^-\right\rangle \delta(t'-\delta t), \tag{5.32}$$

then Eq.(5.31) follows directly from Eq.(5.23). The purpose of introducing Eq.(5.24) was to calculate the prefactor 2τ in Eq.(5.32). The Dirac delta function in Eq.(5.32) physically means that we have a finite autocorrelation concentrated over a correlation time τ much shorter than all the other relevant timescales of the problem.

Matsumoto *et al.*[78][79],[80],[81],[82] apparently used

$$\left\langle \Delta J^-(t_1)\Delta J^-(t_1+\delta t-t')\right\rangle = \left\langle \Delta J^-\Delta J^-\right\rangle \delta(t'-\delta t) \tag{5.33}$$

The only explicit statement of Eq.(5.33) in the many papers of Matsumoto *et al.* can be found in Ref.[85]. The dimensions in this equation are not consistent since the dimension of a δ-function is the inverse of the dimension of its argument[84].

As has been remarked before, the actual representation of the correlation function used in Eq.(5.24) does not matter. For instance, it is straightforward to show that $e^{-|t'-\delta t|/\tau}$ also gives Eq.(5.31). From Eq.(5.31), an expression for the memory function $\alpha(t')$ follows

$$\alpha(t') = \frac{1}{2\tau}\frac{\langle \Delta J^-(t_1)\Delta J^e(t_1+t')\rangle}{\langle \Delta J^-\Delta J^-\rangle} \tag{5.34}$$

The induced evaporation flux follows from averaging Eq.(5.18). Since the system is stationary, t_1 is arbitrary and is set to 0.

$$\langle J^e_{induced}\rangle = \left\langle J^-\right\rangle \int_0^\infty \alpha(t')dt' = \frac{\langle J^-\rangle}{2}\frac{\int_0^\infty \langle \Delta J^-(0)\Delta J^e(t')\rangle\, dt'}{\int_0^\infty \langle \Delta J^-(0)\Delta J^-(t')\rangle\, dt'} \tag{5.35}$$

Here τ has been replaced, using Eq.(5.25). Since the correlation time τ associated with $\langle \Delta J^-(0)\Delta J^-(t')\rangle$ is much smaller than the relevant time-scale for $\langle \Delta J^-(0)\Delta J^e(t')\rangle$, $\langle \Delta J^-(0)\Delta J^-(t')\rangle$ and hence τ should be calculated with shorter sampling intervals than is necessary for $\langle \Delta J^-(0)\Delta J^e(t')\rangle$. The fraction

of condensing molecules that induces molecular exchange, using Eq.(5.5), is

$$\frac{\left\langle J^c_{inducing} \right\rangle}{\langle J^c \rangle} = \frac{1}{2\sigma_c} \frac{\int_0^\infty \langle \Delta J^-(0) \Delta J^e(t') \rangle \, dt'}{\int_0^\infty \langle \Delta J^-(0) \Delta J^-(t') \rangle \, dt'} \tag{5.36}$$

Here $\sigma_c = \langle J^c \rangle / \langle J^- \rangle$ is the average condensation probability, i.e. the condensation coefficient. The expression (5.36) is suitable for molecular dynamics simulation.

The effective condensation coefficient can be written as

$$\begin{aligned} \sigma_c' &= \frac{\left\langle J^c_{eff} \right\rangle}{\langle J^- \rangle} = \sigma_c - \frac{\left\langle J^c_{inducing} \right\rangle}{\langle J^- \rangle} \\ &= \sigma_c - \frac{1}{2} \frac{\int_0^\infty \langle \Delta J^-(0) \Delta J^e(t') \rangle \, dt'}{\int_0^\infty \langle \Delta J^-(0) \Delta J^-(t') \rangle \, dt'} \end{aligned} \tag{5.37}$$

A similar formula for σ_e' can be given using Eqs.(5.7) and (5.35). Matsumoto *et al.* used

$$\sigma_c' = 1 - \frac{1}{\left\langle (\Delta J^-)^2 \right\rangle} \int_0^\infty \langle \Delta J^-(0) \Delta J^+(t') \rangle \, dt' \tag{5.38}$$

where J^+ is the total flux out from the interphase, the sum of the total evaporation and reflection fluxes. Eqs.(5.37) and (5.38) are not directly comparable, but the dimensions in Matsumoto's expression obviously are not consistent, σ_c' is dimensionless but the last term in Eq.(5.38) has dimension of time. Hence, the values Matsumoto *et al.* found for the condensation coefficient in Refs.[78][79],[80],[81],[82] seem to be not correct.

5.4 Conclusion

If the molecular exchange mode is assumed to be the standard non-drifting half Maxwellian with the liquid temperature, molecular exchange has no effect on the gas-kinetic description of evaporation and condensation, the boundary condition outside the interphase is not altered by the inclusion of the exchange mechanism. The fraction of condensing molecules that kick out another molecule can be calculated in molecular dynamics simulations from the correlation between the incident flux and the evaporation flux.

Acknowledgement 1 *Financial support from the Norwegian Council of Research is gratefully acknowledged. I wish to thank Professor Skullerud for stimulating discussions.*

Chapter 6

Strong Evaporation

6.1 Introduction

The nonlinear case of strong evaporation for sonic conditions downstream was considered in a moment solution by Anisimov[9]. Ytrehus[16] extended the moment solution to arbitrary subsonic Mach numbers and calculated the structure of the Knudsen layer. Finite difference solutions of the BKW equation and Monte Carlo simulations of strong evaporation further clarified the field. Yen[86] showed that the type of kinetic equation or intermolecular potential had little influence on properties like the density ratio, pressure ratio and mass flux. Murakami [53] showed that evaporation into vacuum gave a maximum Mach number of unity. Sone *et al.*[87] and Kogan and Abramov [68] clarified the existence region for steady evaporation in a half-space.

Experimental results on the temperature profile in the evaporation Knudsen layer is very limited, but Mager *et al.*[88] considered sublimation of solid iodine into a low-density environment. The effect of non-unity evaporation and condensation coefficients for diffuse reflection was considered by Kogan[89], Sone and Sugimoto[90] and by Ytrehus[24]. There have been many attempts to measure the condensation coefficient for various substances, but this appears to be an extremely difficult task, for instance, values for the condensation coefficient for water at a given temperature vary by a factor of 10, see recent reviews[1],[10]. The majority of the kinetic theory results rest upon the assumption that the gas is monatomic, or that internal degrees of freedom do not play any important role. Incorporation of polyatomic effects have been considered by Cercignani[91] and by Frezzotti[92].

Away from the critical point, the interphase between gas and its condensed phase is typically a couple of molecular diameters thick, and molecular dynamics (MD) simulation[37] can resolve this region. Tsuruta[93] used molecular dynamics to simulate stationary evaporation and condensation between two liquid slabs kept at different temperatures. Zhakhovskii and Anisimov[94] simulated evaporation into vacuum by removing all molecules that left the gas region of

the simulation cell, i.e. a completely absorbing wall.

In this chapter only evaporation into an infinite half-space will be considered. At asymptotically large distances from the interphase the flow parameters are assumed to reach uniform values. The Boltzmann equation Eq.(2.1), together with Eq.(2.4) at the interphase and a drifting Maxwellian $n_\infty F_M(T_\infty, u_\infty)$ at infinity as boundary conditions, have been solved by a variety of methods. From physical arguments[16] and numerical simulations[68],[95] of the BKW and Boltzmann equations for $\sigma = 1$, it has been inferred that only one downstream parameter in steady evaporation can be fixed, for instance the velocity at infinity or the pressure ratio between the gas and the liquid. As will be shown later, nonunity condensation coefficient with diffusive reflection leads only to a stretch of the Knudsen layer in the x-direction, and the general predictions for $\sigma = 1$ holds also for $\sigma \neq 1$.

6.2 Moment solution for evaporation for $\sigma_e \neq \sigma_c$

Ytrehus[16] extended Anisimov's moment solution[9] to arbitrarily Mach number below 1 and calculated the structure of the Knudsen layer for Maxwell molecules by adding an equation for the non-conserved moment $\Psi = mc_x^2$. The original work was for $\sigma = 1$, but Ytrehus later extended the solution to equal condensation and evaporation coefficients by means of a transformation[24]. Here the moment solution will be calculated directly for $\sigma_e \neq \sigma_c$. An approximate form of the distribution function is chosen with a few adjustable parameters determined by the boundary conditions and four moment equations. Using Anisimov's and Ytrehus' ansatz

$$\begin{aligned} f &= a_0(x) f^+ + a_\infty^+(x) n_\infty F_\infty^+ + a_\infty^-(x) n_\infty F_\infty^- \\ &= a_0(x) \left[\sigma_e n_s + (1-\sigma_c) n_i\right] F_s^+ + a_\infty^+(x) n_\infty F_\infty^+ + a_\infty^-(x) n_\infty F_\infty^- \end{aligned} \quad (6.1)$$

the boundary conditions can be written as[16]

$$\begin{aligned} a_0(0) &= 1 \qquad a_0(\infty) = 0 \\ a_\infty^+(0) &= 0 \qquad a_\infty^+(\infty) = 1 \\ a_\infty^-(0) &= \beta \qquad a_\infty^-(\infty) = 1 \end{aligned} \quad (6.2)$$

The amplitude of the back-scattering mode at $x = 0$, $\beta = a_\infty^-(0)$, is an unknown that must be obtained from the solution. In fact, β in the general nonlinear case corresponds to $1 + \delta_0$ of Eqs.(4.16) and (4.17) in chapter 4 for the linear case. The Maxwellian distribution at the wall, F_s^+, is affected by a + superscript to underline that it is a restriction of a Maxwellian distribution to $c_x > 0$. Likewise, F_∞^+ and F_∞^- are halfrange restrictions of the distribution function F_∞ at infinity,

$$F_\infty = \frac{1}{(2\pi RT_\infty)^{3/2}} \exp\left(-\frac{(c_x-u)^2+c_y^2+c_z^2}{2RT_\infty}\right). \tag{6.3}$$

Eq.(2.7) gives

$$n_i = \sqrt{\frac{2\pi}{RT_L}} \int\limits_{c_x<0} c_x a_\infty^-(0) n_\infty F_\infty dc_x = n_\infty \sqrt{\frac{T_\infty}{T_L}} \beta E^- \tag{6.4}$$

where E^- is defined in Eq.(6.6).

Using the 3 conserved moments, the state at the interphase and the external equilibrium state are related by

$$\begin{aligned}
\sigma_e n_s \sqrt{\frac{RT_L}{2\pi}} - \sigma_c n_\infty \sqrt{\frac{RT_\infty}{2\pi}} \beta E^- &= n_\infty u_\infty && (6.5a)\\
\sigma_e \tfrac{1}{2} n_s RT_L + \tfrac{1}{2} n_\infty RT_\infty \beta G^- & \\
+(1-\sigma_c)\tfrac{1}{2} n_\infty R\sqrt{T_L T_\infty}\beta E^- &= n_\infty u_\infty^2 + n_\infty RT_\infty && (6.5b)\\
\sigma_e 2 n_s RT_L \sqrt{\tfrac{RT_L}{2\pi}} & \\
-2 n_\infty RT_\infty \sqrt{\tfrac{RT_\infty}{2\pi}} \beta H^- &= n_\infty u_\infty \left(\frac{1}{2}u_\infty^2 + \frac{5}{2}RT_\infty\right) && (6.5c)\\
+(1-\sigma_c) 2RT_L n_\infty \sqrt{\tfrac{RT_\infty}{2\pi}} \beta E^- &
\end{aligned}$$

independent of the particular type of intermolecular potential. Here the functions E^-, G^- and $H^-$are the same as those used by Ytrehus [16], except that we denote by E^- the quantity that was originally denoted by F^-.

$$\begin{aligned}
E^- &= \sqrt{\pi} S_\infty(-1+\operatorname{erf} S_\infty) + e^{-S_\infty^2} && (6.6)\\
G^- &= (2S_\infty^2+1)(1-\operatorname{erf} S_\infty) - \frac{2}{\sqrt{\pi}} S_\infty e^{-S_\infty^2} && (6.7)\\
H^- &= \frac{\sqrt{\pi} S_\infty}{2}(S_\infty^2 + \frac{5}{2})(-1+\operatorname{erf} S_\infty) + \frac{1}{2}(S_\infty^2+2)e^{-S_\infty^2} && (6.8)\\
S_\infty &= \frac{u_\infty}{\sqrt{2RT_\infty}} && (6.9)
\end{aligned}$$

The solution to Eqs.(6.5a),(6.5b) and (6.5c) is obtained like in Ref.[16] and is expressed as

$$\sqrt{\frac{T_\infty}{T_L}} = -\frac{\sqrt{\pi}}{8}S_\infty + \sqrt{1+\frac{\pi}{64}S_\infty^2} \tag{6.10a}$$

$$\beta = \frac{2(2S_\infty^2+1)\sqrt{\frac{T_\infty}{T_L}} - 2\sqrt{\pi}S_\infty}{E^- + \sqrt{\frac{T_\infty}{T_L}}G^-} \tag{6.10b}$$

$$\frac{n_s}{n_\infty} = 2\frac{(1-\sigma_c)\sqrt{\frac{T_\infty}{T_L}}\sqrt{\pi}S_\infty E^- + \sigma_c\frac{T_\infty}{T_L}E^-(2S_\infty^2+1) + \sqrt{\pi}\frac{T_\infty}{T_L}S_\infty G^-}{\sigma_e(E^- + \sqrt{\frac{T_\infty}{T_L}}G^-)}$$

We see that β and $\frac{T_\infty}{T_L}$ are independent of σ_e and σ_c. The density ratio $\frac{n_s}{n_\infty}$ can be written as

$$\begin{aligned}\frac{n_s}{n_\infty} &= \frac{\sigma_c}{\sigma_e}\frac{2\exp(-S_\infty^2)\frac{T_\infty}{T_L}}{E^- + \sqrt{\frac{T_\infty}{T_L}}G^-} + \frac{1-\sigma_c}{\sigma_e}2\sqrt{\pi}S_\infty\frac{T_\infty}{T_L}\frac{\sqrt{\frac{T_L}{T_\infty}}E^- + G^-}{E^- + \sqrt{\frac{T_\infty}{T_L}}G^-} \\ &= \frac{\sigma_c}{\sigma_e}\left(\frac{n_s}{n_\infty}\right)_{\sigma=1} + \frac{1-\sigma_c}{\sigma_e}2\sqrt{\pi}\sqrt{\frac{T_\infty}{T_L}}S_\infty \end{aligned} \tag{6.11}$$

where $\left(\frac{n_s}{n_\infty}\right)_{\sigma=1}$ is the density ratio if $\sigma_e = \sigma_c = 1$,

$$\left(\frac{n_s}{n_\infty}\right)_{\sigma=1} = \frac{2\exp(-S_\infty^2)\frac{T_\infty}{T_L}}{E^- + \sqrt{\frac{T_\infty}{T_L}}G^-}. \tag{6.12}$$

The net evaporated number flux is given by Eq.(6.5a),

$$J(T_L, S_\infty, \sigma_e, \sigma_c) = \sigma_e n_s\sqrt{\frac{RT_L}{2\pi}} - \sigma_c n_\infty\sqrt{\frac{RT_\infty}{2\pi}}\beta E^-, \tag{6.13}$$

where n_∞ and T_∞ are given by Eqs.(6.11) and (6.10a). If $\sigma_e = \sigma_c = \sigma$, then

$$J(T_L, S_\infty, \sigma) = \sigma\left[n_s\sqrt{\frac{RT_L}{2\pi}} - n_\infty\sqrt{\frac{RT_\infty}{2\pi}}\beta E^-\right] \tag{6.14}$$

The number flux for $\sigma = 1$ given by the moment solution is surprisingly accurate for all speed ratios except close to the sonic state[24]. This holds also for $\sigma \neq 1$ since the transformation rule for the moment solution and more accurate solutions of the Boltzmann equation like DSMC is the same, with the slight modification of more accurate values of $\left(\frac{n_s}{n_\infty}\right)_{\sigma=1}$ and $\frac{T_\infty}{T_L}$.

Let T_L and hence n_s be constant. n_∞ is affected if σ is altered, so the mass flow for a given S_∞ is not linear in σ, as may otherwise be expected from Eq.(6.14). We have

$$\frac{J(T_L, S_\infty, \sigma)}{J(T_L, S_\infty, 1)} = \sigma \frac{\left[1 - \frac{n_\infty}{n_s}\sqrt{\frac{T_\infty}{T_L}}\beta E^-\right]}{\left[1 - \left(\frac{n_\infty}{n_s}\right)_{\sigma=1}\sqrt{\frac{T_\infty}{T_L}}\beta E^-\right]} \tag{6.15}$$

where $\left(\frac{n_\infty}{n_s}\right)_{\sigma=1}$ is given by Eq.(6.12). Fig. 6.1 gives a plot of $J/J_{\sigma=1}$ as a function of σ for various values of S_∞

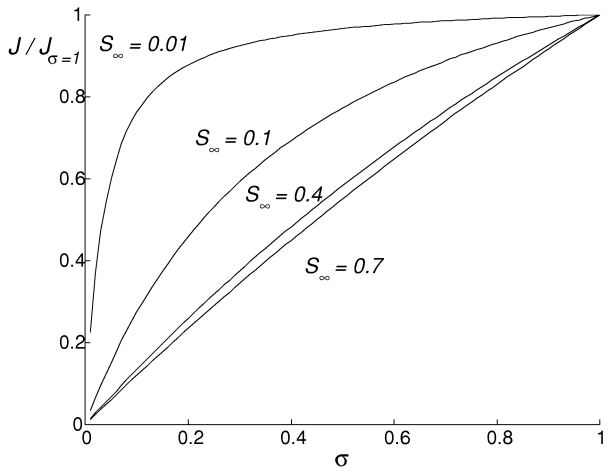

Figure 6.1: Number flux versus σ

The dramatic effect from lowering the coefficient σ can better be seen in a plot of a normalized number flux $\frac{J}{J_s} = \frac{J}{n_s\sqrt{\frac{RT_L}{2\pi}}} = 2\sqrt{\pi}\frac{n_\infty}{n_s}S_\infty\sqrt{\frac{T_\infty}{T_L}}$ versus pressure ratio, as was done by Ytrehus[24], see Fig. 6.2. When σ is lowered, the pressure ratio necessary to achieve the sonic state increases dramatically.

The structure of the Knudsen layer can be found from a forth non-conserved moment. Using the non-conserved moment mc_x^2 and inverse fifth power repulsive Maxwell molecules, Ytrehus[16] found the following solution for $\sigma = 1$:

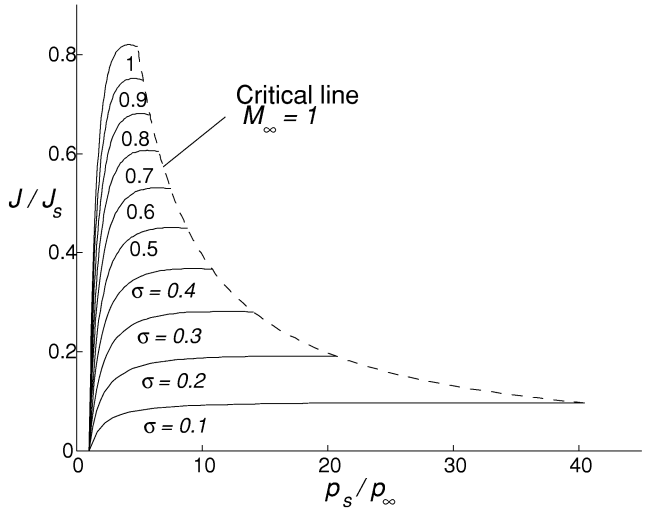

Figure 6.2: Number flux vs pressure ratio, from Ref. [24]

$$\frac{n(x)}{n_\infty} = \frac{u_\infty}{u(x)} = \frac{1}{2}\left[a_\infty^-(x) - 1\right]\phi_1 + 1 \tag{6.16}$$

$$\frac{T(x)}{T_\infty} = \frac{n_\infty}{3n(x)}\left\{2S_\infty^2 + 3 + \left[a_\infty^-(x) - 1\right]\phi_2 - 2S_\infty^2\frac{n_\infty}{n(x)}\right\} \tag{6.17}$$

$$\frac{T_{||}(x)}{T_\infty} = \frac{n_\infty}{n(x)}\left\{1 + 2S_\infty^2\left(1 - \frac{n_\infty}{n(x)}\right)\right\} \tag{6.18}$$

$$\frac{T_\perp(x)}{T_\infty} = \frac{n_\infty}{2n(x)}\left\{\left[a_\infty^-(x) - 1\right]\phi_2 + 2\right\} \tag{6.19}$$

where $||$ and $\perp$ means parallel and normal to the drift velocity respectively, and where

$$\frac{a_\infty^-(x)-1}{a_\infty^-(x)-r} = \frac{\beta-1}{\beta-r} e^{-P(1-r)x/\lambda_s^{\sigma=1}} \tag{6.20}$$

$$P = \frac{\pi}{12}\left(\frac{n_\infty}{n_s}\right)^2_{\sigma=1} \frac{T_\infty}{T_s}(\beta-1)\phi_1\phi_2/\left(1-\frac{T_\infty}{T_L}\right) \tag{6.21}$$

$$r = 1-\frac{2}{\phi_1}+\frac{4S_\infty^2}{\phi_2} \tag{6.22}$$

$$\phi_1 = \frac{1}{\beta-1}\left(\left(\frac{n_s}{n_\infty}\right)_{\sigma=1} - 2 + \beta(1-\operatorname{erf} S_\infty)\right) \tag{6.23}$$

$$\phi_2 = \frac{1}{\beta-1}\left(\left(\frac{n_s}{n_\infty}\right)_{\sigma=1} \frac{T_L}{T_\infty} - 2 + \beta(1-\operatorname{erf} S_\infty)\right) \tag{6.24}$$

Here $\lambda_s^{\sigma=1}$ is a reference mean free path, $\lambda_s^{\sigma=1} = \frac{\mu(T_L)}{mn_s^{\sigma=1}}\sqrt{\frac{\pi}{2RT_L}}$. As seen from Eq.(6.20), there is an approach to equilibrium, $a_\infty^- = 1$, only for $r \leq 1$, which confines S_∞ to the interval $[0, 0.907]$. This corresponds to an upper Mach number of $M_\infty = \sqrt{\frac{6}{5}}S_\infty = 0.994$. Given the approximate nature of the moment solution this is interpreted as an upper limit at Mach 1, i.e. at the sonic singularity.

Although the jump conditions are independent of the interaction law, the structure and in particular the relaxation towards equilibrium flow are not, [86]. This is evident from the above relations, since the collisional properties of Maxwell molecules are the basis for the relaxation exponent $P(1-r)/\lambda_s^{\sigma=1}$, and must be born in mind when comparing moment solutions with molecular dynamics simulations.

For diffuse reflection of molecules at the interphase, the Knudsen layer structure for $\sigma \neq 1$ can be found from an equivalent $\sigma = 1$ solution. This is seen from the boundary condition, Eq.(2.4). The two solutions are identical if the saturation densities are related by

$$n_s^{\sigma=1} = \sigma_e n_s + (1-\sigma_c)n_i = \sigma_e n_s + (1-\sigma_c)J^-\sqrt{\frac{2\pi}{RT_L}} \tag{6.25}$$

Eq.(6.25) is the basis for the standard transformation of densities and pressures originally given in Ref.[89] and also considered in Refs.[90],[24]. But $n_s^{\sigma=1}$ can also be calculated from Eq.(6.12), holding n_∞ fixed, since $\left(\frac{n_s}{n_\infty}\right)_{\sigma=1}$ is only a function of the speed ratio S_∞. This is a different interpretation of Eq.(6.11) than in the original derivation, n_∞ can be kept fixed while $n_s^{\sigma=1}$ vary. Since the solution for $\sigma = 1$ with $n_s^{\sigma=1}$ given by Eq.(6.25) is equivalent to the $\sigma \neq 1$ solution, the ideal value $\left(\frac{n_s}{n_\infty}\right)_{\sigma=1}$ is used in all expressions for the Knudsen layer, but then the solution is given in terms of $x/\lambda_s^{\sigma=1}$. It is better to use the

physical n_s and plot the Knudsen layer in units of λ_s,

$$\lambda_s = \frac{\mu(T_L)}{\rho_s}\sqrt{\frac{\pi}{2RT_L}} = \frac{1}{\sqrt{2}n_s\pi d_{eff}^2}. \tag{6.26}$$

We regard σ here as a free parameter that can be varied independently of μ and d_{eff}. The "real" mean free path is related to the ideal $\sigma = 1$ case by

$$\lambda_s = \frac{1}{\sqrt{2}n_s\pi d_{eff}^2} = \frac{n_s^{\sigma=1}}{n_s}\frac{1}{\sqrt{2}n_s^{\sigma=1}\pi d_{eff}^2} = \frac{(n_s/n_\infty)_{\sigma=1}}{n_s/n_\infty}\lambda_s^{\sigma=1} \tag{6.27}$$

The last equality follows since the Knudsen layers are equal and n_∞ in the nominator and denominator is invariant. When the Knudsen layer is plotted in units of λ_s, a solution for $\sigma = 1$ can be transformed to $\sigma_e \neq \sigma_c \neq 1$ just by scaling the x-axis or stretching the graph in the x-direction. If the evaporation and condensation coefficients are equal, $\sigma_e = \sigma_c = \sigma$, $\sigma < 1$ gives a stretch of the graphs in the x-direction (active viewpoint) relative to the $\sigma = 1$ solution, or equivalently a compression of the x/λ_s-axis (passive viewpoint).

To test the transformation of the Knudsen layer, two DSMC simulations are performed for the same Mach number ($M_\infty = 0.78$) but for different values of the common parameter $\sigma_e = \sigma_c = \sigma$. In the first simulation $\sigma = 1$, and in the second simulation $\sigma = 0.7$. Then $\frac{n_s/n_\infty}{(n_s/n_\infty)_{\sigma=1}} \approx 1.35$ and the $\sigma = 1$ solution stretched in the x-direction by a factor 1.35 overlaps the direct $\sigma = 0.7$ simulation, see Fig.6.3. The small discrepancy between the graphs is due to statistical noise in the DSMC simulation, and two corresponding BKW solutions would overlap completely.

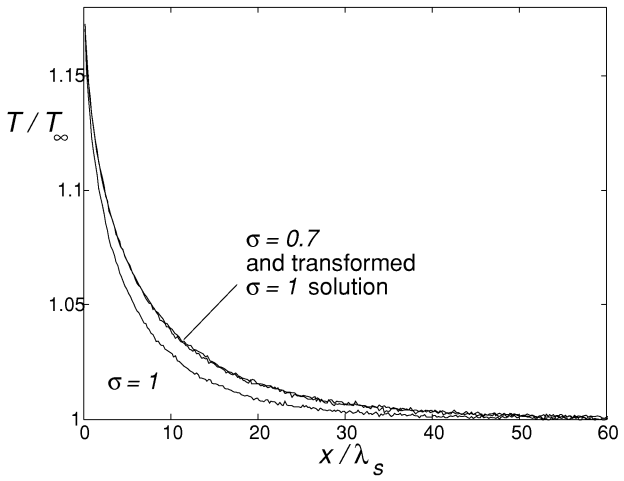

Figure 6.3: Transformation of DSMC simulations, $M_\infty = 0.78$

The moment solution of the Knudsen layer structure for $\sigma_e \neq \sigma_c$ can be given directly, Eq.(6.27) is inserted into Eq.(6.20) with the result

$$\frac{a_\infty^-(x)-1}{a_\infty^-(x)-r} = \frac{\beta-1}{\beta-r} e^{-P(1-r)\frac{(n_s/n_\infty)_{\sigma=1}}{n_s/n_\infty} x/\lambda_s} \tag{6.28}$$

where n_s/n_∞ and $(n_s/n_\infty)_{\sigma=1}$ are given respectively by Eqs.(6.11) and (6.12). Note that $\left(\frac{n_s}{n_\infty}\right)_{\sigma=1}$ in Eqs.(6.21), (6.22), (6.23) and (6.24) shall not be replaced by $\frac{n_s}{n_\infty}$, as could be concluded from a statement made by Cercignani[2], page 291, 'we can easily modify all the formulas obtained for the case $\sigma = 1$, by simply replacing n_s, whenever it occurs by the expression (6.11)'. For evaporation, if the evaporation and condensation coefficients are equal, $\sigma < 1$ gives a stretch of the Knudsen layer in the x-direction (active viewpoint) relative to the $\sigma = 1$ solution, or equivalently a compression of the x/λ_s-axis (passive viewpoint). This can also be seen from the characteristic length l in $a_\infty^-(x)$ given by Eq.(6.28)

$$\frac{l}{\lambda_s} = \frac{n_s/n_\infty}{(n_s/n_\infty)_{\sigma=1}} \frac{1}{P(1-r)} \tag{6.29}$$

The scaled length $\frac{l}{\lambda_s}$ is a function of S_∞ and σ, for high Mach numbers $\frac{l}{\lambda_s}$ is very sensitive to the value of the condensation coefficient, as can be seen in Fig. 6.4

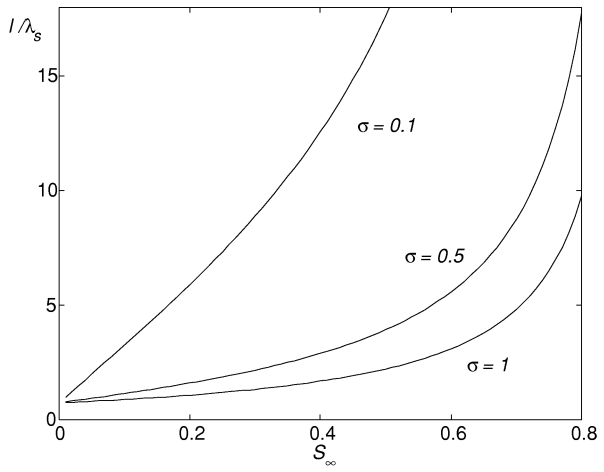

Figure 6.4: Characteristic length in the Knudsen layer, from Eq.(6.29)

All solutions related by the transformation would be equal if they were plotted on a x/λ_∞-scale instead of x/λ_s-scale. This can be accomplished by replacing $\lambda_s^{\sigma=1}$ in Eq.(6.20) by

$$\lambda_s^{\sigma=1} = \frac{1}{\sqrt{2} n_s^{\sigma=1} \pi d_{eff}^2} = \frac{n_\infty}{n_s^{\sigma=1}} \frac{1}{\sqrt{2} n_\infty \pi d_{eff}^2} = \left(\frac{n_\infty}{n_s} \right)_{\sigma=1} \lambda_\infty \qquad (6.30)$$

where $\left(\frac{n_\infty}{n_s}\right)_{\sigma=1}$ is a function of S_∞ only, the moment method gives Eq.(6.12). λ_∞ is invariant.

6.3 Molecular dynamics

Molecular dynamics [37] techniques offer the possibility to study the liquid-gas interphase in detail. The condensation coefficient and the distribution function outside the interphase can be determined by counting the molecules that condense and evaporate.

6.3.1 Simulation box

The molecular dynamics simulation is conducted in a box of non-cubic shape, see Fig.4.5. An elongated box in the x-direction is used so the gas region can be relatively long with the number of liquid molecules limited. We are not interested in the dynamics in the liquid, calculation of the trajectories of liquid molecules is computationally expensive since the liquid molecules have more neighbors than the gas molecules. But the interphase must be correctly reproduced and this requires a liquid slab of say 10 molecular diameters thickness.

The dimensions of the box is given by L_x, which is the longest side, and L_y and L_z that are equal. The ratio between length and width of the simulation box has been varied from 16 for equilibrium simulations to 100 for high Mach number evaporation simulations. In the middle of the liquid a thermostat keeps the temperature fixed. Fluctuations of the center of mass of the liquid can be larger than the width of the interphase. Such behavior would 'smear out' density profiles, etc. Therefor the liquid slab is kept in the middle by shifting the x-coordinates, this does not change the relative distance between the molecules. We may specify the condition that the center of mass of all the particles should not move[98], but in our simulations the length of the gas phase divided by the thickness of the liquid layer is comparable to the liquid density divided by the gas density, hence fluctuations in the gas density far from the interphase may perturb the center of mass. Instead, the shifting is determined by the requirement that there shall be an equal number of molecules in both halves of the box, a primitive bisection search algorithm is used. Particles that are moved outside of the x-boundaries in the centering algorithm, are inserted on the opposite side with the opposite x-component of velocity since the drift velocities in the two halves are opposite. This algorithm conserves momentum only on the average.

6.3.2 Quasi-periodic boundary conditions

In equilibrium simulations periodic boundary conditions are used, as though the simulation box were periodically replicated. A molecule that crosses one side of the simulation box is inserted on the opposite side with the same velocity, and assuming that the cut-off distance for the potential is small compared to the box size, only molecules near one boundary of the box interact with molecules on the opposite boundary. During net evaporation there is a flow away from the liquid, i.e. the drift velocities are opposite in the two parts of the box. The boundary conditions for a nonequilibrium simulation have to be adjusted compared to the completely periodic version for equilibrium, a quasi-periodic approach is used here.

A molecule crossing boundaries with y- or z-constant can be treated as in the equilibrium case, the position is shifted to the opposite side and the velocity is retained. 'Periodic' interaction across the cell boundaries is also correct since the neighboring molecules experience the same environment, macroscopic variables such as temperature and drift velocity should on the average be equal. But a molecule close to the boundary x-constant interacts with neighbors in the adjacent box with opposite drift velocity. This is not correct and an error is introduced, its effect will be discussed later. What happens to a molecule that crosses the constant x boundary is the key to a successful evaporation algorithm and this will be considered in the next chapter.

6.3.3 Evaporation algorithm

In the gas region there is a flow away from the liquid due to the net evaporation of molecules at the interphase. The density, temperature and velocity in the gas phase vary in the x-direction until a uniform state is reached far from the interphase, here denoted ∞.

We now look at the right half of the simulation box in Fig.4.5, the treatment of the other half differs only in the sign of the x-component of the velocity. The gas phase has length L where L is big enough so the fluid reaches the equilibrium flow conditions far out in the gas phase. In evaporation, only one parameter can be specified[2], we chose the velocity at 'infinity'. The way the velocity is specified is to force the velocity distribution function at L to be symmetric about u_∞, see Fig. 6.5, as was done by Frezzotti[99] in a DSMC simulation of evaporation. No assumption on the shape of the distribution function is made, if the simulation domain is long enough the distribution should become a drifting Maxwellian. The mirrored velocity about u_∞ corresponding to $\mathbf{c}$ is $\mathbf{c}' = 2u_\infty \widehat{\mathbf{x}} - \mathbf{c}$. Then for the x-component $u_\infty - c'_x = c_x - u_\infty$, i.e. symmetric about u_∞. Hence we stipulate

$$F_\infty(\mathbf{c}') = F_\infty(2u_\infty \widehat{\mathbf{x}} - \mathbf{c}) = F_\infty(\mathbf{c}) \tag{6.31}$$

When a molecule with velocity c_x leaves the box at $x = L$, it is reinjected at the boundary if $c'_x < 0$ with a probability $|c'_x| / c_x$. The probability con-

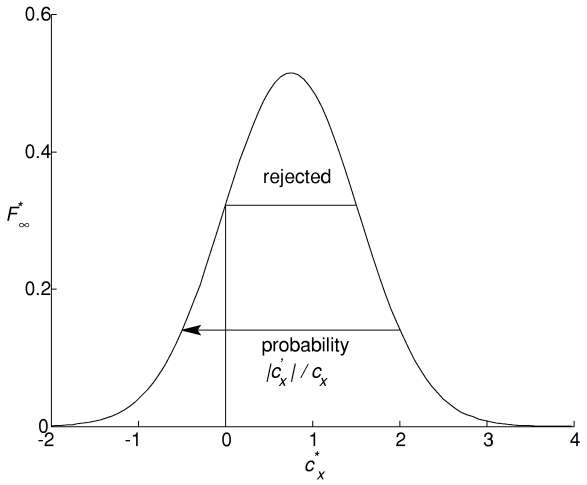

Figure 6.5: Boundary condition at ∞

dition follows from the ratio of the differential fluxes for molecules entering, $|c'_x|\, n_\infty F_\infty(\mathbf{c}')$, and leaving the box, $c_x n_\infty F_\infty(\mathbf{c})$,

$$\frac{|c'_x|\, n_\infty F_\infty(\mathbf{c}')}{c_x n_\infty F_\infty(\mathbf{c})} = \frac{|c'_x|}{c_x}. \tag{6.32}$$

since $F_\infty(\mathbf{c}') = F_\infty(\mathbf{c})$. Hence only a fraction $|c'_x|/c_x$ of the molecules with mirrored velocity $c'_x < 0$ should be reinjected. The temperature and hence Mach number is a result of the computation.

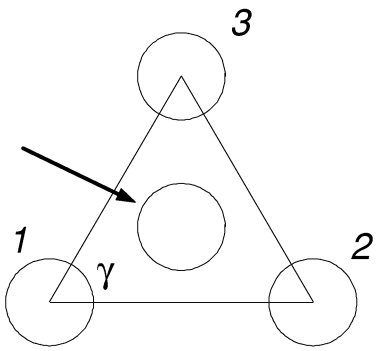

Figure 6.6: Insertion of a molecule in the liquid. The molecular diameter is not drawn to scale, the molecules actually have large overlaps

The molecules that are not allowed to reenter the gas domain are inserted in

the liquid to maintain a steady evaporation flux. Just inserting the molecule at a random position in the middle of the liquid should not be attempted since that may cause large overlaps of the repulsive cores giving unphysically large repulsive forces that can cause numerical failure of the finite-difference algorithm. Instead we locate a small hole nearby the randomly chosen position and try to expand it in a controlled way. The algorithm works as follows : Pick the molecule nearest the random position chosen, here denoted molecule 1. Its closest neighbor is denoted molecule 2. A molecule 3 is chosen among the other successively nearest neighbors of molecule 1 so that the angle γ between the vectors $\mathbf{r}_2-\mathbf{r}_1$ and $\mathbf{r}_3-\mathbf{r}_1$ is between 30 and 90 degrees. The molecule removed from the gas is inserted in the middle of the triangle given by the center of the nodes, $(\mathbf{r}_1+\mathbf{r}_2+\mathbf{r}_3)/3$. This procedure is shown in Fig.6.6. The algorithm ensures that there are no molecules closer to the inserted molecule than those in the triangle. Assuming a nearest neighbor distance of r_0, the distances between the inserted molecule and the molecules at the nodes of the triangle are approximately 0.6 r_0. The forces are strongly repulsive and the inserted molecule creates a larger hole by itself. To avoid unphysically large velocities, the speeds of the inserted molecule and the 3 molecules in the triangle are rescaled for some timesteps after the insertion, the direction is maintained, but the speed is cut at 3 equilibrium standard deviations. The velocities are rescaled for so many timesteps it takes a molecule with the rescaled velocity to move $0.4r_0$. After the procedure, the distances between the inserted molecule and the nearest neighbors are approximately r_0. The excess kinetic energy is removed by the thermostat.

The simulation is started with the molecules in a lattice, or in an old configuration for a different state if it is available. In our simulation the number of molecules and the average density are specified. If a lattice is used, an auxiliary high temperature thermostat in the 'gas end' of the box is used in the beginning together with the thermostat in the liquid to set up a two-phase system. To speed up the formation of an initial liquid layer, all molecules in the simulation box can be thermostatted with a staircase temperature profile. Afterwards the temperature in the gas is decreased until it has the same temperature as the liquid thermostat. Then the evaporation algorithm described above is activated. The system needs considerable time to relax to the steady state. As a rule of thumb, a start-up period of 10 times the time it takes for a soundwave to travel through the gas phase is not included in the sampling of the macroscopic quantities.

If $M_\infty > 0.4$, the gas can be so rarefied that the average density including the liquid is comparable with the gas saturation density at the liquid temperature. To avoid that the liquid film disappears when the temperature of the auxiliary thermostat is lowered, the average density is set larger in the beginning and gradually lowered to the desired value as the evaporation algorithm is activated.

Two trial simulations were performed to test the algorithm. With $u^*_{\infty,set} = 0.025$ the set velocity was reached, see Fig.6.7, but in Fig.6.8 the velocity undershoots 4% of the set value for $u^*_{\infty,set} = 0.2$.

This may be due to the fact that the interactions are not represented correctly at the constant x boundary: there is an interaction between molecules

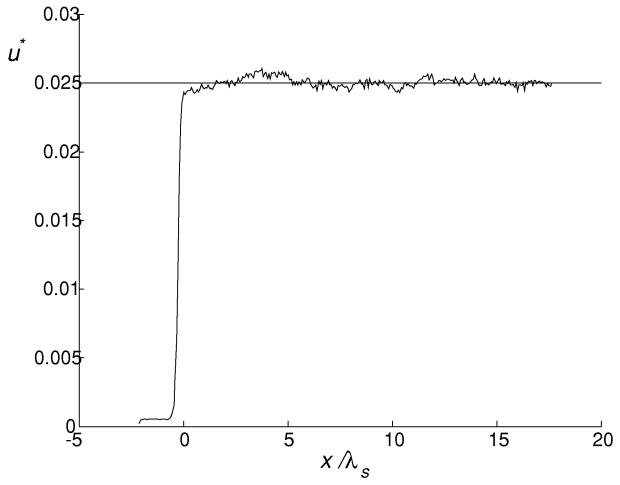

Figure 6.7: Macroscopic velocity, $u^*_{\infty,set} = 0.025$

with opposite drift velocity. The forces are not 'periodic' in the x-direction but this feature was retained from the equilibrium implementation because it makes the programming easier. Of course an infinite box can not be simulated. An alternative way would be to completely remove the periodic force in the x-direction, as though there were no molecules outside the vertical boundary, but that would introduce an error of the same order, as was also evident in a test simulation. How to achieve the set velocity was not resolved. But quasiperiodic boundary conditions give profiles that are stationary and flat far from the interphase as they should be. Hence, the solutions should be valid for the new velocity that deviates slightly from the set value, and this approach is used in all calculations henceforth.

6.4 Tabulated results

We have performed 20 molecular dynamics simulations of net evaporation, covering Mach numbers from 0.025 to near sonic conditions. The number of molecules varied from 4680 for simulation with low Mach numbers to 10800 for high Mach numbers. The time interval of sampling after steady state has been reached, is typically $t^* = 30000$. The target temperature of the thermostat in the liquid was $T^*_{liq} = 0.65$ in all simulations. But strong heating due to molecule insertions made the temperature in the liquid slightly higher than T_{liq}. The liquid temperature T^*_L used in gas-kinetic calculations and here associated with the temperature at the liquid boundary in MD, varies between 0.642 and 0.649 in the simulations. The reference mean free path λ_s is only a function of the liquid temperature and varies slightly around $7.8r_0$.

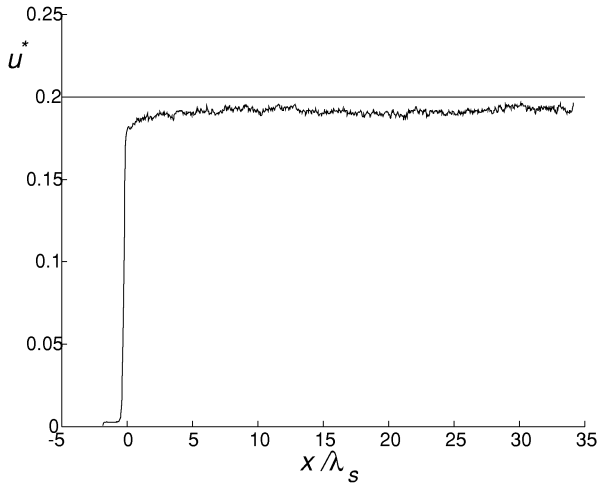

Figure 6.8: Macroscopic velocity, $u^*_{\infty,set} = 0.2$

In Fig. 6.9, T_∞/T_L, which according to gas-kinetic calculations is independent of σ, has been plotted as a function of M_∞. The MD values have been compared with a numerical solution of the BKW equation[100], DSMC solution of the Boltzmann equation for hard spheres[99], and Anisimov's and Ytrehus' moment solution. The experimental values are for sublimation of iodine, the values have been taken from a plot in an article[88] and are only approximate. It is seen that the MD values for $\frac{T_\infty}{T_L}$ correspond nicely with the gas-kinetic calculations.

M_∞	J/J_s	T_∞/T_L	T_0/T_L	n_∞/n_s	n_0/n_s	λ^*_∞
0.097	0.24	0.97	0.96	0.81	0.85	9.3
0.20	0.42	0.92	0.92	0.69	0.74	11
0.30	0.54	0.88	0.89	0.60	0.67	12.5
0.41	0.61	0.84	0.87	0.52	0.61	14.7
0.52	0.65	0.81	0.85	0.45	0.57	16.3
0.62	0.69	0.77	0.84	0.40	0.54	17.6
0.73	0.70	0.74	0.82	0.36	0.54	19.1
0.78	0.72	0.72	0.83	0.34	0.53	19.1
0.83	0.72	0.71	0.82	0.33	9.53	20.3
0.91	0.70	0.68	0.82	0.30	0.53	22.9
0.94	0.71	0.67	0.82	0.29	0.53	23.4

Table 6.1: Simulation results for net evaporation

Various characteristics of the simulations have been summarized in Tables 6.1 and 6.2. The width of the Knudsen layer is denoted x_K. Formally the

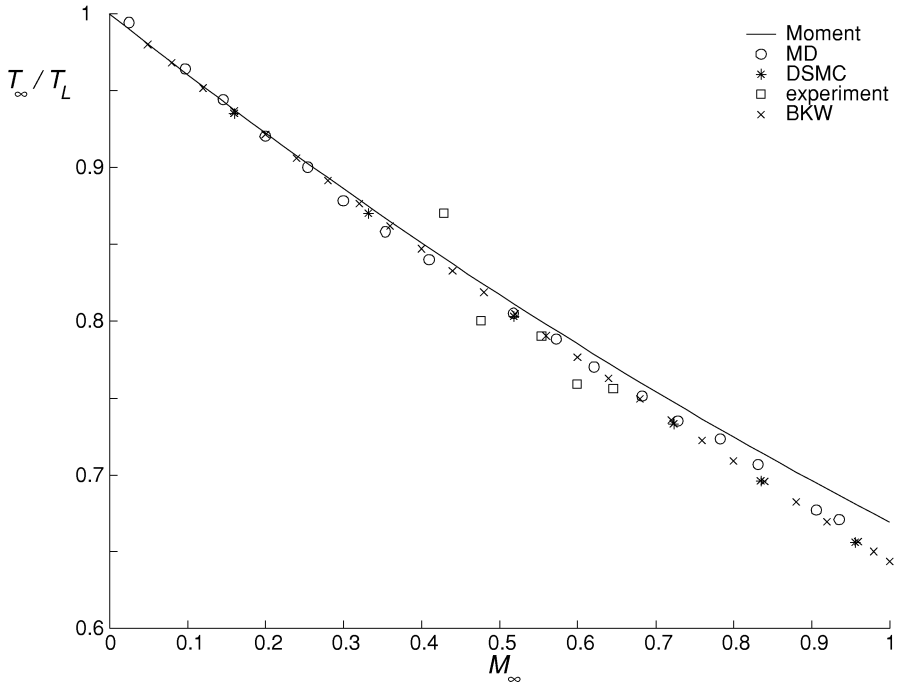

Figure 6.9: Temperature ratio versus Mach number. The simulated values from molecular dynamics are compared with numerical solution of the BKW equation[100], DSMC solution of the Boltzmann equation for hard spheres[99], Ytrehus' moment solution[16] and experimental values for sublimation of iodine[88].

Knudsen layer ends at the point where the flow has reached local equilibrium. A more practical criterion is used instead, x_K is here defined as the position where the difference between the parallel temperature $T_{||}$ and the normal temperature $T_\perp$ given by Eq.(3.28) is less than 1%. As expected, the width of the Knudsen layer increases with the Mach number. x_{99}^U is the position where $u(x) = 0.99u_\infty$. x_∞ is the length of the gas phase and the position where the boundary conditions are applied. $\delta_\infty = n_\infty^{-1/3}$ is the mean molecular spacing. d_{eff} is the effective molecular diameter and δ_∞/d_{eff} is a measure of deviation from ideal gas, Bird[23] uses $\delta_\infty/d_{eff} > 7$ as limit for dilute gas, this is never fulfilled in our simulations. The thickness of the interphase was approximately $5.5r_0$ in all simulations. The compression factor $Z_\infty = \frac{p}{\rho RT}$ varied from 0.9 for low M_∞ to 0.92 for close to critical conditions, hence the correction due to attractive interaction dominates over the repulsive interaction.

M_∞	x_K/λ_s	x^u_{99}/λ_s	x_∞/λ_s	δ^*_∞	δ_∞/d_{eff}
0.097	0.6	4.7	35	4.3	3.1
0.20	2.3	3.8	34	4.6	3.3
0.30	3.7	3.5	37	4.8	3.4
0.41	5.0	7.3	36	5.1	3.6
0.52	13	10	40	5.4	3.7
0.62	15	17	74	5.5	3.8
0.73	16	19	113	5.6	3.9
0.78	17	30	121	5.7	3.9
0.83	24	45	119	5.8	3.9
0.91	24	72	144	6	4.1
0.94	22	69	146	6.1	4.1

Table 6.2: Simulation results for evaporation, continued

6.5 Knudsen layer

In strong evaporation, there is a Knudsen layer where $T_{||}$ and $T_\perp$ are differing significantly, see Fig.6.10. The same thickness $\Delta x \approx 0.3 r_0$ of the sampling intervals has been used both in the liquid and in the gas, the thickness has been determined by the requirement that the interphase shall be resolved.

As noted by Yen[86] and implicit in works of Mager[88] and Frezzotti[99] and also seen in Fig. 6.9, for the one-dimensional evaporation problem, properties like the density ratio, pressure ratio and mass flux do not depend much upon the type of kinetic equation, i.e. Boltzmann or BKW, or intermolecular potential used, for identical condensation coefficient. But the relaxation rate towards the uniform state at infinity is not the same for the Boltzmann and BKW solutions,[86].

Let us assume for the moment that the evaporation and condensation coefficients are equal, and denote the common value by σ. Fig. 6.11 shows a comparison for $M_\infty = 0.78$ between the MD simulation for LJ-spline molecules and the Ytrehus' moment solution of the Boltzmann equation[16] for Maxwell molecules, for two different values of σ. For the MD plot, λ_s is given by Eq.(3.23), as usual. The MD simulation and the moment solutions look rather similar, except for the parallel temperature at the smaller x/λ_s-values.

From the $T_{||}$ plot it may look as though the gas boundary in the MD simulation has been put too far from the interphase. But if the gas boundary is shifted closer to the liquid, $T^{MD}_{||}$ will actually increase. This is shown in Fig.6.12 which is a plot of $T_{||}$ in the interphase and in the Knudsen layer. The drop in $T_{||}$ is much larger for the moment solution with Maxwell molecules than for the MD simulation with LJ-spline potential. For a DSMC simulation of hard spheres the discrepancy is still there, but only half as big.

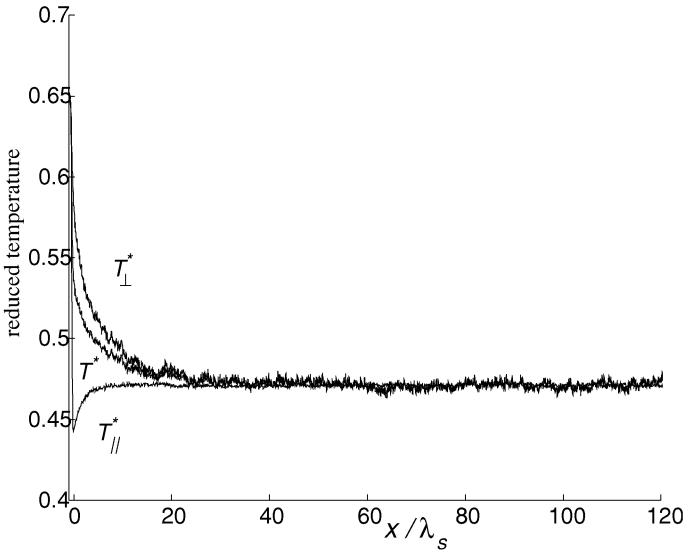

Figure 6.10: Plot of the temperatures for $M_\infty = 0.78$

6.6 Boundary condition at the interphase

The Boltzmann equation can only describe the behavior in the gas phase. In gas-kinetics, the dynamics in the interphase is replaced by a boundary condition at the gas boundary. Here we will use molecular dynamics to determine this boundary condition and compare it with existing models.

6.6.1 Condensation coefficients

There are several ways to calculate the condensation coefficient, any relation given by the moment solution can be compared with molecular dynamics simulations. We will first make the common assumption that the evaporation and condensation coefficients are equal. The distribution function Eq.(2.4) reduces to

$$f^+ = n^+ F^+ = \left[\sigma n_s + (1-\sigma) n_i\right] F_s \tag{6.33}$$

where the number density is given by

$$2n^+ = \sigma n_s + (1-\sigma) n_i \tag{6.34}$$

The factor 2 comes from different normalization of F^+ and F_s, F^+ is normalized to 1 on $c_x > 0$ whereas F_s is normalized on $-\infty < c_x < \infty$. A 'microscopic' condensation coefficient can be defined from the number density as

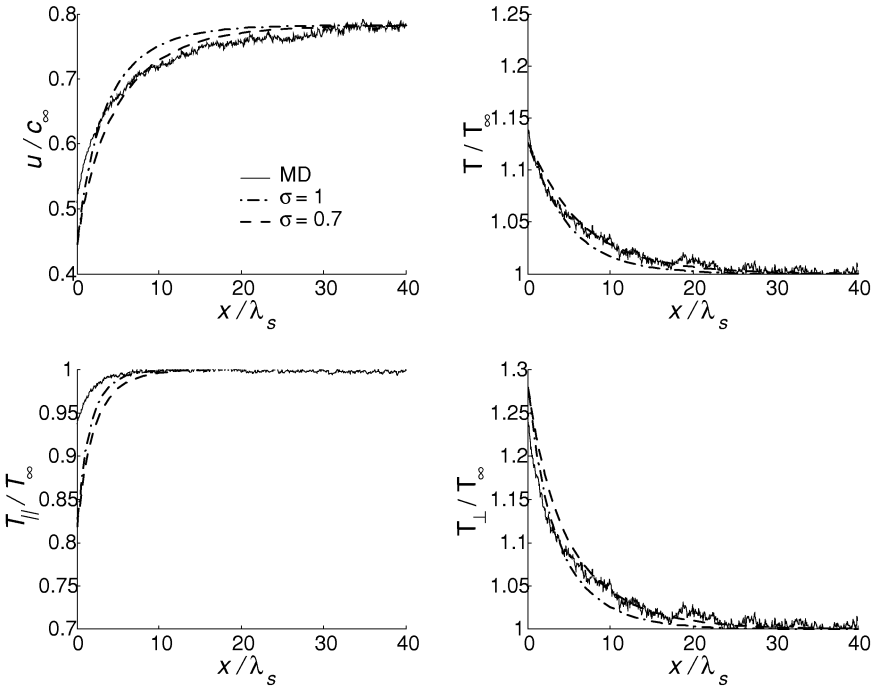

Figure 6.11: Knudsen layer in strong evaporation, $M_\infty = 0.78$. The solid line is a molecular dynamics simulation, and the dashed lines are moment solutions for $\sigma = 0.7$ and $\sigma = 1$.

$$\sigma_{micro} = \frac{n_i - n_s}{n_i - 2n^+} \tag{6.35}$$

In our simulations, n^+ is calculated in a small control volume of thickness $r_0/6 \approx \lambda_s/45$.

A 'macroscopic' relation involving σ can also be used to define an effective coefficient. The $\sigma = 1$ case has been extensively studied by moment and DSMC solutions of the Boltzmann equation. For $\sigma_e = \sigma_c = \sigma$, the transformation of the density, Eq.(6.11) simplifies to

$$\frac{n_s}{n_\infty} = \left(\frac{n_s}{n_\infty}\right)_{\sigma=1} + \frac{1-\sigma}{\sigma} 2\sqrt{\pi}\sqrt{\frac{T_\infty}{T_L}} S_\infty \tag{6.36}$$

Here $\left(\frac{n_s}{n_\infty}\right)_{\sigma=1}$ is a function of S_∞ only, and σ can then be determined from a given value of $\frac{n_s}{n_\infty}$ from MD. We therefore define a 'macroscopic' condensation coefficient as

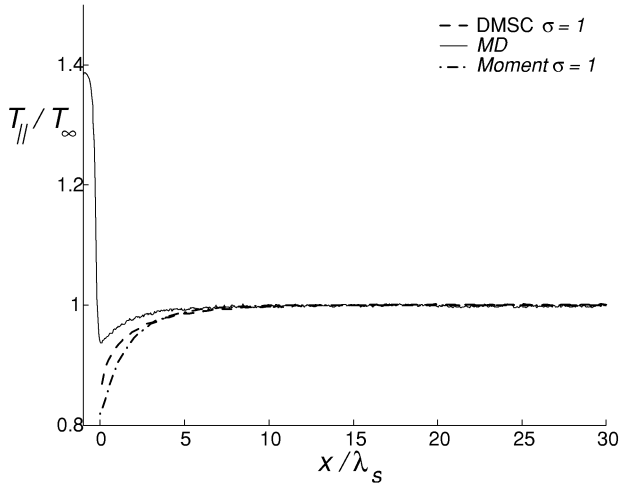

Figure 6.12: Parallel temperature calculated by different methods, $M_\infty = 0.78$.

$$\sigma_{macro} = \frac{2\sqrt{\pi}S_\infty\sqrt{\frac{T_\infty}{T_L}}}{-\left(\frac{n_s}{n_\infty}\right)_{\sigma=1} + \frac{n_s}{n_\infty} + 2\sqrt{\pi}S_\infty\sqrt{\frac{T_\infty}{T_L}}} \tag{6.37}$$

Both Eqs.(6.35) and (6.37) are indeterminate at equilibrium. But the value of σ at equilibrium is of no interest, any value may be used, cancellation occurs and Eq.(6.33) collapses to $f^+ = n_s F_s$.

M_∞	σ_J	σ_{macro}	σ_{micro}	σ_e	σ_c
0	-	-	-	0.67	0.67
0.097	0.73	0.78	0.69	0.71	0.60
0.20	0.80	0.86	0.76	0.74	0.61
0.30	0.83	0.88	0.77	0.76	0.60
0.41	0.84	0.88	0.75	0.78	0.60
0.52	0.83	0.86	0.75	0.78	0.57
0.62	0.84	0.88	0.75	0.79	0.54
0.73	0.85	0.87	0.76	0.79	0.53
0.78	0.85	0.89	0.75	0.80	0.51
0.83	0.86	0.89	0.75	0.80	0.48
0.91	0.84	0.88	0.76	0.79	0.50
0.94	0.85	0.88	0.76	0.80	0.50

Table 6.3: Coefficients calculated from various definitions

The condensation coefficient appears as a parameter in many other expres-

sions, for instance $T(0)/T_L$ and $n(0)/n_s$. In practical applications the evaporation mass flux is important, hence a condensation coefficient defined to give the correct mass flux is useful. The number flux is given by Eq.(6.14), and a 'condensation' coefficient denoted σ_J can be defined to fit the flux. Here we have used values for n_∞, T_∞ and β from the moment solution. In Table (6.3), simulated values for σ, according to the various definitions, have been listed. The coefficients σ_J, σ_{macro} and σ_{micro} are essentially constant for $M_\infty > 0.2$. For low Mach numbers and $\sigma > 0.4$, the mass flux is not much dependent upon the actual value of σ, as can be seen in Fig. 6.1, hence the value of σ_J for $M_\infty < 0.1$ is difficult to calculate accurately. σ_{micro} has nominator and denominator that follow from substraction of two nearly equal numbers and it is very difficult to calculate σ_{micro} accurately for small Mach numbers.

Each method gives a slightly different σ and the theory can not be exact at this point. For high Mach numbers the evaporation mode dominates. Since σ_{micro} defined from the density is lower than σ_J defined from the mass flux, one explanation may be that there is a drift velocity in the evaporation mode. But first we will check if $\sigma_e = \sigma_c$ is a good assumption. In Table 6.3, values for σ_e and σ_c calculated from the definitions in terms of fluxes,

$$\sigma_e = \frac{J^e}{J_s} \tag{6.38}$$

$$\sigma_c = \frac{J^c}{J^-} \tag{6.39}$$

have been listed. The evaporation and condensation coefficients are not equal, the evaporation coefficient increases with M_∞ and the condensation coefficient decreases with M_∞ for net evaporation.

The evaporation and condensation coefficients can also be calculated from the number density. Looking at the boundary condition, Eq.(2.4), we see that $2n^e = \sigma_e n_s$ and $2n^r = (1 - \sigma_c)n_i$. The factor 2 comes from different normalization of F^e and F^r, and F_s, as already remarked. The coefficients calculated from the flux and the number density turn out not to be equal. The number density evaporation coefficient is almost constant, $2n^e/n_s = 2\chi_e \approx 0.66$, χ_e is listed in Table 6.5(chapter 6.6.3). The number density condensation coefficient equals $1 - 2n^r/n_i = 1 - 2\chi_r$ which varies with M_∞, χ_r is listed in Table 6.5. Hence the boundary condition as it is written in Eq.(2.4), and repeated for equal evaporation and condensation coefficients in Eq.(6.33), can not be correct and this is a further motivation for calculating the detailed distribution function at the interphase.

6.6.2 Calculation of the distribution function at the interphase

It is easy to sample the differential flux $\phi^+(c_x)$ of molecules leaving the interphase and entering the gas region. ϕ^+ can furthermore be split into fluxes for

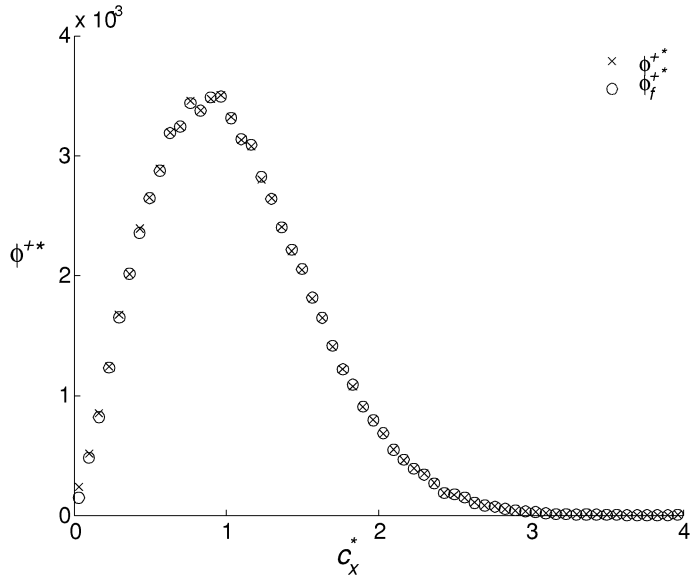

Figure 6.13: Differential flux at the gas boundary for $M_\infty = 0.78$.

evaporation and reflection. The distribution function is related to the differential flux by

$$f^+(c_x) = \phi^+(c_x)/c_x. \tag{6.40}$$

But division by c_x amplifies errors in the flux for small values of c_x, hence this method for calculating the distribution function was not used. Instead evaporating and reflecting molecules are tagged as they leave the interphase and their velocities are sampled in a thin control volume of width $r_0/6 \approx \lambda_s/45$ at the gas boundary. In Fig.6.13 it is shown that this algorithm works, the differential flux calculated from the distribution function, ϕ_f^+, is compared with the differential flux ϕ^+ calculated directly, for $M_\infty = 0.78$.

In Fig. 6.14 the velocity probability distribution $F^+(c_x)$ for molecules crossing from the interphase into the gas is plotted for $M_\infty = 0.78$. F^+ is normalized to 1 for $c_x > 0$. Then n^+ in the total distribution function $f^+ = n^+F^+$ is the physical density of particles crossing the gas boundary. Contrary to the usual assumption in gas-kinetic boundary conditions, there is a drift velocity in $F^+(c_x)$ that can not be neglected, it is comparable to the drift velocity at the gas boundary, $u(0)$. The distribution looks like a Maxwellian, but is not completely symmetric about the maximum. However it is tempting to try to fit a Maxwellian. The natural logarithm of a Maxwellian is a second order polynomial. Using the least squares principle, effective values of temperature and drift velocity can be found, but the ln function makes the lower values of the

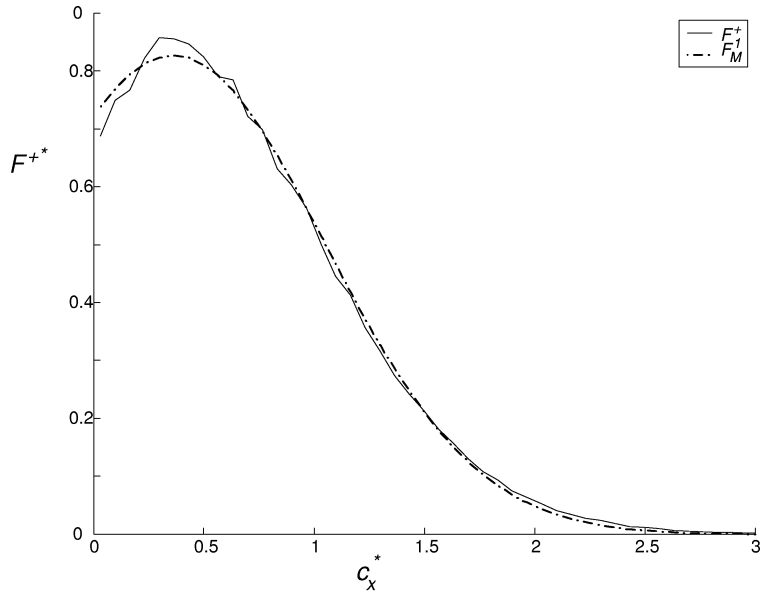

Figure 6.14: Distribution function for molecules crossing into the gas, $M_\infty = 0.78$.

distribution function for higher velocities count more than the more important higher values at lower velocities, and the interval of least squares regression is cut arbitrarily at $c_x^* = 1.7$. This Maxwellian is denoted F_M^1 in Fig.6.14. In Table 6.4 some values for the effective temperature $T_{||}^+$ and drift velocity u^+ in $F^+(c_x)$ have been tabulated. The u^+ and $T_{||}^+$ values are only meant as an illustration. F^+ is not Maxwellian, but the values for u^+ and $T_{||}^+$ give a fair overall fit.

In Fig. 6.15 the distribution for the c_y-component for molecules entering the gas is compared with Maxwellians with temperatures T_L and T_0, where T_0 is the temperature at the gas boundary, for $M_\infty = 0.78$. The distribution looks very much like a Maxwellian, and an effective temperature $T_\perp^+$ is calculated from $F^+(c_y)$. It looks as though $T_\perp^+$ corresponds to the local temperature somewhere in the interphase. This is also the case for other Mach numbers, see Table 6.4.

The normalized distribution function for the c_x-component of the incoming molecules has been plotted in Fig. 6.16 for $M_\infty = 0.3$ and $M_\infty = 0.78$ along with the Maxwellians given by least squares regression. The effective velocity u^- and temperature $T_{||}^-$ are listed in Table 6.4. The drift velocity u^- in the Maxwellian increases with M_∞, hence the distribution for $M_\infty = 0.78$ is more shifted to the right and has relatively more molecules with small incoming c_x-velocity than the $M_\infty = 0.3$ distribution. The distribution function for the c_y-component of the incoming molecules is well described by a Maxwellian, some values for the

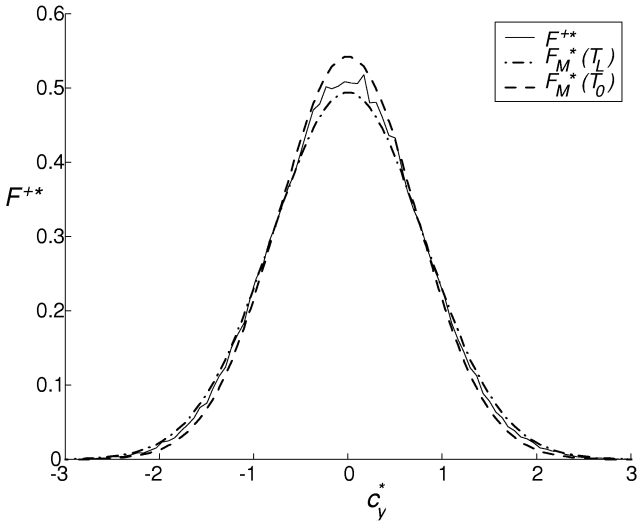

Figure 6.15: Distribution function at the interphase for the normal component of velocity

temperature $T_{\perp}^{-}$ is listed in Table 6.4.

M_∞	$T_{\|\|}^{+}/T_L$	$T_{\perp}^{+}/T_L$	$\frac{u^+}{\sqrt{2RT_L}}$	$\frac{u_0}{\sqrt{2RT_L}}$	$T_{\|\|}^{-}/T_L$	$T_{\perp}^{-}/T_L$	$\frac{u^-}{\sqrt{2RT_L}}$
0.25	0.86	0.95	0.17	0.19	0.91	0.93	0.22
0.41	0.84	0.94	0.21	0.28	0.86	0.90	0.39
0.73	0.75	0.93	0.30	0.37	0.70	0.83	0.43
0.83	0.71	0.93	0.35	0.38	0.73	0.84	0.50

Table 6.4: Effective temperatures and velocities for interphase distributions

There is no evidence of a discontinuity at $c_x = 0$ in $F(c_x)$ for low Mach numbers, but that should not be expected either, since we have effectively averaged the distribution function over a small interval. For $M_\infty > 0.75$ the results are inconclusive, a discontinuity shows in some plots.

To explain the deviation from the standard boundary condition in kinetic theory, it is tempting to use a "mean free path" argument. It is assumed that the molecules, on the average, bring with them the local drift velocity and temperature a mean free path away. Fig.6.17 shows the drift velocity in the interphase region, and Fig.6.10 shows the various temperatures. In the standard boundary condition it is implicit that an evaporating molecule does not collide in the interphase, but this is not a very realistic assumption. In the middle of the interphase the average distance between the molecules is just 1.38 r_0. Hence it is probable that both an evaporating and a reflecting molecule collide for the last time somewhere in the interphase before they cross the gas boundary. If

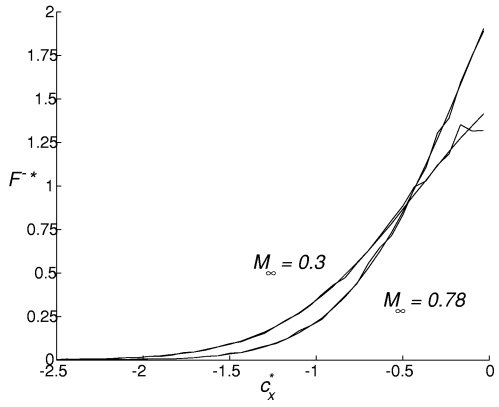

Figure 6.16: Distribution function for incoming molecules.

the mean free path argument is taken literally, the drift velocity as well as the parallel and normal temperatures of $F^+(\mathbf{c})$ should correspond to values in the interphase. At the edge of the interphase $T_{||}$ is smaller than T_0, $T_\perp$ is between T_L and T_0, and u is between 0 and u_0, which is consistent with the values for $T_{||}^+$, $T_\perp^+$ and u^+.

6.6.3 Evaporation and condensation distribution functions

Evaporating and reflecting molecules are tagged. In Fig.6.18 the velocity probability distribution for the evaporated molecules for the component of velocity parallel to the drift velocity, $F^e(c_x)$, is plotted for various M_∞ together with an average over all simulations. The distributions are normalized to 1 for $c_x > 0$. The plots are very similar, it looks like the normalized distribution for evaporation is independent of M_∞. Contrary to the assumption in most gas-kinetic calculations, F^e has a drift velocity away from the interphase. The average is not symmetric about the peak and a drifting Maxwellian gives a rather poor fit.

Fig.6.19 shows the probability distribution for the component of velocity parallel to the drift velocity for the reflected molecules, $F^r(c_x)$ is plotted for various M_∞ along with the average over all simulations. All distributions are normalized to 1 on $c_x > 0$. The plots are again similar, the normalized distribution for reflection is rather independent of M_∞, except for very small c_x, but that is not so important since it is the flux $c_x f^r$ that is used in implementation of the boundary condition. The average looks similar to a Maxwellian with a drift velocity towards the interphase, but least squares regression with a drifting Maxwellian gives a poor fit. This is not unexpected: if F^e and F^r really are independent of M_∞, then they should not be Maxwellians since the sum of two Maxwellians with different drift velocity can not give a Maxwellian with zero drift velocity in equilibrium.

The shape of F^r in Fig. 6.19 shows that reflecting molecules are not 'ther-

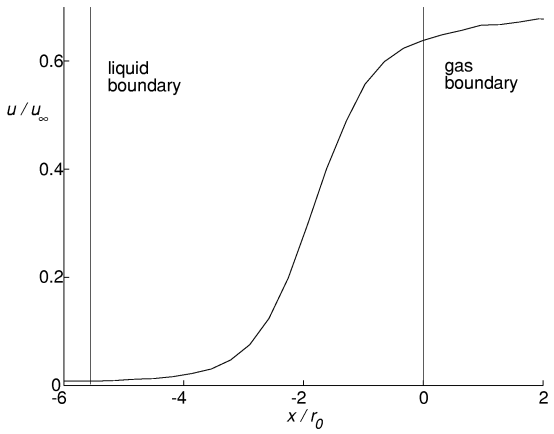

Figure 6.17: Drift velocity in the interphase region.

malized' in the interphase before they are reflected. The form of F^r is similar to what would be expected for high Mach numbers if reflection were specular for evaporation, but F^r has the same shape also for condensation, see Fig. 7.10 on page 100. Besides, reflection can neither be specular nor diffuse or a combination in equilibrium, since it would imply in all cases a Maxwellian with zero drift velocity for the reflection mode, contrary to our results. Tsuruta[93] has also reported similar shifts for the differential flux $\Phi \sim c_x F$ for evaporation and condensation.

We have also calculated the evaporation and condensation velocity distributions when the gas and liquid boundaries have been moved arbitrarily a couple of σ's. The general shape of shifted evaporation and condensation distributions was always observed.

M_∞	χ_e	n^r/n_s	χ_r
0.097	0.29	0.17	0.22
0.20	0.32	0.13	0.24
0.30	0.33	0.10	0.27
0.41	0.34	0.08	0.28
0.52	0.34	0.07	0.29
0.62	0.34	0.06	0.32
0.73	0.34	0.06	0.33
0.78	0.34	0.06	0.33
0.83	0.33	0.06	0.36
0.90	0.34	0.06	0.35
0.94	0.34	0.06	0.36

Table 6.5: Evaporation and reflection mode densities

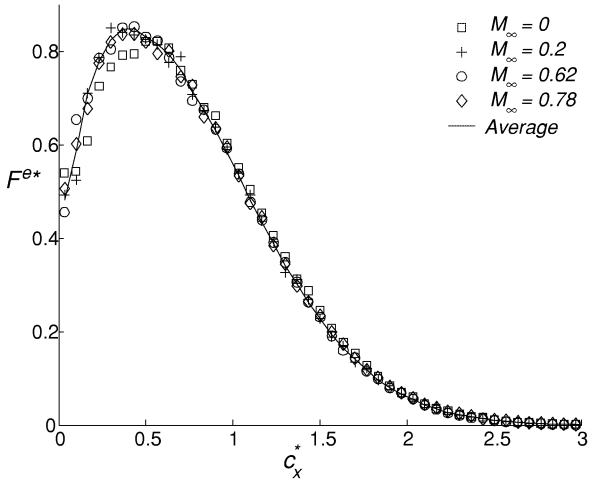

Figure 6.18: Evaporation mode for various Mach numbers.

Number densities for the evaporated and reflected molecules can be calculated, $n^+ = n^e + n^r$, i.e. the density of the molecules escaping from the interphase. The probability distributions in Figs. 6.14, 6.18 and 6.19 are related by

$$f^+ = n^+ F^+ = n^e F^e + n^r F^r \tag{6.41}$$

It is convenient to tabulate n^e in terms of n_s and a dimensionless constant χ_e defined as

$$\chi_e = \frac{n^e}{n_s} \tag{6.42}$$

n^r is proportional to the reflected flux, and hence a reference density for the reflection mode that scales as J^r ought to be used. That quantity is not available and $n_i = J^-/\sqrt{\frac{RT_L}{2\pi}}$ is used instead. If the condensation coefficient were constant, then J^r would be proportional to J^-. This is not the case, and the derived quantity

$$\chi_r = \frac{n^r}{n_i} = n^r \sqrt{\frac{RT_L}{2\pi}}/J^- \tag{6.43}$$

will depend upon M_∞. n^r/n_s is also tabulated since it indicates the diminishing influence of reflected molecules for high Mach numbers. The factor $\chi_e = n^e/n_s$ is almost independent of M_∞, hence the complete evaporation distribution function $f^e = \chi_e n_s F^e$ can be regarded to be constant, independent of the Mach number. It is only the dependence of χ_r on M_∞ that makes f^+ depend on M_∞.

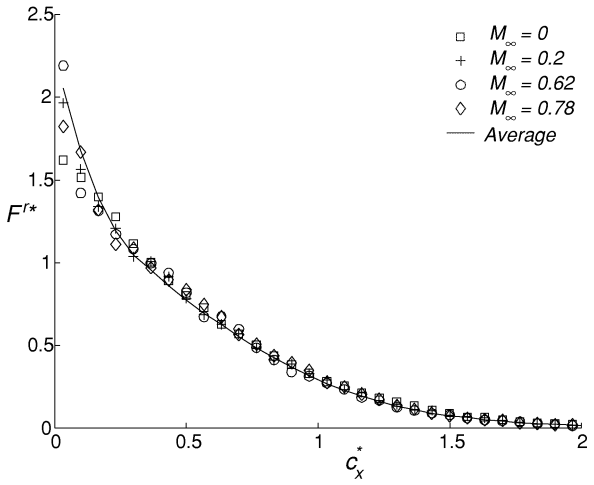

Figure 6.19: Reflection mode for various Mach numbers.

6.6.4 Interpretation of the evaporation and reflection modes

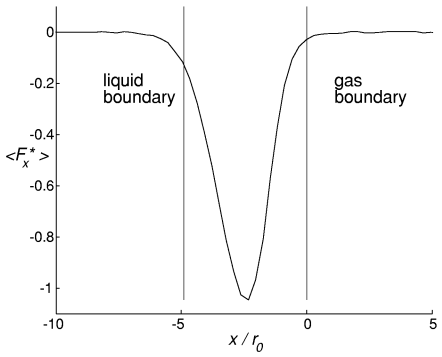

Figure 6.20: Mean force on the molecules

The shift in f^+ can be 'explained' from the fact that the evaporation mode dominates over the reflection mode in evaporation, n^e is much larger than n^r. The shifts in the evaporation and reflection distributions are harder to understand quantitatively, but they may be related to collisional effects in the interphase region, as already suggested at the end of section 6.6.2. It is obvious that the assumed form for the evaporation mode used in most gas-kinetic calculations, nondrifting half Maxwellian with the liquid temperature, can not be correct. Then the interaction the molecules experience while passing through the interphase is completely neglected. The molecules in the interphase experience

a mean force towards the liquid, due to the collective effect of increasing number of molecules towards the liquid side, see Fig. 6.20. A molecule that evaporates has to cross a potential barrier. Assume for the moment that there is no noise in the mean force, which corresponds roughly to the fact that there are no repulsive collisions, only the smooth longer range attraction. The molecules that cross the liquid boundary into the interphase have approximately a half Maxwellian distribution for the velocity normal to the interphase. Only those molecules that have a c_x-velocity such that the kinetic energy contribution from c_x, $1/2mc_x^2$, is larger that the potential difference, can cross the interphase and evaporate. The distribution for evaporated molecules is then the rescaled right tail of a Maxwellian with drift velocity towards the interphase. But we now argue that collisions in the interphase lead to a depletion of small velocities and hence the distribution looks more like a Maxwellian with a drift velocity away from the interphase. Fast molecules are less likely than slow molecules to be scattered significantly, this can be measured by the velocity dependent viscosity or momentum cross sections which are roughly equal to the classical cross section $\pi r_c^2/r_0^2$ for small relative velocities $g^* << 1$, but smaller than $\pi r_0^2/r_0^2 = \pi$ for $g^* >> 1$. r_0 is the relative distance where the potential changes from negative to a positive value. A molecule that has diffused out into the interphase where the density is lower, may escape into the gas if it has kinetic energy greater than the remaining potential barrier. The last obstacle is collisions with other molecules at the edge of the interphase. A slow molecule experiences attractive forces for a longer time during an encounter with an other molecule than a fast one, hence the slow molecule can be drawn so close to the colliding partner that they repulse each other, i.e. they have a large cross section. A fast molecule is less likely to experience a head-on collision at the edge of the interphase and it will retain a greater share of its original kinetic energy after the binding energy has been subtracted. Hence the peak of the distribution function for evaporated molecules is shifted towards higher velocities.

The shape of the reflection distribution may be explained in a similar way. Fast gas molecules entering the interphase have smaller cross sections and are more likely to penetrate far into the interphase, where the density is higher, before undergoing the first 'head on' repulsive interaction. Since the density is higher, it is likely that the incoming molecule will scatter several times and lose its kinetic energy. This is consistent with the condensation probability being larger for molecules with large velocity normal to the interphase, see the condensation probability $\sigma_c(c_x)$ in Fig. 6.22. An incoming molecule with small velocity is more likely to collide with a molecule at the edge of the interphase that also has small velocity. They will attract each other and then scatter significantly due to the repulsive short range force. One or a few such collisions may reflect the incoming molecule out of the interphase and the molecule has on the average not gained more kinetic energy and hence most reflected molecules have low velocity and the reflection distribution function looks more like a Maxwellian with drift velocity towards the interphase.

If this interpretation was correct, the majority of the molecules should be reflected at the edge of the interphase. That is not completely true. Fig.6.21

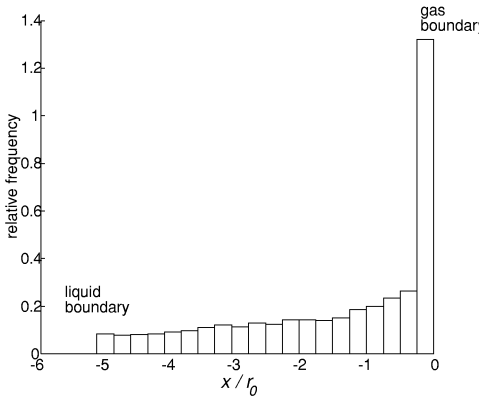

Figure 6.21: Frequency plot of the innermost position in the interphase of reflected molecules

shows a typical frequency plot of the innermost position in the interphase of molecules that are reflected. Although the highest probability is that a molecule is reflected just inside the interphase, half of the molecules penetrate further inside before they are reflected back into the gas.

6.6.5 Condensation probability and velocity dependent coefficients

It has been shown by Tsuruta[93] that the condensation probability is velocity dependent, contrary to the usual assumption in gas-kinetic calculations. The higher the velocity normal to the interphase is, the higher is the probability for condensation, which is a reasonable result. In gas-kinetic calculations the condensation probability is assumed to be a constant, equal to the condensation coefficient.

If σ_e and σ_c are defined from the conventional boundary condition, Eq.(2.4), in terms of non-drifting Maxwellians, the coefficients will be velocity dependent.

$$f^e(\mathbf{c}) = n^e F^e = \sigma_e(c_x) n_s F_s(\mathbf{c}) \quad (6.44)$$

$$f^r(\mathbf{c}) = n^r F^r = [1 - \sigma_r(c_x)]\, n_u F_s(\mathbf{c}) \quad (6.45)$$

The redefined coefficients take into account the deviation from a Maxwellian with no drift velocity for the c_x-probability distributions and give the correct number density. The c_y- and c_z-distributions are not affected, they are the standard Maxwellian distribution with temperature T_L. This is only an approximation, as can be seen from Table 6.4, $T_\perp^+$ is 5-10% lower than T_L. The reference density n_u has not been specified but it should be equal to n_s in equilibrium.

We have used the term 'reflection' coefficient since it is not immediately apparent that the reflection coefficient in general is equal to the condensation

probability, i.e. velocity dependent condensation coefficient. However, in equilibrium

$$f^+ = [\sigma_e(c_x) n_s(T_L) + (1 - \sigma_r(c_x))\, n_u]\, F_s = n_s F_s \tag{6.46}$$

and $n_u = n_s$, hence $\sigma_e(c_x) = \sigma_r(c_x)$. In equilibrium the evaporation and condensation fluxes are equal.

$$\int_{c_x>0} c_x \sigma_e(c_x) n_s F_s dc_x = \int_{c_x<0} \sigma_c(|c_x|)\, |c_x|\, n^- F^- dc_x \tag{6.47}$$

Also $n_s F_s = n^- F^-$, and $\sigma_c(c_x) = \sigma_e(c_x) = \sigma_r(c_x)$ in equilibrium. The surprising result of non-Maxwellian distribution functions for evaporation and condensation is equivalent to a velocity dependent condensation probability, which is plausible.

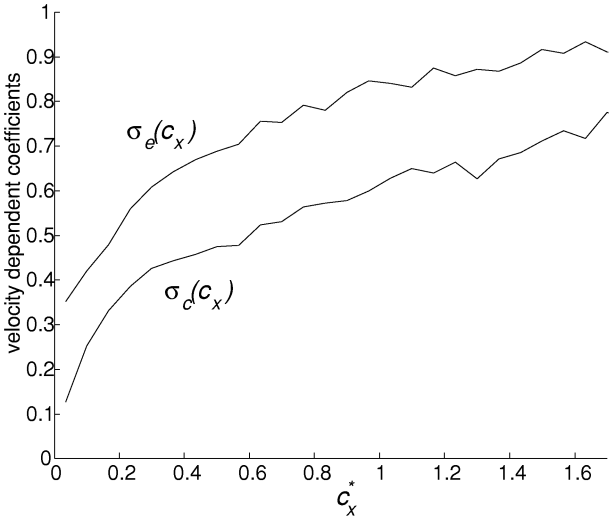

Figure 6.22: Velocity dependent coefficients for the case of $M_\infty = 0.78$.

It is sometimes claimed that $\sigma_c(c_x) = \sigma_e(c_x)$ also in nonequilibrium[101],[102], but to the best of our knowledge a proof is still lacking. Our simulations indicate that the velocity dependent coefficients are not equal outside equilibrium. In Fig. 6.22, $\sigma_e(c_x)$ and $\sigma_c(c_x)$ have been plotted for $M_\infty = 0.78$.

The condensation and evaporation coefficients listed in Table 6.3 should be interpreted as the average condensation probability and the average evaporation coefficient.

$$\overline{\sigma}_c = \frac{\int\limits_{c_x<0} \sigma_c(|c_x|)|c_x| f^- d\mathbf{c}}{\int\limits_{c_x<0} |c_x| f^- d\mathbf{c}} \tag{6.48}$$

$$\overline{\sigma}_e = \frac{\int\limits_{c_x>0} \sigma_e(c_x) c_x f_s d\mathbf{c}}{\int\limits_{c_x>0} c_x f_s d\mathbf{c}} \tag{6.49}$$

6.6.6 Representation of the boundary condition

Our simulations indicate that there is no simple representation of the distribution function just outside of the interphase. The evaporation distribution $f^e(c_x) = n^e F^e$ and the normalized reflection distribution $F^r(c_x)$ are roughly independent of M_∞. They are probably dependent upon the liquid temperature and the type of substance, but this has not been checked. $F^+(c_\perp)$ is a Maxwellian with a temperature slightly less than T_L, but the deviation will be neglected. The best representation of the boundary condition outside the interphase seems to be

$$\begin{aligned} f^+(\mathbf{c}) &= n^+ F^+ \approx \left[n^e F^e(c_x) + n^r F^r(c_x)\right] F_M(c_y, c_z, T_L) \\ &= \left[\chi_e n_e F^e + \chi_r n_i F^r\right] F_M(c_y, c_z, T_L) \end{aligned} \tag{6.50}$$

where χ_e is independent of M_∞. Values for χ_e and χ_r are given in Table 6.5 for the Lennard-Jones-spline potential. The 'base functions' F^e and F^r must also be parameterized.

An alternative way is suggested by Figs.6.14 and 6.15. The distribution function may be approximated with

$$f^+ = n^+ F^+ = \left[n_s \sigma_{micro} + (1 - \sigma_{micro}) n_i\right] F_M(c_x, u^+, T_{||}^+) F_M(c_y, c_z, T_L) \tag{6.51}$$

Some values for u^+ and $T_{||}^+$ are given Table 6.4.

6.7 Conclusion

The evaporation algorithm presented makes it possible to do molecular dynamics simulations for net evaporation for arbitrary Mach number below 1. It is then feasible to do comparisons between molecular dynamics simulations and results from gas-kinetic calculations, and in addition verify if the conventional boundary condition used in most gas-kinetic calculations is accurate.

The simulated temperature ratio T_∞/T_L as a function of the Mach number agrees very well with gas-kinetic calculations. Contrary to a common approximation, the average condensation and evaporation coefficients found are not

equal outside equilibrium, the condensation coefficient decreases with increasing Mach number, the evaporation coefficient increases with increasing Mach number. A significant drift velocity shows in $f^+(c_x)$ that can not be neglected, it is comparable to the drift velocity at the gas boundary. The evaporation and reflection distribution functions deviate from the conventional representation as nondrifting half-Maxwellians, the evaporation mode has a drift velocity away from the interphase, and the reflection mode has a drift velocity towards the interphase. However, the evaporation and reflection velocity probability functions appear to be independent of the Mach number.

If the observed form of the distribution function f^+ can be extrapolated to weak conditions, the gas-kinetic prediction for an inverted temperature profile in chapter 4, based upon nondrifting Maxwellians, may not be correct.

Acknowledgement 2 *Financial support from the Norwegian Council of Research and the Italian State, and CPU time at the department of Chemistry, NTNU, and NOTUR's supercomputers, are gratefully acknowledged.*

Chapter 7

Strong Condensation

7.1 Introduction

The case of net condensation of a vapor on a liquid surface is of equal importance as is evaporation, and the gas-kinetic formulations of the two problems have been developed more or less in parallel over the last three decades. The nonlinear case of strong condensation was considered in various moment solutions by Labuntsov & Kryukov[96], Hatakeyama & Oguchi[97] and Ytrehus and Alvestad[17]. Sone *et al.* [87] and Aoki *et al.*[21] used numerical solutions of the BKW equation and Kogan and Abramov[68] used DSMC to find the existence region for steady condensation in a half-space. If the condensation coefficient is less than approximately 0.97, subsonic condensation solutions do not exist above a critical Mach number, this is the so-called blocking effect[68],[24].

The interphase between the gas and its condensed phase is typically a couple of molecular diameters wide, and molecular dynamics (MD) simulation[37] is hence ideally suited. Tsuruta[93] used molecular dynamics to simulate stationary evaporation and condensation between two liquid slabs kept at different temperatures. Hafskjold[98] simulated condensation on a liquid film with molecules inserted in a 'molecule reservoir' a couple of mean free paths from the interphase to maintain steady condensation flux.

Here only condensation of a gas in an infinite half-space will be considered. At asymptotically large distances from the interphase the flow parameters reach uniform values. The Boltzmann equation (2.1) together with Eq.(2.4) at the interphase and a drifting Maxwellian at infinity, $n_\infty F_M(T_\infty,u_\infty)$, as boundary conditions, has been solved by a variety of methods. From numerical simulation of the BKW and Boltzmann equations for $\sigma = 1$ it has been inferred that two parameters in steady condensation can be held fixed, for instance the temperature ratio between the gas and the liquid, and the pressure ratio or the velocity at infinity[21],[67], [68].

7.2 Effect of nonunity condensation coefficient

For $\sigma_e, \sigma_c \neq 1$ and diffuse reflection, values for $\frac{n_s}{n_\infty}$ can be found from an equivalent $\sigma = 1$ solution. For evaporation this was shown from the moment solution but it results from a general transformation[89],[90], [24]. This is seen from the boundary condition, Eq.(2.4). The $\sigma_e, \sigma_c \neq 1$ and $\sigma = 1$ solutions are identical if the saturation density $n_s^{\sigma=1}$ of the latter is given by

$$n_s^{\sigma=1} = \sigma_e n_s + (1-\sigma_c) n_i = \sigma_e n_s + (1-\sigma_c) J^- \sqrt{\frac{2\pi}{RT_L}} \tag{7.1}$$

The solutions are identical in all respects, except for quantities depending upon n_s, which is different in the two cases. The number flux at the interphase is

$$J = \int\limits_{c_x>0} c_x f^+ dc + \int\limits_{c_x<0} c_x f^- dc \tag{7.2}$$

The first integral can be evaluated from the assumed form of the boundary distribution function, Eq. (2.4), the second we denote by J^-. The number flux at infinity is $n_\infty u_\infty$ and

$$n_s^{\sigma=1} \sqrt{\frac{RT_L}{2\pi}} - J^- = n_\infty u_\infty \tag{7.3}$$

Since J^- is the same, Eq.(7.1) simplifies to

$$\sigma_c n_s^{\sigma=1} = \sigma_e n_s - (1-\sigma_c) \sqrt{\frac{2\pi}{RT_L}} n_\infty u_\infty \tag{7.4}$$

Dividing by n_∞ we have

$$\frac{n_s}{n_\infty} = \frac{\sigma_c}{\sigma_e} \left(\frac{n_s}{n_\infty} \right)_{\sigma=1} + \frac{1-\sigma_c}{\sigma_e} 2\sqrt{\pi} \sqrt{\frac{T_\infty}{T_L}} S_\infty \tag{7.5}$$

$$= \frac{\sigma_c}{\sigma_e} \left(\frac{n_s}{n_\infty} \right)_{\sigma=1} + \frac{1-\sigma_c}{\sigma_e} \sqrt{\frac{10\pi}{3}} \sqrt{\frac{T_\infty}{T_L}} M_\infty \tag{7.6}$$

Eq.(7.5) is identical to the transformation rule for evaporation derived directly from a moment solution, Eq.(6.25), but for condensation the speed ratio $S_\infty = \frac{u_\infty}{\sqrt{2RT_\infty}}$ and the Mach number $M_\infty = \frac{u_\infty}{\sqrt{\gamma RT_\infty}}$ are negative. For monatomic ideal gases the ratio of the heat capacities $\gamma = c_p/c_v$ equals 5/3 and $M_\infty = \sqrt{\frac{6}{5}} S_\infty$. Eq.(7.5) can be used in two different ways. If we stipulate that the solutions are equal, then the equation gives the connection between n_s for nonunity coefficients and $n_s^{\sigma=1}$ for $\sigma = 1$. But we can also keep n_s, and for instance S_∞

and $\frac{T_\infty}{T_L}$ constant and vary the coefficients, the solutions are then no longer equivalent and n_∞ will change. If we hold S_∞ and T_∞/T_L constant and assume that $\sigma_e = \sigma_c = \sigma$, then the effect of the transformation is easy to predict. For condensation, if σ decreases, the effect is :

$$\begin{aligned} n_s \text{ fixed} &\implies n_\infty \text{ increases} \\ n_\infty \text{ fixed} &\implies n_s \text{ decreases} \end{aligned}$$

For evaporation, if σ decreases, the effect is :

$$\begin{aligned} n_s \text{ fixed} &\implies n_\infty \text{ decreases} \\ n_\infty \text{ fixed} &\implies n_s \text{ increases} \end{aligned}$$

For the one-dimensional evaporation problem properties like the density ratio, pressure ratio and mass flux does not depend much upon the type of kinetic equation (Boltzmann or BKW) or intermolecular potential used as long as the condensation coefficient is the same. But the relaxation rate towards the uniform state at infinity differs[86]. We will assume that the same applies for the one dimensional condensation problem also, hence $\left(\frac{n_s}{n_\infty}\right)_{\sigma=1} = g(S_\infty, \frac{T_\infty}{T_L})$ can be calculated from numerical solution of the simpler BKW equation instead of DSMC[23] solution of the Boltzmann equation.

The number flux J for condensation is given approximately by the Schrage expression[48],[24]

$$\begin{aligned} J(T_L, T_\infty, S_\infty, \sigma_e, \sigma_c) &= \sigma_e n_s \sqrt{\frac{RT_L}{2\pi}} - \sigma_c n_\infty \sqrt{\frac{RT_\infty}{2\pi}} E^-(S_\infty) \quad (7.7) \\ &= \sigma_e n_s \sqrt{\frac{RT_L}{2\pi}} - \sigma_c n_\infty \sqrt{\frac{RT_\infty}{2\pi}} E^+(|S_\infty|) \quad (7.8) \end{aligned}$$

where n_∞ is given by Eq.(7.5) and

$$\begin{aligned} E^+(S_\infty) &= \sqrt{\pi} S_\infty (1 + \operatorname{erf} S_\infty) + e^{-S_\infty^2} \quad (7.9) \\ E^-(S_\infty) &= \sqrt{\pi} S_\infty (-1 + \operatorname{erf} S_\infty) + e^{-S_\infty^2} \quad (7.10) \end{aligned}$$

Here we have used $E^-(S_\infty) = E^+(-S_\infty)$, since S_∞ is negative for condensation.

There is a transformation of the number flux similar to the transformation for number density[24]. First it is assumed that all quantities except the saturation density are equal. From Eq.(7.4) we have

$$\begin{aligned} J_s &= n_s(T_L)\sqrt{\frac{RT_L}{2\pi}} = \left[\frac{\sigma_c}{\sigma_e}(n_s)_{\sigma=1} + \frac{1-\sigma_c}{\sigma_e} 2\sqrt{\pi}\sqrt{\frac{T_\infty}{T_L}} \frac{n_\infty u_\infty}{\sqrt{2RT_\infty}}\right] \sqrt{\frac{RT_L}{2\pi}} \\ &= \frac{\sigma_c}{\sigma_e}(J_s)_{\sigma=1} + \frac{1-\sigma_c}{\sigma_e} J \quad (7.11) \end{aligned}$$

and

$$\frac{J_s}{J} = \frac{\sigma_c}{\sigma_e}\left(\frac{J_s}{J}\right)_{\sigma=1} + \frac{1-\sigma_c}{\sigma_e} \tag{7.12}$$

$\left(\frac{J}{J_s}\right)_{\sigma=1}$ is a function of $\frac{p_\infty}{p_s}$ or S_∞, and $\frac{T_\infty}{T_L}$, but the dependence upon $\frac{T_\infty}{T_L}$ is weak[24]. It is more interesting to keep n_s and hence J_s constant and see what happens to J when the coefficients are varied for the same values of S_∞ and $\frac{T_\infty}{T_L}$. If $\sigma_e = \sigma_c = \sigma$, it is easy to see that the absolute value of the number flux for $\sigma < 1$ is always less than for $\sigma = 1$.

For diffuse reflection of molecules at the interphase, the Knudsen layer structure for $\sigma \neq 1$ can be found from an equivalent $\sigma = 1$ solution with $n_s^{\sigma=1}$ given by Eq.(7.1). But if λ_s is used to make the distance nondimensional, the relaxation rate will depend upon σ_e and σ_c since n_s and $n_s^{\sigma=1}$ are different. The mean free path is related to the ideal $\sigma = 1$ case by Eq.(6.27) derived in chapter 6, here repeated

$$\lambda_s = \frac{1}{\sqrt{2} n_s \pi d_{eff}^2} = \frac{(n_s/n_\infty)_{\sigma=1}}{n_s/n_\infty}\lambda_s^{\sigma=1} \tag{7.13}$$

If the evaporation and condensation coefficients are equal, $\sigma_e = \sigma_c = \sigma$, for condensation $\sigma < 1$ gives a compression of the graphs in the x-direction (active viewpoint) relative to the $\sigma = 1$ solution, or equivalently a stretch of the x/λ_s-axis (passive viewpoint). For evaporation the situation is opposite.

To test the transformation of the Knudsen layer for condensation, two DSMC simulations are performed for the same Mach number ($M_\infty = -0.284$) and temperature fraction ($T_\infty/T_L = 1.63$), but different σ. In the first simulation $\sigma = 1$ and in the second $\sigma = 0.85$. Then $\frac{(n_s/n_\infty)_{\sigma=1}}{n_s/n_\infty} \approx 1.3$ and the $\sigma = 1$ solution compressed in the x-direction by a factor 1.3 overlaps the direct $\sigma = 0.85$ simulation, see Fig. 7.1, the small discrepancy is due to statistical noise in the DSMC simulations. All solutions related by the transformation would be equal if they were plotted on a x/λ_∞-scale instead of x/λ_s-scale.

7.3 Molecular Dynamics Simulations

7.3.1 Simulation box

As for evaporation, the simulation is conducted in a elongated box so the gas region can be relatively long with the number of liquid molecules limited. Fig. 4.5 shows a snapshot of the configuration in an equilibrium simulation. The ratio between the temperatures far out in the gas and in the middle of the liquid is $\frac{T_\infty}{T_{liq}} = 1.75$ in all simulations. The ratio between length and width has been varied from 30 for moderate Mach numbers to 80 for lowest Mach number

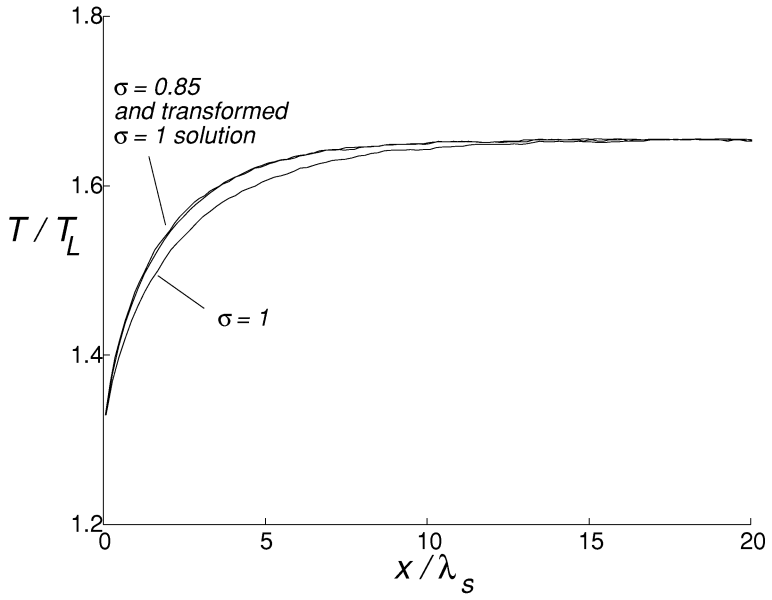

Figure 7.1: Test of transformation, $\sigma = 0.85$ compared with transformed $\sigma = 1$ solution.

simulated, $M\infty = -0.11$. The drift velocity 'compresses' the nonuniform region in condensation.

In the middle of the liquid the temperature is kept fixed by a thermostat. The thermostat has been implemented by a crude method, the velocity is rescaled to give the desired temperature. A temperature gradient keeps the liquid in the middle of the box, but fluctuations of the center of mass of the liquid can still be larger than the width of the interphase. Such behavior would 'smear out' density profiles, etc., in the interphase. Therefor the liquid slab is kept in the middle by shifting the x-coordinates, this does not change the relative distance between the molecules. The shifting is determined by the requirement that there shall be an equal number of molecules in both halves of the box. Molecules that are moved outside of the x-boundaries in the centering algorithm are inserted on the opposite side with the opposite x-component of velocity since the drift velocities in the two halves are opposite.

7.3.2 Condensation algorithm

Two parameters in steady condensation can be fixed, here the temperature ratio between the gas and the liquid and the velocity at infinity are chosen. In the gas regions there is a flow towards the liquid, i.e. the drift velocities are opposite in the two parts of the box. The density, temperature and velocity in the gas phase varies in the x-direction until a uniform state is reached far from the interphase.

It is the boundary conditions that sets up the condensation flow. A molecule crossing boundaries with y or z constant can be treated as in the equilibrium case, it is inserted on the opposite side with the velocity retained. 'Periodic' interactions across y or z cell boundaries are also correct since the neighboring molecules experience the same environment, macroscopic variables as temperature and drift velocity should on the average be equal. But a molecule close to the boundary x-constant interacts with neighbors in the adjacent box with opposite drift velocity. This is not correct and an error is introduced, the effect of this 'quasi periodic' boundary condition will be discussed later. There is no velocity scaling thermostat in the gas phase, the temperature there is set by specifying the distribution for the molecules inserted.

In simulation of condensation, the liquid is used as a molecule reservoir to replace the gas molecules that have condensed. Particles are removed from the liquid and inserted in the gas phase to exactly cancel the net condensation flux. The molecules must be inserted in the gas with a Maxwellian distribution with a given temperature and velocity. The problem is then how often molecules should be moved, since we already have fixed two parameters, the condensation flux can not be specified.

We now look at the left half of the simulation box in Fig. 4.5 , the treatment of the other half differs only in the sign of the x-component of the velocity. For the left half the drift velocity u_∞ and condensation flux are positive. The gas phase has length L, where L is big enough so the fluid reaches the equilibrium conditions far out in the gas phase, here denoted ∞. The distribution function far from the interphase should be a drifting Maxwellian with temperature T_∞ and drift velocity u_∞.

$$F_\infty(\mathbf{c}) = \frac{1}{(2\pi RT_\infty)^{\frac{3}{2}}} e^{-\frac{(c_x-u_\infty)^2+c_y^2+c_z^2}{2RT_\infty}} \tag{7.14}$$

The velocity distribution for molecules inserted at the left end of the box is hence the corresponding normalized differential flux[23], for $c_x > 0$ we have

$$\begin{aligned} \Phi(c_x) &= \frac{c_x F_\infty(c_x)}{\int\limits_{c_x>0} c_x F_\infty dc_x} \qquad (7.15) \\ &= \frac{c_x}{\left[\frac{u_\infty}{2} + \sqrt{\frac{RT_\infty}{2\pi}} e^{-\frac{u_\infty^2}{2RT_\infty}} + \frac{1}{2} u_\infty \operatorname{erf}(\frac{u_\infty}{\sqrt{2RT_\infty}})\right]} \frac{1}{(2\pi RT_\infty)^{\frac{1}{2}}} e^{-\frac{(c_x-u_\infty)^2}{2RT_\infty}} \end{aligned}$$

For the right boundary, the negative of samples from $\Phi(c_x)$ are used. The probability distribution for tangential components of velocities are the standard Maxwellians. Samples from this distribution is generated by the acceptance-rejection method[23], then $\Phi/\Phi^{\max}$ must be calculated. The maximum value of Φ is attained for a value $c_x^{\max}$

$$c_x^{\max} = \frac{u_\infty}{2} + \frac{1}{2}\sqrt{u_\infty^2 + 4RT_\infty} \tag{7.16}$$

and we have

$$\frac{\Phi}{\Phi^{\max}} = \frac{c_x \exp\left(-\frac{(c_x-u_\infty)^2}{2RT_\infty} + \frac{1}{2} - \frac{u_\infty}{2\sqrt{2RT_\infty}}\sqrt{\frac{u_\infty^2}{2RT_\infty}+2} + \frac{u_\infty^2}{4RT_\infty}\right)}{\left(\frac{u_\infty}{2} + \frac{1}{2}\sqrt{u_\infty^2 + 4RT_\infty}\right)} \tag{7.17}$$

Since only two parameters can be specified in condensation, here chosen to be T_∞/T_L and u_∞, the net mass flux can not be specified and is a result of the molecular dynamics simulation. The fluxes of molecules entering and leaving the left boundary are

$$J^{in} = \int_{c_x>0} c_x n_\infty F_M(u_\infty, T_\infty) d\mathbf{c} \tag{7.18}$$

and

$$J^{out} = \int_{c_x<0} |c_x| n_\infty F_M(u_\infty, T_\infty) d\mathbf{c}. \tag{7.19}$$

J^{in} and J^{out} are here defined to be positive. The molecule density at infinity, n_∞, is unknown, but it does not appear in the fraction J^{in}/J^{out},

$$x = \frac{J^{in}}{J^{out}} = \frac{|S_\infty|\sqrt{\pi} + \mathrm{erf}(|S_\infty|)|S_\infty|\sqrt{\pi} + e^{-S_\infty^2}}{-|S_\infty|\sqrt{\pi} + \mathrm{erf}(|S_\infty|)|S_\infty|\sqrt{\pi} + e^{-S_\infty^2}} \tag{7.20}$$

Here $S_\infty = \frac{u_\infty}{\sqrt{2RT_\infty}}$, the speed ratio. Absolute values have been used since u_∞ is defined positive for evaporation and negative for condensation. J^{in}/J^{out} is only a function of T_∞ and u_∞, which are specified in advance. Instantaneous values of J^{out} is calculated and averaged over a short period so rapid fluctuations are absent, in this work an averaging interval of $\Delta t^* = 200$ was used.

The molecules crossing the vertical boundary of the box are inserted immediately with new velocities drawn from the distribution $\Phi(\mathbf{c})$. The flux of molecules that is moved from the liquid to the gas is equal to the net flux

$$J = J^{in} - J^{out} = J^{out}(x-1) \tag{7.21}$$

and the same for the right part. The moves are implemented as a Poisson process, for every step there is a probability that a molecule will be moved such that on the average the correct flux is achieved.

The simulation is started with the molecules in a lattice or in an old configuration for a different state, if it is available. In our simulation the number of molecules and the average density are specified. If a lattice is used, an auxiliary high temperature, velocity rescaling thermostat in the 'gas end' of the box is used in the beginning together with the thermostat in the liquid to set up a two-phase system. To speed up the formation of an initial liquid layer, all molecules in the simulation box can be thermostatted with a staircase temperature profile. Then the condensation algorithm described above is activated. The system needs considerable time to relax to the steady state. This can be seen for instance from the number of liquid molecules plotted as a function of time. As a rule of thumb the start-up period is 10 times the time it takes for a soundwave to travel through the gas phase. The start-up period is not included when the macroscopic quantities are sampled. The box must be so long that the gas relaxes to a uniform state, the uniform region should be at least a couple of mean free paths.

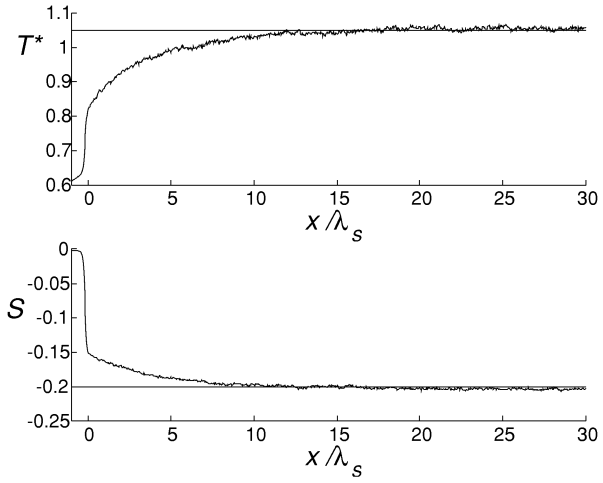

Figure 7.2: Molecular dynamics simulation of condensation

A trial simulation to test the algorithm was performed with $T^*_{liq} = 0.6$, $T^*_\infty = 1.05$ and $|S_\infty| = 0.2$. The temperature profile from the simulation and the dimensionless drift velocity $S = \frac{u}{\sqrt{2RT_\infty}}$ are shown in Fig. 7.2. $\lambda_s = \frac{\mu(T_L)}{mn_s}\sqrt{\frac{\pi}{2RT_L}}$ is a reference mean free path, n_s is the saturation density, i.e. gas density in two-phase equilibrium, and μ is the viscosity for the Lennard-Jones-spline potential. The set temperature in the gas was attained but the speed ratio overshoots 2% the set value. This may be an effect of the fact that the interactions are not represented correctly at the constant x boundary, there is an interaction between molecules with opposite drift velocity. The forces are not 'periodic' in the x-direction, but this feature was retained from the equilibrium

$\|M_\infty\|$	$\|J\|/J_s$	T_∞/T_L	T_0/T_L	n_∞/n_s	$(n_\infty/n_s)_{\sigma=1}$	n_0/n_s	λ_s/r_0
0.11	0.32	1.73	1.15	0.68	0.73	1.06	12.6
0.17	0.54	1.72	1.23	0.77	0.82	1.11	11.1
0.22	0.85	1.68	1.31	0.92	0.95	1.24	9.2
0.25	1.07	1.69	1.34	1.01	1.01	1.33	9.5
0.28	1.34	1.65	1.35	1.15	1.10	1.48	8.3
0.31	1.62	1.68	1.39	1.24	1.16	1.57	9
0.35	2.08	1.66	1.45	1.46	1.27	1.76	8

Table 7.1: Simulation results for condensation

implementation because it makes the programming easier. Of course an infinite box can not be simulated. An alternative way would be to completely remove the periodic force in the x-direction, as though there were no molecules outside the vertical boundary, but that would introduce an error of the same order, as was also evident in a test simulation. How to achieve the set speed ratio was not resolved. But quasi-periodic boundary conditions gives profiles that are stationary and flat far from the interphase as they should be. Hence, the solutions should be valid for the new speed ratio that deviates slightly from the set value, and this approach is used in all calculations henceforth. For the simulations shown in Fig. 7.2, $S_\infty = -0.204$ is the achieved value. For larger S_∞, the deviation increases, for a set value $|S_\infty| = 0.3$ the attained speed ratio is 5% larger than the set value.

7.4 Results

We have performed 7 molecular dynamics simulations of net condensation, covering Mach numbers from -0.11 to -0.35, for $T_\infty/T_{liq} = 1.75$. The ratio between length and width has been varied from 30 for moderate Mach numbers to 80 for low Mach number, the drift velocity 'compresses' the nonuniform region in condensation. The number of molecules varied from 2700 for simulation with moderate Mach numbers to 8600 for the smallest Mach number simulated, $M_\infty = 0.11$. We did not attempt to simulate smaller Mach numbers since a finite large temperature difference and small drift velocity makes the nonuniform region very long. The time interval of sampling after steady state was reached, was typically $t^* = 30000$. The target temperature of the thermostat in the liquid was $T^*_{liq} = 0.6$ in all simulations. T^*_L, the liquid temperature used in gas-kinetic calculations and here associated with the temperature at the liquid boundary in MD simulations, is slightly higher and varies in simulations due to heat conduction in the liquid and the fact that the thickness of the liquid layer is not the same in all simulations.

Various characteristics of the simulations have been tabulated in Tables 7.1 and 7.2. x^U_{99} is the position where $u(x) = 0.99u_\infty$. x_∞ is the length of the gas phase and the position where the boundary conditions are applied. $\delta_\infty = n_\infty^{-1/3}$

$\|M_\infty\|$	λ_∞/r_0	x^u_{99}/λ_s	x_∞/λ_s	δ_∞/r_0	δ_∞/d_{eff}	Z_∞
0.11	23.2	35.7	67	5.5	4.3	0.99
0.17	18.1	21	37	5	4	0.98
0.22	12.5	12.7	30	4.4	3.5	0.97
0.25	11.6	11	21	4.3	3.4	0.97
0.28	8.9	8.5	34	4	3.2	0.96
0.31	9	8	18	4	3.2	0.96
0.35	6.8	6	35	3.6	2.9	0.95

Table 7.2: Simulation results for condensation, continued

is the mean molecular spacing. d_{eff} is the effective molecular diameter defined from the mean free path at infinity, $\lambda_\infty = \frac{1}{\sqrt{2} n_\infty \pi d_{eff}^2}$, and δ_∞/d_{eff} is a measure of the deviation from ideal gas, Bird [23] uses $\delta_\infty/d_{eff} > 7$ as limit for dilute gas, this criterion is never fulfilled in our simulations. The thickness of the interphase was approximately $5r_0$ in all simulations. The compression factor is here defined as $Z_\infty = \frac{p_\infty}{\rho R T_\infty}$. λ_s, the reference mean free path defined from viscosity, Eq.(3.23), is only a function of the liquid temperature and varied slightly around 10 r_0 in the simulations. $(n_\infty/n_s)_{\sigma=1}$ is calculated from a finite difference solution of the BKW equation.

7.5 Knudsen layer

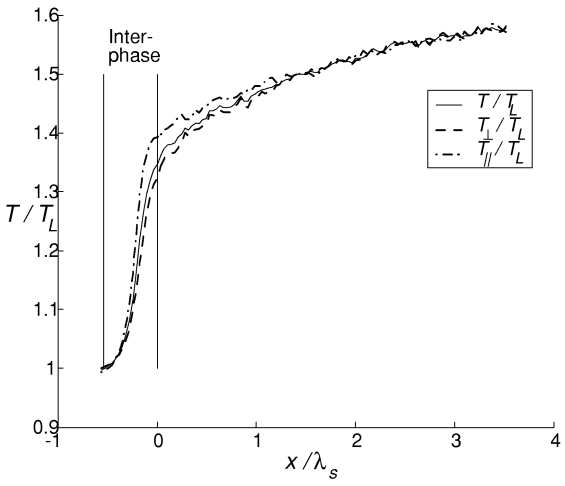

Figure 7.3: Knudsen layer for $M_\infty = -0.28$.

Fig.7.3 shows a plot of the various temperatures T, $T_{||}$ and $T_\perp$ for $M_\infty =$

-0.28. The temperatures deviate from each other slightly from midway in the interphase to approximately $1.5\ \lambda_s$. The Knudsen layer for condensation is much less pronounced than for evaporation.

As noted by Yen[86] and implicit in works of Mager[88] and Frezzotti[99], for the one-dimensional evaporation problem properties like the density ratio and mass flux does not depend much upon the type of kinetic equation or intermolecular potential used (for the same condensation coefficient). But the relaxation rate towards the uniform state at infinity is not the same according to Yen[86]. In Fig.7.4 we make a comparison for the temperature between an MD simulation, a numerical solution of the BKW equation and a DSMC simulation, for $M_\infty = -0.28$ and $T_\infty/T_L = 1.65$. For the MD simulation, defining an appropriate σ so a comparison with the gas-kinetic solutions can be made is not easy, see Table 7.3 for values from various definitions. Since σ_{macro} is determined by n_s/n_∞ and it is just the density that is involved in the rescaling of the gas-kinetic solutions for various σ's, $\sigma \approx 1$ may be a good choice. The BKW and DSMC solutions are hence for $\sigma = 1$, hard spheres collision cross section has been used for both. The graphs from the various simulation methods do not differ much. It is seen that the BKW solution relaxes faster than the corresponding DSMC solution.

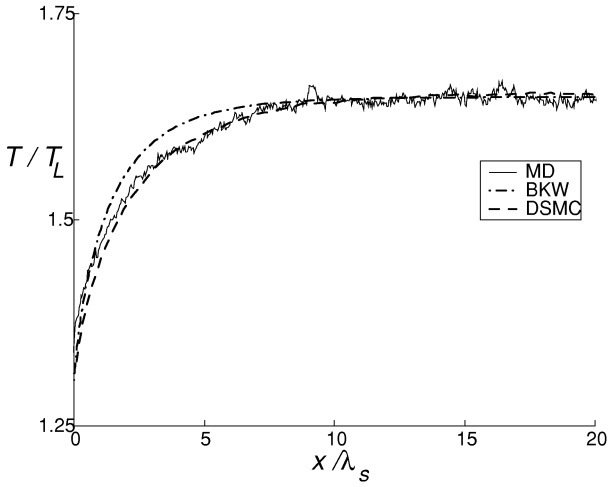

Figure 7.4: Comparison of DSMC and BKW for $\sigma = 1$, and MD

In Fig.7.5 we make a comparison of the velocity for a MD simulation, a DSMC solution of the Boltzmann equation and a BKW solution, $M_\infty = -0.28$ and $T_\infty/T_L = 1.65$. For the DSMC and BKW solutions $\sigma = 1$. The MD and DSMC simulations are similar.

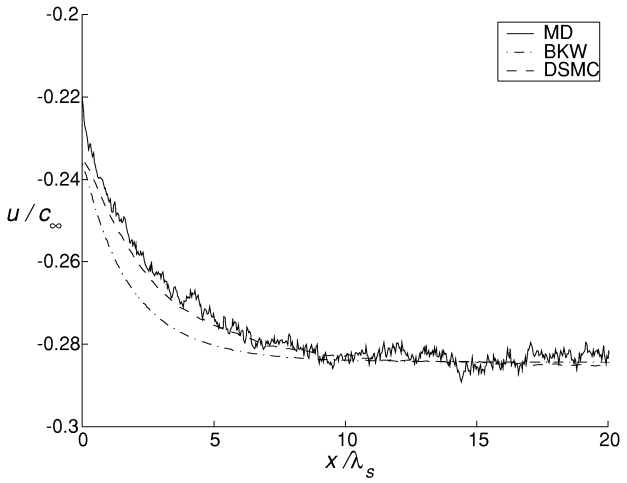

Figure 7.5: Comparison of DSMC and BKW solutions for $\sigma = 1$, and a MD simulation, at identical conditions.

7.6 Boundary condition at the interphase

The Boltzmann equation can only describe the behavior in the gas phase. In gas-kinetics the dynamics in the interphase is replaced by a boundary condition at the gas boundary defined above. Here we will use molecular dynamics to determine this boundary condition and compare it with existing models.

7.6.1 Condensation coefficients

As in the evaporation case, several possible ways exist to calculate the coefficients. First we will recapitulate the various simulation expressions for the coefficients and give the corresponding values from MD simulations.

We will first make the common assumption that the evaporation and condensation coefficients are equal. The distribution function, Eq.(2.4) becomes

$$f^+ = n^+ F^+ = \left[\sigma n_s + (1-\sigma) n_i\right] F_s, \qquad c_x > 0 \tag{7.22}$$

where the number density is given by

$$2n^+ = \sigma n_s + (1-\sigma) n_i \tag{7.23}$$

The factor 2 comes from different normalization of F^+ and F_s, F^+ is normalized to 1 on $c_x > 0$ whereas F_s is normalized on $-\infty < c_x < \infty$. A 'microscopic' condensation coefficient can be defined from the number density

$$\sigma_{micro} = \frac{n_i - n_s}{n_i - 2n^+} \tag{7.24}$$

n^+ is calculated in our simulations in a small control volume of thickness $r_0/6 \approx \lambda_s/55$.

A 'macroscopic' relation involving σ can also be used to define an effective coefficient. The transformation of the density, Eq.(7.6) for $\sigma_e = \sigma_c = \sigma$ is

$$\frac{n_s}{n_\infty} = \left(\frac{n_s}{n_\infty}\right)_{\sigma=1} + \frac{1-\sigma}{\sigma}\sqrt{\frac{10\pi}{3}}\sqrt{\frac{T_\infty}{T_L}}M_\infty \tag{7.25}$$

$\left(\frac{n_s}{n_\infty}\right)_{\sigma=1}$ is a function of M_∞ and $\frac{T_\infty}{T_L}$ for condensation, and σ can then be determined from a given value of $\frac{n_s}{n_\infty}$,

$$\sigma_{macro} = \frac{\sqrt{\frac{10\pi}{3}}\sqrt{\frac{T_\infty}{T_L}}M_\infty}{-\left(\frac{n_s}{n_\infty}\right)_{\sigma=1} + \frac{n_s}{n_\infty} + \sqrt{\frac{10\pi}{3}}\sqrt{\frac{T_\infty}{T_L}}M_\infty} \tag{7.26}$$

σ_{macro} has been calculated with $\left(\frac{n_s}{n_\infty}\right)_{\sigma=1}$ from a numerical solution of the BKW equation. Both expressions (7.24) and (7.26) are indeterminate at equilibrium. But the value of σ at equilibrium is of no interest, any value may be used, cancellation occurs and Eq.(2.4) collapses to $f^+ = n_s F_s$.

In practical applications the evaporation mass flux is important, hence a condensation coefficient should be defined to give the correct flux, here the new coefficient is denoted σ_J. The flux is given by Eq.(7.7), with $\sigma_e = \sigma_c = \sigma$,

$$J = \sigma n_s\sqrt{\frac{RT_L}{2\pi}} - \sigma n_\infty\sqrt{\frac{RT_\infty}{2\pi}}F^-(\sqrt{5/6}M_\infty) \tag{7.27}$$

Values for n_∞ from MD simulations are not used, n_∞ is found by transforming numerical BKW solutions of $\left(\frac{n_\infty}{n_s}\right)_{\sigma=1}$, since this is the most likely approach to be used in application of the mass flux formula. σ_J is defined as the value where the graph $J(\sigma)$ crosses the line given by the simulated flux. In Table 7.3 the various coefficients have been listed. Uncertainty estimates in the coefficients ought to be included, but the statistical uncertainty is much smaller than the uncertainty in the definitions of the coefficients themselves, which are difficult to estimate. For instance, there is no unique way to define the positions of the gas- and liquid boundaries.

Each method gives different σ's and the theory can not be exact. Hence we should check if $\sigma_e = \sigma_c$ is a good assumption. In Table 7.3, values for σ_e and σ_c calculated from their definitions have also been listed. It looks as though the assumption that $\sigma_c = \sigma_e$ outside equilibrium is not valid, the evaporation coefficient decreases when the strength of the condensation process is increased, whereas the condensation coefficient is fairly constant.

$\lvert M_\infty \rvert$	σ_J	σ_{macro}	σ_{micro}	σ_e	σ_c
0.11	0.55	1.21	1.05	0.69	0.77
0.17	0.76	1.14	1.01	0.61	0.76
0.22	0.88	1.05	0.96	0.60	0.76
0.25	0.89	0.99	0.94	0.57	0.74
0.28	0.91	0.97	0.90	0.55	0.76
0.31	0.92	0.96	0.90	0.55	0.77
0.35	0.92	0.93	0.89	0.45	0.75

Table 7.3: Condensation coefficients for various Mach numbers.

7.6.2 Calculation of the distribution function at the interphase

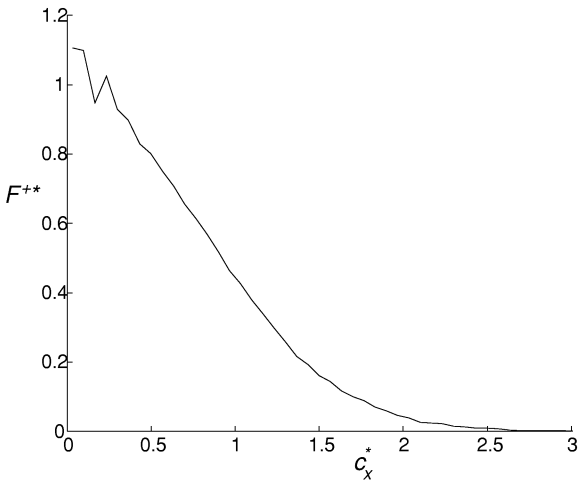

Figure 7.6: Distribution function for molecules escaping the interphase, for $M_\infty = -0.31$.

Fig.7.6 shows the probability distribution $F^+(c_x)$ for molecules crossing from the interphase into the gas, for $M_\infty = -0.31$. F^+ is normalized to 1 for $c_x > 0$. Then n^+ in $f^+ = n^+F^+$ is the physical density of molecules leaving the interphase and entering the gas. F^+ looks like a Maxwellian with a small drift-velocity towards the interphase.

In Fig.7.7 the distribution for the c_y-component for molecules entering the gas is compared with Maxwellians with temperatures T_L and T_0, the temperature at the gas boundary, for $M_\infty = -0.31$. The distribution looks like a Maxwellian, but with a temperature that corresponds to somewhere in the interphase.

The normalized distribution function for the c_x-velocity for the incoming

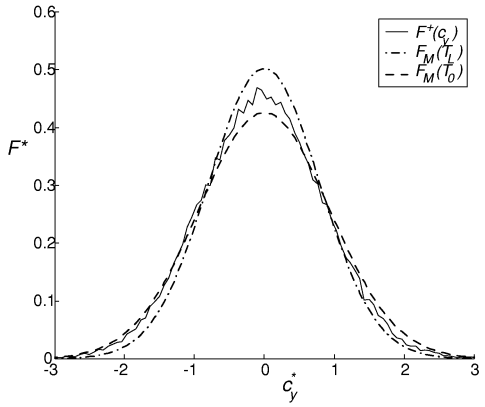

Figure 7.7: Distribution function at the interphase for the normal component of velocity

molecules has been plotted in Fig. 7.8 for $M_\infty = -0.31$, the distribution looks like Maxwellian with a drift velocity towards the interphase.

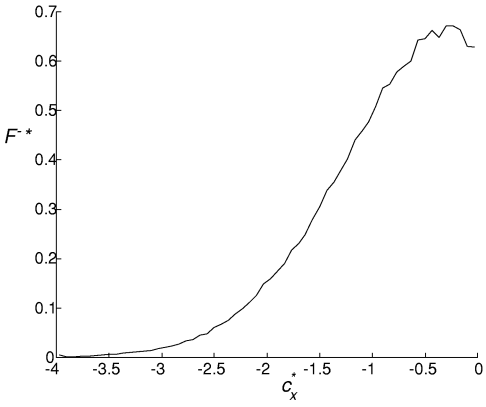

Figure 7.8: Distribution function for incoming molecules, $M_\infty = -0.31$.

7.6.3 Evaporation and condensation distribution functions

Evaporating and reflecting molecules are tagged. Fig.7.9 shows the probability distributions for the evaporated molecules for the component of velocity parallel to the drift velocity, for various values of M_∞. The distributions are normalized to 1 for $c_x > 0$. The plots are very similar, although not identical, but this may be due to poor statistics. Contrary to the assumption in most gas-kinetic

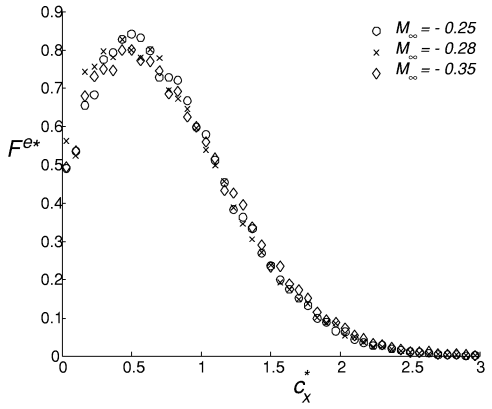

Figure 7.9: Evaporation mode for varoius Mach numbers.

calculations, F^e has a drift velocity away from the interphase. This was also the case for net evaporation, Fig.6.18, and the evaporation distributions look very similar for net evaporation and net condensation.

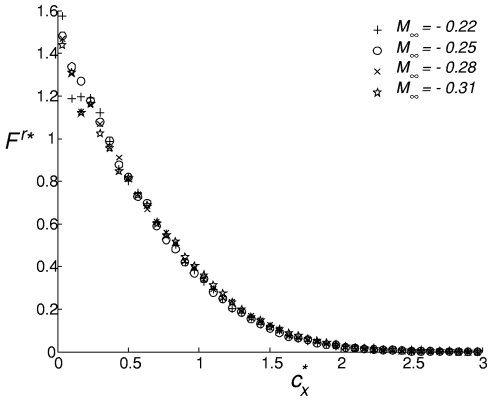

Figure 7.10: Reflection mode for various Mach numbers.

In Fig. 7.10 the probability distribution for the normal component of velocity for the reflected molecules is plotted for various M_∞. All distributions are normalized to 1 on $c_x > 0$. The plots are again similar, the normalized distribution for reflection is rather independent of M_∞, as was the case for net evaporation too. Tsuruta[93] has also reported similar shifts for the differential flux $\Phi \sim c_x F$ for evaporation and condensation.

Number densities for the evaporated and reflected molecules can be calculated, n^e is the density for evaporated molecules just outside the gas boundary,

$\lvert M_\infty \rvert$	χ_e	n^r/n_s	χ_r
0.11	0.30	0.19	0.15
0.17	0.27	0.23	0.15
0.22	0.26	0.26	0.14
0.25	0.23	0.31	0.14
0.28	0.23	0.35	0.14
0.31	0.23	0.35	0.13
0.35	0.18	0.45	0.13

Table 7.4: Nondimensional evaporation and reflection densities

n^r is the density for reflected molecules and $n^+ = n^e + n^r$, i.e. the density of the molecules escaping from the interphase and entering the gas. The probability distributions in Figs. 7.6, 7.9 and 7.10 are related by

$$f^+ = n^+ F^+ = n^e F^e + n^r F^r \tag{7.28}$$

It is convenient to tabulate n^e in terms of n_s and a dimensionless constant χ_e, defined as

$$\chi_e = \frac{n^e}{n_s} \tag{7.29}$$

Similarly, the reflection density is nondimensionalized as

$$\chi_r = \frac{n^r}{n_i} = n^r \sqrt{\frac{RT_L}{2\pi}} / J^- \tag{7.30}$$

n^r/n_s is also listed in Table 7.4 since it indicates the increasing influence of reflected molecules for higher negative Mach numbers.

7.6.4 Condensation probability and velocity dependent coefficients

In gas-kinetic calculations the condensation probability is assumed to be a constant, equal to the condensation coefficient. However, it has been shown by Tsuruta[93] that the condensation probability $\sigma_c(c_x)$ is velocity dependent, contrary to the usual assumption in kinetic theory. The higher the velocity normal to the interphase is, the higher is the probability for condensation, which is a reasonable result.

If σ_e is defined from the conventional boundary condition, Eq.(2.4), in terms of non-drifting Maxwellians, the coefficient will be velocity dependent

$$f^e(\mathbf{c}) = n^e F^e = \sigma_e(c_x) n_s F_s(\mathbf{c}) \tag{7.31}$$

The redefined coefficient $\sigma_e(c_x)$ takes into account the deviation from a Maxwellian with no drift velocity for the c_x-velocity probability distributions and gives the correct number density. The c_y- and c_z- distributions are not affected, they are assumed to be the standard Maxwellian distribution with temperature T_L. It is easy to show that $\sigma_c(c_x) = \sigma_e(c_x)$ at equilibrium, see section 6.6.5. It is sometimes claimed that $\sigma_c(c_x) = \sigma_e(c_x)$ also in nonequilibrium[101],[102], but to the best of our knowledge a proof is still lacking. Our simulations indicate that the velocity dependent coefficients are not equal outside equilibrium. In Fig.7.11, $\sigma_e(c_x)$ and $\sigma_c(c_x)$ has been plotted for $M_\infty = -0.31$.

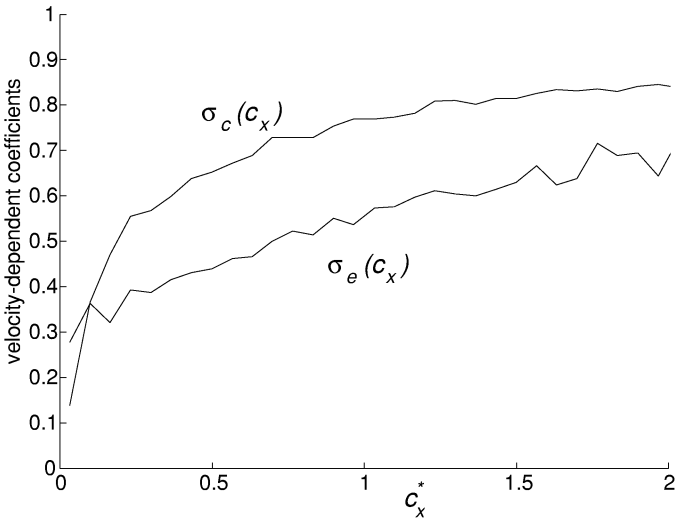

Figure 7.11: Velocity-dependent coefficients for $M_\infty = -0.31$.

J^c/J^- listed in Table 7.3 should be interpreted as the average condensation probability and $J^e/(n_s\sqrt{\frac{RT_L}{2\pi}})$ is the average evaporation coefficient

$$\overline{\sigma}_c = \frac{\int\limits_{c_x<0} \sigma_c(|c_x|)|c_x|f^- d\mathbf{c}}{\int\limits_{c_x<0} |c_x|f^- d\mathbf{c}} \tag{7.32}$$

$$\overline{\sigma}_e = \frac{\int\limits_{c_x>0} \sigma_e(c_x)c_x f_s d\mathbf{c}}{\int\limits_{c_x>0} c_x f_s d\mathbf{c}} \tag{7.33}$$

We see from Fig.7.11 that $\sigma_c(c_x)$ is larger than $\sigma_e(c_x)$ for condensation, whereas it is the opposite for evaporation. This is consistent with the values for the average evaporation and condensation coefficients for both cases.

7.6.5 Blocking

The blocking effect restricts the attainable Mach numbers for condensation according to gas-kinetic calculations[68]. The blocking effect is due to reflection of the incoming molecules. In a DSMC or a MD simulation a certain temperature difference T_∞/T_L and Mach number are forced upon the system. Assume that the average condensation probability can be decreased, this is easy in DSMC, just adjust the rate with which molecules are inserted at the boundary, but for MD it is a 'gedanken' experiment. More molecules are reflected and the incoming flux must be increased to give the desired Mach number, but this gives more reflected molecules and below a certain critical average condensation probability, dependent upon the Mach number, the result is a runaway process. From Eq.(7.6) it follows for $\sigma_e = \sigma_c = \sigma$ that $\frac{n_s}{n_\infty}$ is zero and n_∞ is infinite for a subsonic Mach number if σ is below a certain value σ_{crit}, weakly depending on the temperature ratio

$$\sigma_{crit} = \left[1 - \left(\frac{n_s}{n_\infty}\right)_{\sigma=1, M_\infty=1} \sqrt{\frac{3}{10\pi}\frac{T_L}{T_\infty}}\right]^{-1} \tag{7.34}$$

Ytrehus[24] used $\sigma_{crit} \approx 0.97$.

We have not managed to simulate net condensation for higher negative Mach numbers than -0.35. When higher $|M_\infty|$ was prescribed, the code crashed, regardless of the average density in the simulation cell. It is natural to suspect this is due to the blocking effect, although a rapid increase in n_∞/n_s was not observed for the simulations listed in Table 7.1.

7.7 Conclusion

The condensation algorithm presented makes it possible to do molecular dynamics simulations for net condensation for arbitrary Mach number up to blocking. It is then feasible to compare molecular dynamics simulations and results from gas-kinetic calculations, and in addition verify if the conventional boundary condition used in most gas-kinetic calculations of condensation is accurate.

Contrary to a common approximation, the average condensation and evaporation coefficients found are not equal outside equilibrium. The condensation coefficient increases with the strength of the condensation process, whereas the evaporation coefficient decreases. The evaporation and reflection distribution functions deviate from the conventional representation as nondrifting half-Maxwellians. The evaporation mode has a drift velocity away from the interphase, and the reflection mode has a drift velocity towards the interphase. However, the evaporation and reflection velocity probability functions appear to be independent of the Mach number and rather similar to the corresponding functions for equilibrium and net evaporation.

Acknowledgement 3 *Financial support from the Norwegian Council of Research and the Italian State, and CPU time at the department of Chemistry, NTNU are gratefully acknowledged.*

Appendix A

Main notation

A.1 Latin letters

A	general property
$\mathbf{a}$	acceleration vector
$a_0, a_K^+, a_\infty^+, a_\infty^-$	weight factors in moment ansatz
$C(f)$	collision integral
$\mathbf{c} = (c_x, c_y, c_z)$	molecular velocity
c_p	constant pressure specific heat capacity
c_v	constant volume specific heat capacity
c_∞	speed of sound
d_{eff}	effective molecular diamter
$d\mathbf{c}$	velocity element
$d\mathbf{r}$	volume element
$\mathbf{F}$	force
F	velocity probability density
F_M	Maxwellian velocity probability density
F_s	standard Maxwellian
f	distribution function
f^e	evaporation distribution function
f^r	reflection distribution function
f^+	distribution function of molecules leaving the interphase
f^-	incident distribution function
g	relative velocity
h	specific enthalpy
J	number flux
J^e	evaporation number flux
J^{ex}	exchange number flux
J^{in}	number flux inserted in the gas for condensation
J_m	mass flux
J^{out}	number flux leaving the box
J_s	number flux corresponding to half Maxwellian
J^r	reflection number flux

J^-	incident number flux
$\mathbf{K}$	external force
K	thermal conductivity
Kn	Knudsen number
k	Boltzmann's constant
L	latent heat
L_x	length of simulation box
L_y	width of simulation box
l	characteristic lenght in gas phase
M_∞	Mach number
m	molecular mass
N	number of molecules
n	number density
n^e	density of evaporating particles
n_s	saturation density
n^r	density of reflecting particles
n^+	density of particles escaping from the interphase
n^-	density of incident particles
O	order of symbol
p	pressure
p_{normal}	pressure normal to the interphase
p_{SRK}	Soave-Redlich-Kwong equation of state
$p_{transverse}$	pressure parallel to the interphase
$p_\perp$	pressure normal to the drift velocity
$p_{\|\|}$	pressure parallel to the drift velocity
Q	moment
R	gas constant per unit mass
r_c	cut-off distance for potential
r_L	neighborlist cut-off
r_s	inflection point for LJ-potential
S_∞	speed ratio
T_L	liquid temperature
T_K	temperature outside the Knudsen layer
T_∞	temperature at infinity
t	time
u_p	specific potential energy
v	$1/\rho$
Z_∞	compression factor

A.2 Greek letters

β	normalized latent heat
$\underline{\beta}_c$	criticallity parameter for the inverted temperature gradient
$\overline{\beta}_c$	redefined criticallity parameter for the inverted temperature gradient
γ	c_p/c_v
δ	average distance between molecules
$\Delta\widehat{\sigma}$	deviation between the condensation and evaporation coefficients
λ	mean free path
μ	viscosity
ρ	mass density
ν	colission frequency
σ_c	condensation coefficient
σ_e	evaporation coefficient
σ_μ	viscosity cross section
Φ_1	pertubation in distribution function
Φ	normalized differential flux
φ	differential flux
$\varkappa$	deflection angle

A.3 Abbreviations

BGK	Bhatnagar,Gross and Krook
DSMC	direct simulation Monte Carlo
gb	gas boundary
lb	liquid boundary
LJ	Lennard-Jones
MD	molecular dynamics
NEMD	nonequilibrium molecular dynamics
SRK	Soave-Redlich-Kwong

Bibliography

[1] I. W. Eames, N. J. Marr and H. Sabir, The evaporation coefficient of water : a review, *Int. J. Heat Mass Transfer*, 40, 2963-2973, 1997.

[2] C. Cercignani, Rarefied Gas Dynamics, Cambridge University Press 2000.

[3] J. H. Ferziger and H.G. Kaper, Mathematical theory of transport processes in gases, North-Holland, 1972.

[4] W.G Vincenti and C.H. Kruger, Introduction to Physical Gas Dynamics, Wiley, 1965.

[5] P. Résibois and M. De Leener, Classical kinetic theory of fluids, Wiley 1977.

[6] H. Hertz, Ueber die Verdünstung der Flüssigkeiten, insbesondere des Quecksilbers im luftleere Raume, *Ann. Phys. Chem*, 17, 177, 1882.

[7] M. Knudsen, Die maximale Verdampfungsgeschwindigkeit des Quecksilbers, *Ann. Phys. Chem, 47, 697, 1915.*

[8] J.S. Rowlinson and B. Widom, Molecular theory of capillarity, Oxford science publications, 1982.

[9] S. I. Anisimov, Vaporization of metal absorbing laser radiation, JETP 27,1 182-183, 1968

[10] R. Marek and J. Straub, Analysis of the evaporation coefficient and the condensation coefficient of water, *Int. J. Heat Mass Transfer,* 44, 39-53, 2001.

[11] P.N. Shankar and F. E. Marble, Kinetic Theory of Transient Condensation and Evaporation at a Plane Surface, *Phys. Fluids* 14, 3, 510-516, 1971.

[12] K. Aoki, S. Takata and S. Kosuge, Vapor flows caused by evaporation and condensation on two parallel plane surfaces: Effect of the presence of a noncondensible gas, *Phys. Fluids* 10, 6, 1519-1533, 1998.

[13] C. Cercignani, The Boltzmann equation and its applications, Springer verlag, 1988.

[14] H.M. Mott-Smith, The solution of the Boltzmann equation for a shock wave, *Phys. Rev* 82, 885-892, 1951.

[15] C. Y. Liu and L. Lees, Kinetic theory description of a plane compressible Couette flow, in *Rarefied Gas Dynamics*, edited by L. Talbot, 391-428. Academic Press, 1961.

[16] T. Ytrehus, Theory and experiments on gas kinetics in evaporation, in *Rarefied Gas Dynamics*, edited by J.L. Potter, vol. 51 of *Progr. Aeronaut.* AIAA, 1197-1212, 1977.

[17] T. Ytrehus and J.A. Alvestad, A Mott-Smith solution for nonlinear condensation, in *Rarefied Gas Dynamics,* Vol. 74 of *Progr. Astronaut-Aeronaut*, edited by S. Fischer, 330-345, AIAA, 1981.

[18] P.L. Bhatnagar, E.P. Gross and M. Krook, A model for collision processes in gases. *Phys. Rev.*, 94, 3, 511-525, 1954.

[19] K. Aoki and N. Masukawa, Gas flows caused by evaporation and condensation on two parallel condensed phases and the negative temperature gradient: Numerical analysis by using a nonlinear kinetic equation, *Phys. Fluids* 6, 3, 1379-1395, 1994.

[20] Y. Sone, Kinetic theory of evaporation and condensation - Linear and nonlinear problems, *J. Phys. Soc. Jpn.* 45, 315-320, 1978.

[21] K. Aoki, Y. Sone and T. Yamada, Numerical analysis of gas flows condensing on its plane condensed phase on the basis of kinetic theory, *Phys. Fluids* A 2, 1867-1878, 1990.

[22] G. A. Bird, Approach to Translational Equilibrium in a Rigid Sphere Gas, *Phys. Fluids* 6, 1518-1519, 1963.

[23] G. A. Bird, Molecular Gas Dynamics and the Direct Simulation of Gas Flows, Oxford University Press 1994.

[24] T. Ytrehus, Molecular Flow Effects in Evaporation and Condensation at Interfaces, *Multiphase Science and Technology*, Vol. 9, No 3, 205-327. 1997

[25] M. N. Kogan, Kinetic theory in aerothermodynamics, Prog. Aerospace Sci. Vol. 29, 271-354, 1992.

[26] B. J. Alder and T.E. Wainwright, Phase transition for a hard sphere system, *J. Chem. Phys.* 27, 1208-1209, 1957.

[27] A. Rahman, Correlations in the motion of atoms in liquid argon, *Phys. Rev.* 136A, 405-411, 1964.

[28] T. A. Andrea, W.C. Swoope and H. C. Andersen, The role of long ranged forces in determining the structure and properties of liquid water, *J. Chem. Phys.* 79, 4576-4584, 1983.

[29] W.G. Hoover, Computational statistical mechanics, Elsevier, 1991.

[30] D.J. Evans and G. P. Morriss, Statistical mechanics of non-equilibrium liquids, Academic Press, 1990.

[31] J. Koplik, Continuum deductions from molecular hydrodynamics, *Ann. Rev. Fluid Mech.*, 27 : 257-292, 1995.

[32] W. G. Hoover and W. T. Ashurst, Nonequilibrium molecular dynamics, in *Theoretical chemistry: Advances and perspectives*, edited by H. Eyring and D. Henderson, vol. 1, 1-51, Academic Press, 1975.

[33] M.P. Allen, D. J. Tildesley, Computer Simulation of Liquids, Oxford science publications 1987.

[34] D.C. Rapaport, Molecular dynamics simulation, Cambridge university Press 1995.

[35] D. M. Heyes, The liquid state, applications of molecular simulations, Wiley 1998.

[36] D. J. Evans and W. G. Hoover, Flows far from equilibrium via molecular dynamics, *Ann. Rev. Fluid Mech.*, 18 : 243-264, 1986.

[37] J. M. Haile, Molecular dynamics simulation, Wiley, 1992.

[38] J.-P. Hansen, Theory of simple liquids, Academic press, 1986.

[39] W. C. Swope and H.C. Andersen, A computer simulation method for the calculation of equilibrium constants for the formation of physical clusters of molecules: application to small water clusters, *J. Chem. Phys.* 76, 637-649, 1982.

[40] L. Verlet, Computer 'experiments' on classical fluids, Thermodynamical properties of Lennard-Jones molecules, *Phys. Rev.* 159, 98-103, 1967.

[41] I. Wold, Nonequilibrium molecular dynamics simulations of porous media, PhD. thesis, Dept. of physical chemistry, Norwegian University of Science and Technology, 1997.

[42] B.L. Holian, D.J. Evans, Shear viscosities away from the melting line. A comparison of equilibrium and nonequilibrium molecular dynamics. *J.Chem.Phys.*, 78, 5147-5150, 1983.

[43] A. Røsjorde, D. W. Fossmo, D. Bedeaux, S. Kjelstrup and B. Hafskjold, Nonequilibrium Molecular Dynamics Simulations of Steady-State Heat and Mass Transport in Condensation. I. Local Equilibrium, *Journal of Colloid and Interface Science*, 232, 178-185, 2000.

[44] P.A. Thompson, Compressible-Fluid Dynamics, McGraw-Hill, 1971.

[45] D. Kondepudi and I. Prigogine, Modern thermodynamics, Wiley 1998.

[46] C.B.P. Finn, Thermal Physics, Chapman & Hall, 1993.

[47] J.A. Barker and D. Henderson, Pertubation Theory and Equation of State for Fluids. II. A Successful Theory of Liquids, *J. Chem. Phys.* 47, 4714-4721, 1967.

[48] R. W. Schrage, A theoretical study of interphase mass transfer. Colombia University Press, 1953.

[49] A.J. Patton and G.S. Springer, A kinetic theory description of liquid-vapor phase change, in *Rarefied Gas Dynamics*, edited by L. Trilling and H.Y. Wachman, 410-419, 1969.

[50] Y.-P. Pao, Application of kinetic theory to the problem of evaporation and condensation, *Phys. Fluids* 14, 306-311, 1971.

[51] Y.-P. Pao, Temperature and density jumps in the kinetic theory of gases and vapors, *Phys. Fluids* 14, 1340-1346, 1971.

[52] J.W. Cipolla, J.H. Lang and S.K. Loyalka, Kinetic Theory of Evaporation and Condensation, in *Rarefied Gas Dynamics,* edited by K. Karamcheti, 179-188, 1973.

[53] M. Murakami and K. Oshima, Kinetic approach to the transient evaporation and condensation problem, in *Rarefied Gas Dynamics*, edited by M. Becker and M. Fiebig, vol. I, F.6, DFLVR Press, 1974.

[54] P. Gajewski, A. Kulicki, A. Wisniewski and M. Zgorelski, Kinetic theory approach to the vapor-phase phenomena in a non-equilibrium condensation process, *Phys. Fluids* 17, 321-327, 1974.

[55] Y. Sone and Y. Onishi, Kinetic Theory of Evaporation and condensation-Hydrodynamic Equations and Slip-boundary Conditions., *J. Phys. Soc. Jpn.*, 35, 1981-1994, 1978.

[56] T. Matsushita, An analytical study of the problem of evaporation and condensation using the finite element method, in *Rarefied Gas Dynamics*, edited by M. Becker and M. Fiebig, vol. II, F.3-1-12, DFLVR Press, 1974

[57] K. Aoki, C. Cercignani, Evaporation and condensation on two parallel plates at finite Reynolds numbers. *Phys. Fluids 26*, 1163-1164, 1983.

[58] L.D Koffman, M.S Plesset & L. Lees, Theory of Evaporation and Condensation, *Phys. Fluids* 27, 876-880. 1984.

[59] C. Cercignani, W. Fiszdon and A. Frezzotti, The paradox of the inverted temperature profiles between an evaporation and a condensing surface, *Phys. Fluids* 28, 3237-3240, 1985.

[60] Y. Sone, T. Ohwada and K. Aoki, Evaporation and condensation of a rarefied gas between its two parallel plane condensed phases with different temperatures and negative temperature-gradient phenomenon-Numerical analysis of the Boltzmann equation for hard-sphere molecules, in Mathematical Aspects of Fluid and Plasma Dynamics, edited by G. Toscani, LNM 1460, 186-202, Springer-Verlag, 1991.

[61] T. Ytrehus and T. Aukrust, Mott-Smith Solution for Weak condensation, in *Rarefied Gas Dynamics*, edited by V. Boffi and C. Cercignani, Vol. II, 271-279, 1986.

[62] T. Ytrehus, The Inverted Temperature Gradient in Condensation, Revisited, in *Rarefied Gas Dynamics*, edited by R.Brun, R. Campargue, R.Gatignol and J,-C.Lengrand, Vol. 1, 471-478, 1999.

[63] Y. Sone and Y. Onishi, Kinetic theory of evaporation and condensation, *J. Phys. Soc. Jpn.*, 35, 1773, 1973.

[64] R.E. Caflisch, Asymptotic Expansions of Solutions for the Boltzmann equation. *Transp. Theory. Stat. Phys.* 16, 701-725. 1987

[65] K. Aoki, K. Nishino, Y. Sone and H. Sugimoto, Numerical analysis of steady flows of gas condensing on or evaporating from its plane condensed phase on the basis of kinetic theory, *Phys. Fluids* A 3, 2260-2275, 1991

[66] M. Plesset, Note on the flow between liquid surfaces, *Journal of chemical physics*, 20, 790-793, 1952.

[67] Y. Sone. K. Aoki and J. Yamashito, A study of strong condensation on a plane condensed phase with special interest in formation of a steady profile, in *Rarefied Gas Dynamics,* editef by V. Boffi and C. Cercignani, Vol. II, 323-333,B. G. Teubner, 1986.

[68] M.N. Kogan, and A.A. Abramov, Direct Simulation Solution of the Strong Evaporation and Condensation Problem, in *Rarefied Gas Dynamics*, 1251-1257, edited by A. Beylich, VCH, 1991.

[69] K. Aoki and Y. Sone, Gas flows around the condensed phase with strong evaporation or condensation - Fluid dynamic equations and its boundary condition on the interface and their application, in Advances in Kinetic Theory and Continuum Mechanics, edited by R. Gatignol and Soubbaramayer, 43-54, Springer-Verlag, 1991.

[70] L. J. F. Hermans and J. J .M Beenakker, The temperature paradox in the kinetic theory of evaporation, *Phys. Fluids* 29(12), 4231-4232, 1986.

[71] A.C.L. Opitz, Molecular Dynamics Investigation of a Free Surface of Liquid Argon, *Phys. Lett.* 47A, 439-440, 1974.

[72] G.A. Chapela and G. Saville, *J. chem. Soc. Faraday Trans.* II, 73, 1133-1144, 1977.

[73] A. Røsjorde, S. Kjelstrup, D. Bedeaux and B. Hafskjold, Nonequilibrium Molecular Dynamics Simulations of Steady-State Heat and Mass Transport in Condensation. II. Transfer coefficients , *Journal of Colloid and Interface Science*, 240, 355-364, 2001.

[74] D. Bedeaux, L.J.F. Hermans and T. Ytrehus, Slow evaporation and condensation, *Physica A*, 169, 263-280, 1990.

[75] S. Kjelstrup and D. Bedeaux, Irreversible thermodynamics of heterogenous systems, lecture notes Norwegian University of Science and Technology, 1999.

[76] K. Yasuoka and M. Matsumoto, Evaporation and condensation at a liquid surface. I. Argon, *J. Chem. Phys*, 101 (9), 1994.

[77] T. Tsuruta and G. Nagayama, Interphase mass transfer rate between liquid and vapor based in molecular dynamics, Proceedings of 11. Int. Symp. on Transport Phenomena, 527-532, 1998.

[78] M. Matsumoto, K. Yasuoka, Y. Kataoka, Microscopic Features of Evaporation and Condensation at Liquid Surfaces: Molecular Dynamics Simulation, *Thermal Science & Engineering*, Vol. 2, No 1, 64-69, 1994.

[79] M. Matsumoto, K. Yasuoka, Evaporation and Condensation at a Liquid Surface. 1. Argon, *J. Chem. Phys.,* 101 (9), 7904-7911. 1994.

[80] M. Matsumoto, K. Yasuoka, Evaporation and Condensation at a Liquid Surface. 2. Methanol, *J. Chem. Phys.,* 101 (9), 7912-7917. 1994.

[81] M. Matsumoto, K. Yasuoka, Y. Kataoka, Molecular Mechanism of Evaporation and Condensation, *Thermal Science & Engineering*, Vol. 3, No 3, 27-31, 1995.

[82] M. Matsumoto, Molecular Dynamics of Liquid Surfaces, *Molecular Simulation*, Vol. 16, 209-217, 1996.

[83] J. Goodisman, Statistical Mechanics for Chemists, Wiley 1997.

[84] S. P. Pope, Turbulent flows, Cambridge University Press, 2000.

[85] S. Fujikawa, M. Kotani, H. Sato, M. Matsumoto, Molecular Study of Evaporation and Condensation of an Associating Liquid, *Heat Transfer-Japanese Research*, 23 (7), 595-610, 1994.

[86] S. Yen and T. J. Akai, Nonlinear Numerical Solutions for an Evaporation-Effusion Problem, in *Rarefied Gas Dynamics*, edited by J.L. Potter, 1175-1183, 1977.

[87] Y. Sone, K. Aoki, H. Sugimoto and T. Yamada, Steady evaporation and condensation on a plane condensed phase, *Phys. Fluids,* 10, 1867-1878, 1990.

[88] R. Mager, G. Adomeit and G. Wortberg, Theoretical and Experimental Investigation of the Strong Evaporation of Solids, in *Rarefied Gas Dynamics : Physical Phenomena,* edited by E.P. Muntz, D. P. Weaver and D. H. Campbell, 460-469, 1989.

[89] M. N. Kogan and N.K. Makashev, Knudsen layer in the theory of heterogeneous reactions, *Fluid. Dynam.* 6, 913-921, 1971.

[90] Y. Sone and H. Sugimoto, Strong evaporation from a plane condensed phase, in Adiabatic waves in liquid-vapor systems, edited by G. Meier, 293-303, 1990.

[91] C. Cercignani, Strong evaporation of a polyatomic gas, in *Rarefied Gas Dynamics,* edited by S. Fisher, 305-320, 1981.

[92] A. Frezzotti, Numerical investigation of the strong evaporation of a polyatomic gas, in *Rarefied Gas Dynamics,* edited by A. Beylich, 1243-1250, 1991.

[93] T. Tsuruta, H. Tanaka and T. Masuoka, Condensation/evaporation coefficient and velocity distributions at liquid-vapor interface, *International Journal of Heat and Mass Transfer*, 42, 4107-4116, 1999.

[94] V.V. Zhakhovskii, S.I. Anisimov, Molecular-dynamics simulation of evaporation of a liquid, *JETP* 84 (4), 734-745, 1997.

[95] Y. Sone, K. Aoki and I. Yamada, Steady evaporation and condensation on the plane condensed phase, *Theoretical and Applied Mechanics* **14,** 89-93, Bulgarian Academy of Sciences, 1988.

[96] D. A. Labuntsov and A.P. Kryukov, Analysis of intensive evaporation and condensation, *Int. J. Heat and Mass Transfer* **22**, 989-1002, 1979.

[97] M. Hatakeyama and H. Oguchi, Kinetic approach to nonlinear condensation in flowing vapor, in *Rarefied Gas Dynamics,* edited by R. Campargue, II, 1293-1303, 1979.

[98] B. Hafskjold and S. Ratkje, Criteria for local equilibrium in a system with transport of heat and mass, *Journal of Statistical Physics*, 78, 463-493, 1995.

[99] A. Frezzotti, Kinetic Theory Description of the Evaporation of Multi-Component Substances, in *Rarefied Gas Dynamics,* edited by C. Shen, *837-846,* 1997.

[100] Y. Sone, Kinetic Theoretical Studies of the Half-Space Problem of Evaporation and Condensation, *Transport Theory and Statistical Physics*, 29(3-5), 227-260, 2000.

[101] F. Sharipov, Onsager-Casimir reciprocity relations for open gaseous systems at arbitrary rarefaction I General theory for single gas , *Physica A* 203, 437-456, 1994.

[102] Private communication with F. Sharipov and C. Cercignani